# SYNTHESIS AND CHARACTERIZATION OF MAGNETIC NANOPARTICLES

by

NARAYAN POUDYAL

Presented to the Faculty of the Graduate School of

The University of Texas at Arlington in Partial Fulfillment

of the Requirements

for the Degree of

MASTER OF SCIENCE IN PHYSICS

THE UNIVERSITY OF TEXAS AT ARLINGTON

December 2005

ACKNOWLEDGEMENTS

I would like to express my sincere gratitude to my advisor, Professor J. Ping Liu, for providing invaluable guidance to research and constant supports to my study. I highly appreciate Prof. Liu for introducing me to scientific research, giving me a chance to accelerate my research skills, and encouraging me to work in the field of nanotechnology. His expertise in nanostructured magnetism along with his vision of nanotechnology has been the source of inspiration to me for further research in the field. The present research work would, therefore, have never been completed without his proper guidance, regular supervision, and constant encouragement.

I would like to thank Professors Suresh C. Sharma and Qiming Zhang for serving on my thesis supervisory committee. I am grateful to them for their careful and critical reading of my thesis and invaluable suggestions. Their comments and suggestions would not only help to improve my research skill but also would be a great help to have deeper insight in future research.

I would also like to thank Dr. Baki Altuncevahir for his invaluable suggestions, guidance, and encouragement. His technical support with equipments was a great help. I am thankful to Dr. Zhiqiang Jin, Dr. Yang Li, Grace Liu, Vamsi M. Chakka, and Dhurva Karki who have reviewed my thesis.

I am thankful to our collaborator, Dr. Z.L. Wang in Georgia Institute of Technology for his cooperation in HRTEM analysis. I am also grateful to Dr. Jing Li

and Dr. Zhiqiang Jin for their HRTEM analysis at Georgia Institute of Technology. I am thankful to Micheal Coviello for the technical support in operating the Transmission Electron Microscope and the assistance in processing TEM images.

I would like to thank my colleagues, Vamsi M. Chakka, Vikas Nandwana, Tejaswi Vedantam, Kung-Te Chu, Kevin Elkins, and Daren Li, for their cooperation in the laboratory activities. I would also like to thank my friends, Yogendra Panta and Rajan Lamichhane for helping me assemble materials. I express my indebtedness to these friends for their encouragement to complete this work.

There can be no adequate acknowledgement for the loving encouragement I have received from my parents, brothers and sisters and all family members. Without their constant support and inspirations all this would never have been possible.

This work was supported by Defense Advanced Research Projects Agency (DARPA) through ARO under Grant No. DAAD 19-03-1-0038.

August 5, 2005

# ABSTRACT

## SYNTHESIS AND CHARACTERIZATION OF MAGNETIC NANOPARTICLES

Publication No. _____

Narayan Poudyal, M.S.

The University of Texas at Arlington, 2005

Supervising Professor: J. Ping Liu

Synthesis of uniform nanoparticles (<100 nm) of hard and soft magnetic materials have attracted much attention in the last two decades because of their unique magnetic properties and potential for many applications such as high density recording media, biotechnology, ferrofluids, and fabrication of exchange-coupled nanocomposite permanent magnets. In this thesis, synthesis and characterization of hard (FePt) and soft ($Fe_3O_4$ and $CoFe_2O_4$) magnetic nanoparticles with different sizes are reported. Monodisperse FePt, $Fe_3O_4$ and $CoFe_2O_4$ nanoparticles were synthesized by chemical solution methods. Particle diameter was tuned from 3 to 20 nm by varying reaction

conditions or by seed-mediated growth method. Monodisperse face-centered tetragonal (fct) FePt nanoparticles were prepared by annealing at 700$^{o}$C the disodered face-centered cubic (fcc) FePt nanopaticles in NaCl matrix to convert the fcc particles into ordered fct structure. Morphological, structural, and compositional characterizations of the nanoparticles were performed by Transmission Electron Microscopy (TEM), High resolution TEM (HRTEM), Laser Particle-Size Analyzer, X-ray Diffractometer (XRD), Energy Dispersive X-ray (EDX), and Inductively Coupled Plasma (ICP). Magnetic properties of nanoparticles of different sizes at different temperatures were studied by Anternating Gradiant Magnetometer (AGM), and Superconducting Quantum Interference Device (SQUID) magnetometer. It has been found that all the as-synthesized $Fe_3O_4$ nanoparticles up to 20 nm are superparamagnetic at room temperatue while $CoFe_2O_4$ nanoparticles larger than 12 nm are ferromagnetic. An exchange bias field up to 3 kOe was observed for 3 nm $CoFe_2O_4$ nanoparticles in field cooling measurements. Very high coercivity of the isolated fct FePt nanoparticles up to 30 kOe at room temperature has been obtained. Interesting experimental results on the size dependent magnetic properties for both the hard and soft magnetic nanoparticles at different temperatures have been found.

TABLE OF CONTENTS

LIST OF ILLUSTRATIONS

# CHAPTER 1

# FUNDAMENTAL OF MAGNETISM AND MAGNETIC MATERIALS

## 1.1 Introduction

Magnetism is a phenomenon by which materials exert an attractive or repulsive force on other materials. All materials are influenced to one degree or another by the presence of a magnetic field, although in most cases the influence is too small to be detected if without any special equipment. Magnetic field is seen whenever electrically charged particles are in motion. This can arise either from the movement of electrons in an electric field, resulting in "electromagnetism", or from the constant subatomic movement of electrons, resulting in what is known as "permanent magnetism" [1-2].

## 1.2 Atomic Origins of Magnetism

From the atomic view of matter, there are two kinds of electronic motion: the orbital motion, and the spin motion. Except some nucleic magnetic effects, which are much smaller, these two types of electronic motions are the sources of the macroscopic magnetic phenomena in materials. Each electron may also be thought of as spinning around an axis of itself, which brings about spin moment. Another magnetic moment originates from this electronic spin, which is directed along the orbit around the nucleus

of the atom as shown in Figure 1.1. The net magnetic moment of an atom is just the sum of the magnetic moments of each of the constituent electrons, including both orbital and spin contributions. Moment cancellations due to opposite direction of electrons moment paired are also needed to be taken into account [1-5]. Materials composed of atoms having completely filled electron shells are not capable of being permanently magnetized.

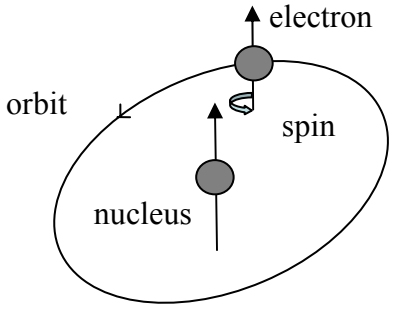


Figure 1.1 The orbit of a spinning electron about the nucleus of an atom

The types of magnetism include diamagnetism, paramagnetism, and ferromagnetism; in addition, antiferromagnetism and ferrimagnetism are considered to be subclasses of ferromagnetism [3]. These will be discussed in section 1.4. All materials exhibit at least one of these types of magnetism, and the behavior depends on the response of electron and atomic magnetic dipoles to the application of an externally applied magnetic field.

## 1.3 Magnetic Fields and Variables

The magnetic field strength (or intensity) is usually represented by *H*. The magnetic moment per unit volume of a magnetic material is measured by *M,* the magnetization (or polarization). *M* results from two atomic motions: orbital and spin motions of electrons as mentioned above. Magnetic induction, *B* is defined as [2, 3]

$$B = H + 4\pi M \qquad \text{[CGS]} \tag{1.1}$$

The nature of *H, M* and *B* is fundamentally all the same, as implied by equation (1.1). The units of these three parameters are also similar, and depend on the system of units being used. There are currently three systems of units that are widely used, including CGS or Gaussian system and SI system (See Appendix A).

Magnetic Susceptibility and Permeability: -The magnetic properties of a material are characterized not only by the magnitude of *M* but also by the way in which *M* varies with *H*. The ratio of these two quantities is called susceptibility [2]

$$k = \frac{M}{H}. \tag{1.2}$$

This susceptibility is unitless, as seen by the equation (1.2).

A quantity closely related to the susceptibility is the permeability μ which is defined by

$$\mu = \frac{B}{H}. \tag{1.3}$$

The physical meaning of equation (1.4), especially if it is written as $B = \mu H$, is that a current generated magnetic field $H$, when applied to a material of large permeability is enhanced by the factor of $\mu$ to create a large field $B$.

From equations (1.1), (1.2), and (1.3), it is obtained that

$$\mu = 1 + 4\pi k. \tag{1.4}$$

## 1.4 Types of Magnetism in Materials

The origin of magnetism lies in the orbital and spin motions of electrons. Electron interactions have also strong effect of magnetism. In some materials there is no collective interaction of atomic magnetic moments, whereas in other materials there are very strong interactions among atomic moments. The way to classify the different types of magnetism depends on how materials respond to magnetic fields. The magnetic behavior of materials can be classified into diamagnetism, paramagnetism and ferromagnetism in which anitferromagnetism and ferrimagnetism are considered to be it's subclasses [3].

### *1.4.1 Diamagnetism*

Diamagnetism is a fundamental property of all matter, although it is usually very weak. It is due to the non-cooperative behavior of orbiting electrons when exposed to an applied magnetic field. Diamagnetic substances are composed of atoms which have no net magnetic moments (i.e., all the orbital are filled and there are no unpaired electrons).

However, when exposed to a field $H$, the orbiting electrons either accelerate or decelerate, so that their magnetic moments are in the opposite direction from the external field. Once the external field is removed, the diamagnetic material losses its magnetization, and a negative magnetization is produced, and thus, the susceptibility $\chi_m$ is < 0 (order of $-10^{-5}$) for a diamagnetic material, resulting in very low moments [1-6].

*1.4.2 Paramagnetism*

For this class of materials, some of the atoms or ions in the material have a net magnetic moment due to unpaired electrons in partially filled orbitals. However, the individual magnetic moments do not interact magnetically, and like diamagnetism, the net magnetization is zero when the field is removed. In the presence of a field, there is a partial alignment of the atomic magnetic moments in the direction of the field, resulting in a net positive magnetization and susceptibility $\chi_m$ is > 0 (order of $10^{-5}$ to $10^{-2}$) for paramagnetic materials [1-3]. In addition, the efficiency of the field in aligning the moments is opposed by randomizing effects of temperature. This results in a temperature dependent susceptibility, known as the Curie Law.

*1.4.3 Ferromagnetism*

Ferromagnetic materials exhibit parallel alignment of permanent magnetic moments resulting in a large net magnetization even in the absence of a magnetic field. These moments originate from the overall contribution of electron spin and orbital magnetic moment [4]. The elements Fe, Ni, and Co and many of their alloys are typical

ferromagnetic materials. Magnetic susceptibilities as high as $10^6$ are possible for ferromagnetic materials. Two distinct characteristics of ferromagnetic materials are their spontaneous magnetization and the existence of magnetic ordering temperature. The spontaneous magnetization is the net magnetization that exists inside a uniformly magnetized microscopic volume in the absence of a field. As the temperature increases, the arrangement of atomic moments is disturbed by the thermal agitation, thus resulting in temperature dependence of spontaneous magnetization. In spite of the presence of spontaneous magnetization, a block of ferromagnetic or ferromagnetic substance is usually not spontaneously magnetized but exits rather demagnetized state. This is because the interior of the block is divided into many magnetic domains, each of which is spontaneously magnetized. Since the direction of domain magnetization varies from domain to domain, the resultant magnetization can be changed from zero to the value of spontaneous magnetization [1]. The saturation magnetization ($H_{sat}$) is the maximum induced magnetic moment that can be obtained in a magnetic field beyond this field no further increase in magnetization occurs. Saturation magnetization is an intrinsic property, independent of particle size but dependent on temperature.

*1.4.4 Antiferromagnetism*

In some other types of materials, the magnetic moment coupling between adjacent atoms or ions results in antiparallel alignment of the magnetic dipoles. This phenomenon of the alignment of spin moments of neighboring atoms or ions in exactly opposite directions is termed antiferromagnetism. The opposing magnetic moments

cancel one another resulting in zero net magnetization of the material [2, 4]. For example in manganese oxide (MnO), the A and B sub-lattice moments are exactly equal but opposite, and thus the net moment is zero.

*1.4.5 Ferrimagnetism*

Ferrimagnetism is another type of magnetic ordering. In ferrimagnets, the moments of adjacent atoms or ions are in an antiparallel alignment, but they do not cancel each other. The best example of a ferromagnetic mineral is magnetite ($Fe_3O_4$) in which two iron ions are trivalent while another is divalent. The two trivalent ions align with opposite moments and cancel one another, so the net moment arises from the divalent. The structural formula for magnetite is $[Fe^{3+}]A[Fe^{3+},Fe^{2+}]BO_4$. This particular arrangement of cations on A and B sublattice is called an inverse spinel structure. With negative AB exchange interactions, the net magnetic moment of magnetite is due to the B-site $Fe^{2+}$. Ferrimagnetism is therefore similar to ferromagnetism. It exhibits all the hallmarks of ferromagnetic behavior- spontaneous magnetization, Curie temperatures, hysteresis, and remanence. However, ferro and ferrimagnets have very different magnetic ordering.

## 1.5 Important Concepts about Ferromagnetism [1-5]

Curie Temperature- Even though electronic exchange forces in ferromagnets are very large, thermal energy eventually overcomes the exchange interaction and produces a randomizing effect. This occurs at a particular temperature called the Curie

temperature ($T_c$). Below the Curie temperature, the ferromagnet is ordered and above it, disordered. The saturation magnetization goes to zero at the Curie temperature. The Curie temperature is an intrinsic property of material and is a diagnostic parameter that can be used for mineral identification. However, it is not full proof because different magnetic minerals, in principle, can have the same Curie temperature.

Magnetic Domains-Any ferromagnetic material at a temperature below Curie temperature $T_c$ is composed of small-volume regions known as domains, in which there is mutual alignment of the magnetic moments in the same direction, as illustrated in Fig. 1.2(A). Each domain is magnetized to its saturation magnetization and adjacent domains are separated by domain walls, across which the direction of magnetization gradually changes (See Fig. 1.2(B)).

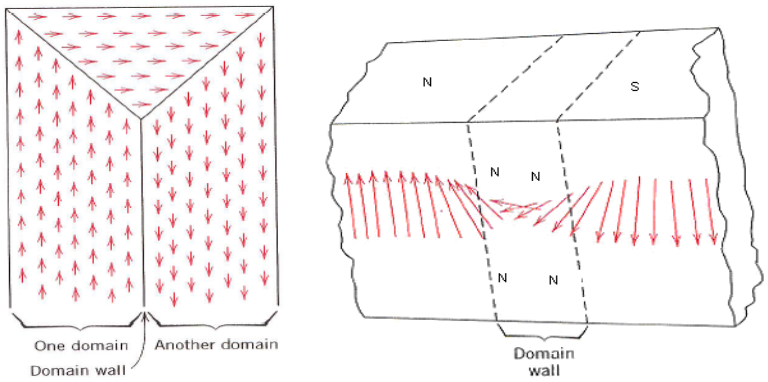


(A) (B)

Figure 1.2 (A) Creation of domain and domain wall and (B) spin orientation rotation through domain (Bloch) wall [4]

Hysteresis- Ferromagnet can retain a memory of an applied field even after the field is removed. This behavior is called hysteresis and a plot of the variation of magnetization with magnetic field is called a hysteresis loop. The hysteresis loop is a means of characterizing magnetic materials, and various parameters can be determined from it.

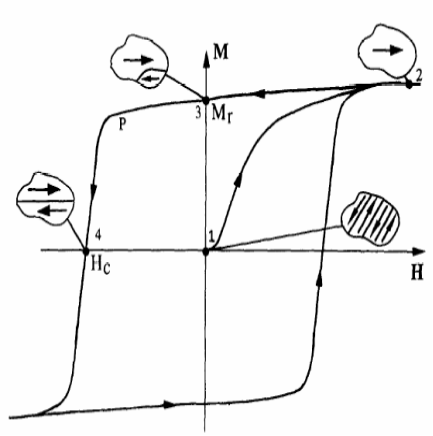


Figure 1.3 The magnetization curve and hysteresis loop of a permanent magnet showing the magnetic domain structure in the virgin state (1), at saturation (2), at remanence (3), and at the coercive field (4)[9].

Initially, the moments of the constituent domains are randomly oriented such a way that there is no net *B (or M)* field. As shown in figure 1.3, on the application of a field to an unmagnetized sample the polarization increases initially by the growth of favorably oriented domains, which will be magnetized in the easy direction of the crystal. When the polarization can increase no further by the growth of domains, the direction of magnetization of the domains then rotates away from the easy axis to align with the field. When all of the domains have fully aligned with the applied field saturation is reached and the polarization can increase no further. The maximum value

of $M$ is called the saturation magnetization $M_s$ and the resultant $M$-$H$ curve is called the initial magnetization curve. Starting from the saturation point (see figure 1.3), when the $H$ field is reduced, the curve does not retrace its original path. A hysteresis effect is produced in which the $M$ field lags behind the applied $H$ field, or decrease at a lower rate. At zero $H$ field, a residual $M$ that is called the remanence or remanent magnetization $M_r$ is retained, indicating that the material remains magnetized even in the absence of an external $H$ field. The polarization will only decrease after a sufficiently high field is applied to: (1) nucleate and grow domains favorably oriented with respect to the applied field or (2) rotate the direction of magnetization of the domains towards the applied field. After applying a high enough reversal field, saturation polarization will be achieved in the negative direction. If the applied field is then decreased and again applied in the positive direction then the full hysteresis loop is plotted (figure 1.3). The area contained within the loop indicates the amount of energy absorbed by the material during each cycle of the hysteresis loop. The reverse field required to bring the magnetic induction B of specimen to zero is called the inductive coercivity, $H_b$, whereas the reverse field required to bring the magnetization M to zero is called the intrinsic coercivity, $H_c$. The remanence ratio $M_r/M_s$ is generally used as measure of squareness of the $M$-$H$ loop.

Maximum Energy Product $(BH)_{max}$- In $B$-$H$ loop, the maximum value of the product of $B$ and $H$ is called the maximum energy product, $(BH)_{max}$ and is a measure of the maximum amount of useful work that can be performed by the magnet. $(BH)_{max}$ is used as a figure of merit for permanent magnet materials as shown in figure 1.4. It's

units are KJ/m$^3$ (MGOe). For a permanent magnetic material the $(BH)_{max}$ is twice the maximum magnetostatic energy available from a magnet of optimal shape. The product tends to increase with increasing both coercive field $H_c$ and saturation magnetization $M_s$. However, for materials with sufficiently high $H_c$ values ($H_c > 2\pi M_s$) the theoretical limit for the energy product is limited only by $M_s$ and is given by [16]

$$(BH)_{max} \leq (2\pi M_s)^2 \tag{1.6}$$

The highest value of $(BH)_{max}$ of a material requires an ideal rectangular hysteresis loop.

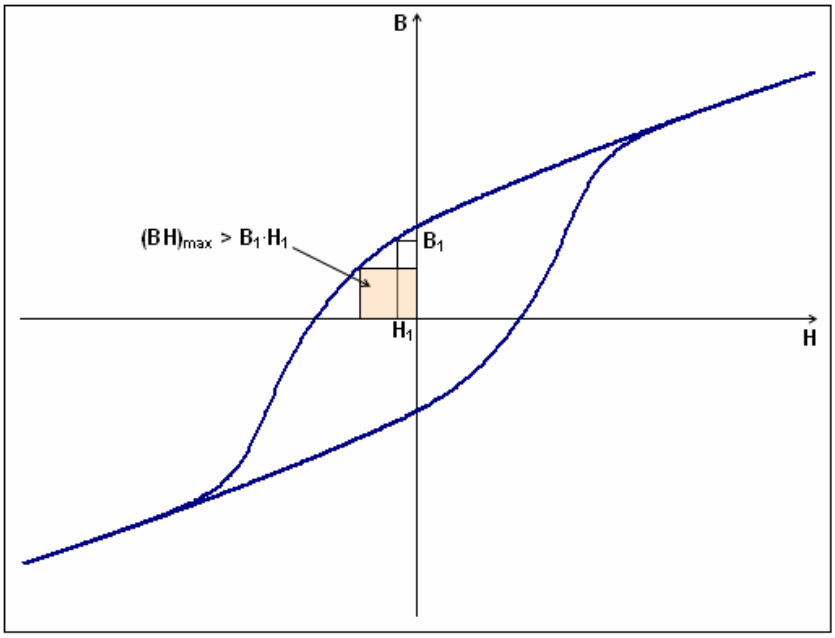


Figure 1.4 A typical hysteresis loop $B$ vs $H$ for ferromagnetic material

## 1.6 Magnetic Anisotropy

In many situations the susceptibility of a material will depend on the direction in which it is measured. Such a situation is called magnetic anisotropy. When magnetic anisotropy exits, the total magnetization of a ferromagnetic $M_s$ will prefer to lie along a special direction called the easy axis or crystal axis. In case of HCP (hexagonal close packed) or tetragonal crystal the easy axis is usually the c-axis. Under an applied field, the magnetic moment derivates from the easy direction and returns to its original alignment with the removal of the field. The energy associated with this alignment is called the anisotropy energy and in its lowest order form is given by

$$E_a = K\sin^2 \theta \tag{1.7}$$

Where θ is the angle between $M_s$ and the easy axis and $K$ is the anisotropy constant (units is ergs/cm$^3$). There are several causes from which anisotropy may occur, including those induced by stress and prior mechanical handling of materials. Two important and common sources of anisotropy, which are magneto crystalline anisotropy and shape anisotropy, will be discussed below.

### *1.6.1 Magnetocrystalline Anisotropy*

Only magnetocrystalline anisotropy, or simply crystal anisotropy, is intrinsic to the material; all other anisotropies are induced. In crystal anisotropy, the ease of obtaining saturation magnetization is different for different crystallographic directions.

The direction of easy magnetization of crystal is the direction of spontaneous domain magnetization in the demagnetized state. An example is a single crystal of iron (see Figure 1.5) for which $M_s$ is most easily obtained in the [100] direction, then less easy for the [110] direction, and most difficult for the [111] directions. The [100] direction is called the easy direction, or easy axis, and because the other two directions have an overall smaller susceptibility.

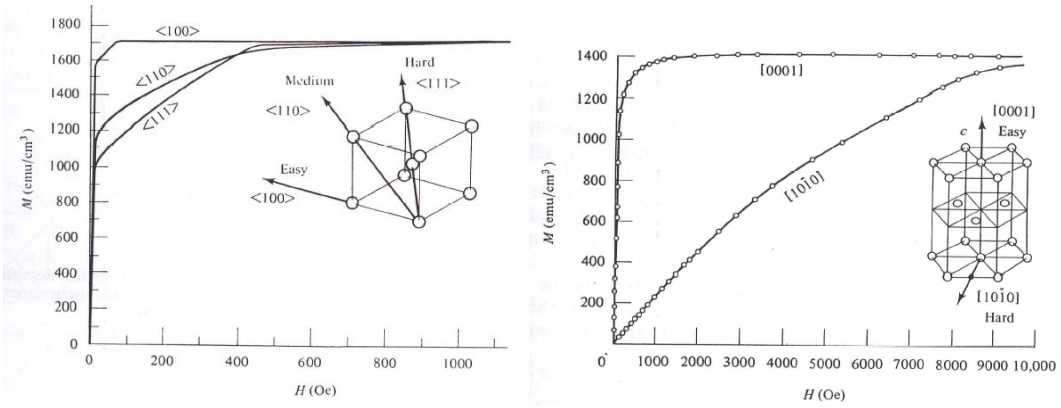


(A) (B)

Figure1.5 Magnetization curves for single crystal of (A) iron, and (B) cobalt [2]

*1.6.2 Shape Anisotropy*

It is easier to induce a magnetization along a long direction of non-spherical piece of material than along a short direction. This is so because the demagnetizing field is less in the long direction, for the reason that the induced poles at the surface are further apart. Thus a smaller applied field will negate the internal, demagnetizing field. The shape anisotropy can be very important for non-spherical materials. The long axis

of specimen plays the same role as the easy axis of the crystal, and the shape anisotropy constant $K_s$ is given by

$$K_s = \tfrac{1}{2}(N_a - N_c)M^2 \qquad (1.8)$$

Magnetization is easy along the c axis and equally hard along any axis normal to *c*. If *c* decreases until it equals *a*, the specimen becomes spherical, $N_a = N_c$, $K_s = 0$, and shape anisotropy disappears.

## 1.7 Coercivity Mechanism

There are various methods of increasing or decreasing the coercivity of magnetic materials, all of which involve the controlling the magnetic domains within the material. For a hard magnetic material it is desirable that the domains cannot easily rotate its direction of magnetization and that the domain walls do not move easily and / or nucleation of reversal domains is difficult. To prevent easy rotation of domains the material could have strong uniaxial magnetocrystalline anisotropy. Alternatively, shape anisotropy can occur in needle-like particles or grains leading to magnetic hardening. In case of shape anisotropy, the magnetostatic energy is less when the magnetization is in the long axis of the needle compared to the short axis. If the size of a magnetic particle or grain decreases, there is a critical size below which the decrease in magnetostatic energy by splitting into two domains is less than the increase in energy due to the introduction of the domain wall. Particles that are below this critical size are known as “single domain particles.” If they have sufficiently high anisotropy to prevent

the easy rotation of the direction of magnetization, the particles will be permanently magnetic and difficult to be demagnetized. Permanent magnets can also achieve their resistance to demagnetization by pinning of the domain walls and by making the new domain nucleation difficult. Nucleation controlled permanent magnets are easily magnetized as the initial state has several domains in each crystal, but are difficult to be demagnetized because this would require the nucleation of new reversal domains.

## 1.8 Classification of Ferromagnetic Materials for Applications [1-5]

Magnetic materials are broadly classified into two main groups, either soft or hard, on the basis of their hysteresis characteristics.

### *1.8.1 Soft Magnetic Materials and Their Applications*

Soft magnetic materials can be easily magnetized and demagnetized by low-strength magnetic field. When applied field is removed, soft magnetic materials will return to a state of relatively low residual magnetization. They are used primarily to enhance or channel the flux produced by an electric current. The main parameter, often used as a figure of merit for soft magnetic materials, is the relative permeability, which is a measure of how readily the material responds to the applied magnetic field. The other main parameters of interest are the coercivity, the saturation magnetization and the electrical conductivity. As shown in Figure 1.6, typical soft materials have intrinsic coercivity less than 100 Oe, high saturation magnetization $M_s$ but low $M_r$. The types of applications for soft magnetic materials fall into two main categories: DC and AC. In

DC applications, the material is magnetized in order to perform an operation and then demagnetized on completion of the operation, e.g. an electromagnet on a crane at a scrap yard will be switched on to attract the scrap steel and then switched off to drop the steel. In AC applications, the material will be continuously cycled from being magnetized in one direction to the other, throughout the period of operation, e.g. a power supply transformer.

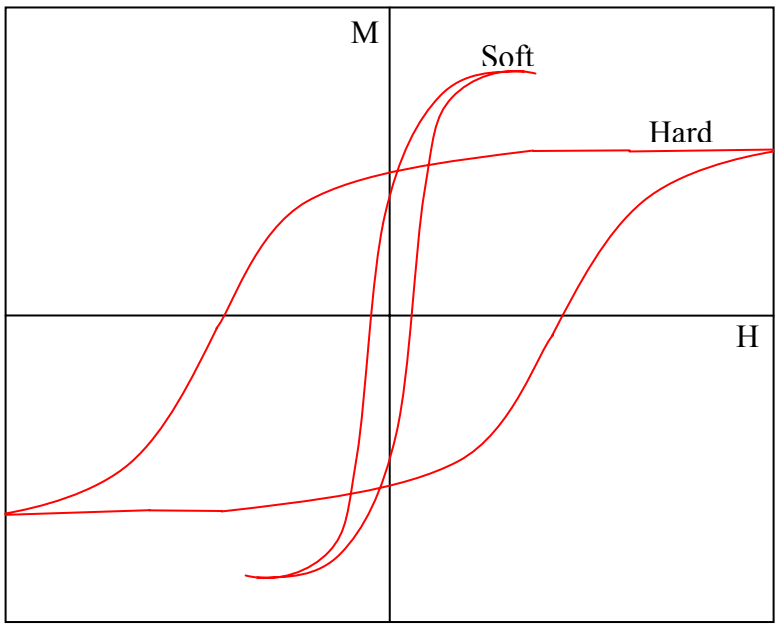


Figure 1.6 *M-H* curves for soft and hard magnets

*1.8.2 Hard Magnetic Materials and Their Applications*

Hard magnets, also referred to as permanent magnets, are magnetic materials that can retain their magnetism after being magnetized. The term hard is used to describe materials that have sufficiently high resistance to demagnetizing field.

Coercivity is, therefore, the key to distinguish between hard and soft phase magnetic materials. As shown in figure 1.6 materials that have an intrinsic coercivity of greater than 1000 Oe, typically high remanece $M_r$ are hard magnetic materials. Such material have high energy product $(BH)_{max}$, which is the figure of merit of hard magnet. Hard magnets are indispensable in modern life and their role in today's technology is growing increasingly. Some of the applications for permanent magnetic materials are given below [55].

Automotive: Starter motors, anti-lock braking systems (abs), motor drives for wipers, injection pumps, fans and controls for windows, seats etc, loudspeakers, eddy current brakes, alternators.

Telecommunications: Loudspeakers, microphones, telephone ringers, electro-acoustic pick-ups, switches and relays.

Data Processing*:* Disc drives and actuators, stepping motors, printers.

Consumer Electronics: DC motors for showers, washing machines, drills, low voltage dc drives for cordless appliances, loudspeakers for TV and audio, TV beam correction and focusing device, compact-disc drives, home computers, video recorders, clocks.

Electronic and Instrumentation: Sensors, contactless switches, NMR spectrometer, energy meter disc, electro-mechanical transducers, crossed field tubes, flux-transfer trip device, dampers.

Industrial: DC motors for magnetic tools, robotics, magnetic separators for extracting metals and ores, magnetic bearings, servo-motor drives, lifting apparatus, brakes and clutches, meters and measuring equipment.

Astro and Aerospace: Frictionless bearings, stepping motors, couplings, instrumentation, travelling wave tubes, auto-compass.

Biosurgical: Dentures, orthodontics, orthopedics, wound closures, stomach seals, repulsion collars, ferromagnetic probes, cancer cell separators, magnetomotive artificial hearts, NMR / MRI body scanner.

Several different types of permanent magnetic materials are now available including a variety of alloys, intermetallics, and ceramics. The most widely studied permanent magnetic materials are: Cobalt-rare earth alloys ($SmCo_5$, or $Sm_2Co_{17}$), and neodymium-iron-boron ($Nd_2Fe_{14}B$), iron-platinum (FePt), cobalt-platinum (CoPt), hard ferrites ($SrO\text{-}Fe_2O_3$ or $BaO\text{-}6Fe_2O_3$), and Alnicos.

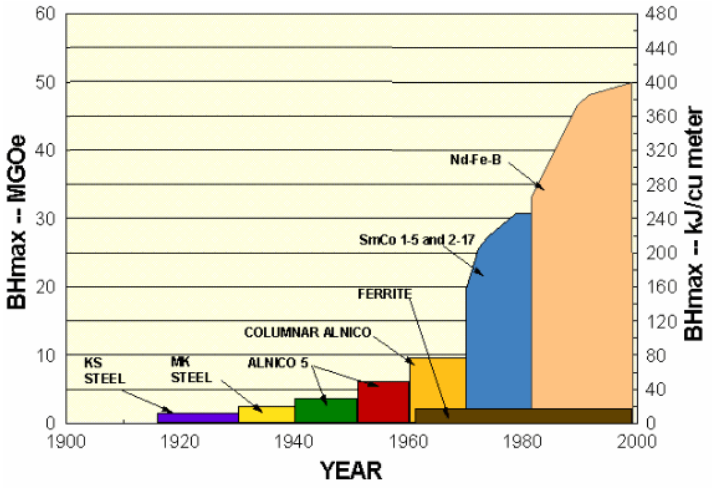


Figure 1.7 Progress in the energy product of permanent magnets in the 20th century

The 20th century has witnessed quite an extraordinary development in hard magnetic materials, where the coercivity and the maximum energy product have been

significant enhanced in rare-earth-transition-metal permanent magnets. Figure 1.7 shows the development of energy products of these materials.

Driven by the limitation as in equation (1.6) [$(BH)_{max} \leq (2\pi M_s)^2$ ], research has focused on developing new high-anisotropy materials with high $M_s$ and Curie temperature $T_c$. Thus, new hard-magnet compounds such as $SmCo_5$, $Sm_2Co_{17}$ and $Nd_2Fe_{14}B$ are made increasing transition metal (TM) rich to enhance $M_s$. Unfortunately, these compounds still have magnetization values significantly lower than that of Co, Fe or $Fe_{65}Co_{35}$, which have $4\pi M_s$ values of 18, 21, and 24 kG, respectively [16]. In 1991 Kneller and Hawig [10] proposed an alternative approach to enhance the TM content to increase $M_s$ by making a nanocomposite of exchange-coupled hard and soft magnetic phases. Such magnets are referred to as "exchange-spring" magnets and provide new approach to increased $(BH)_{max}$. The hard phase provides the requisite magnetic anisotropy and stabilizes the exchange-coupled soft phase against demagnetization and the soft phase provides the high magnetization as shown in Figure 1.8.

First exchange-coupled nanocomposite was observed by Coehoorn et al. [56] in a melt-spun $Nd_{4.5}Fe_{77}B_{18.5}$ sample that, when annealed, consisted of a mixture of $Nd_2Fe_{14}B$, $Fe_3B$ and Fe phases. Skomski and Coey explored the theory of exchange coupled films and predicted that a giant energy product of 120 MGOe might be attainable by exploiting the exchange-spring mechanism in oriented nanostructured magnets [11, 17].

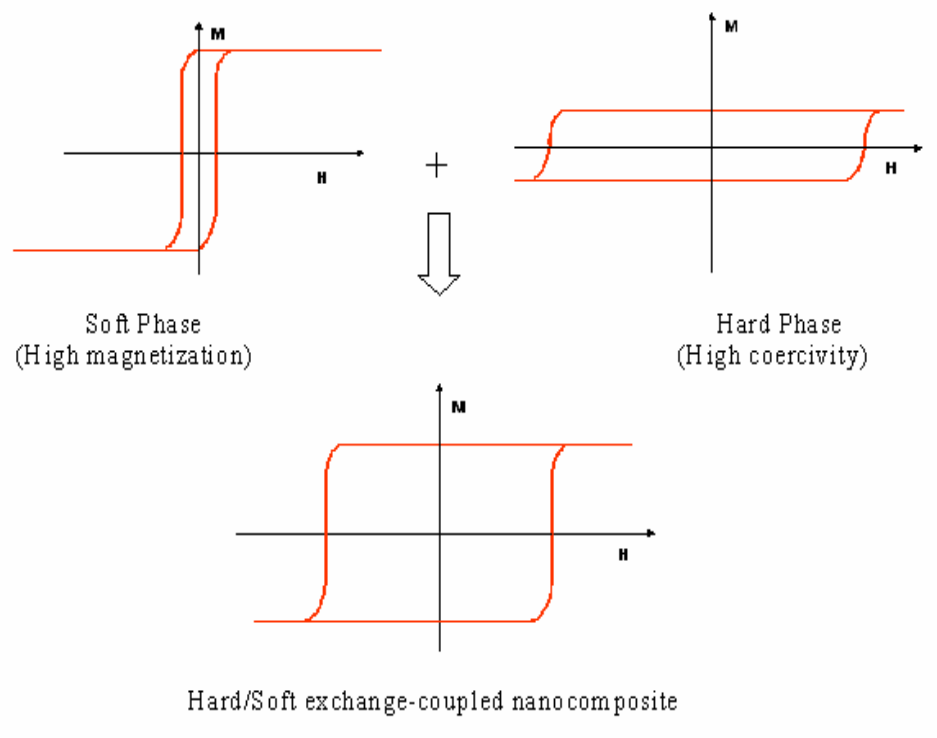


Figure 1.8 Hysteresis loops of soft, hard, and nanocomposite magnets

They also predicated that for effective exchange coupling the grain size of soft phase should not be larger than twice the domain-wall thickness of hard phase. Future applications of exchange-spring magnets will likely be based on a nanodispersed composite geometry obtained in bulk processing [7].

## 1.9 Small Particle Magnetism

Magnetic properties of small ferromagnetic particles such as coercivity are dominated by two key features: (1) a size limit below which the specimen cannot be broken into domains, hence it remains with single domain; (2) the thermal energy in small particles which decouples the magnetization from the particle itself to give rise to the phenomenon of superparamagnetism. These two key features are represented by two key sizes (on length scale): the single domain size and superparamagnetic size [2, 19].

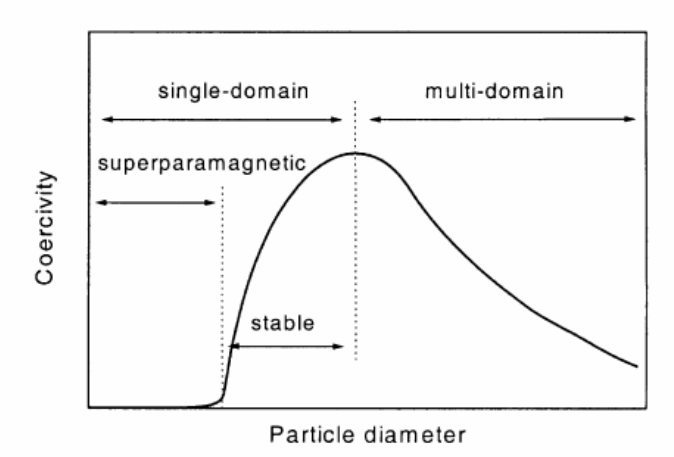


Figure 1.9 Variation of coercivity with particles diameter

### *1.9.1 Single-Domain Particles*

The magnetostatic energy of a ferromagnet could be decreased by restructuring the material into domains. There is a limit to this because formation of domains costs energy due to domain wall formation. Thus in a large body there could be minimum domain size below which the energy cost of domain formation exceeds the benefits

from decreasing the magnetostatic energy. When the size of the particles decreases down to a critical particle diameter, the formation of domain walls is energetically less favorable and the particles have only a single domain. Magnetization reversal in single-domain particles occur via spin rotaion since there are no domian walls to move. Because of this, single-domain particles have a larger coercivity campared to multidomain system as it is harder to rotate the magnetization than to move a domain wall [2,19].

*1.9.2 Superparamagnetism*

Superparamagnetism is a phenomenon by which magnetic materials may behave similar to paramagnetism at temperatures below the Curie or the Neel temperature. It occurs when the materiasl are composed of very small crystallites (usually below10 nm). In this case, even though the temperature is below the Curie or Neel temperatures, the thermal energy is sufficient to overcome the coupling forces between neighboring atoms, leading to change in the direction of magnetization of the entire crystallite. The resulting fluctuations in the direction of magnetization cause the magnetic field to average to zero. The material behaves in a manner similar to paramagnetism, except that instead of each individual atom being independently influenced by an external magnetic field, the magnetic moment of the entire crystallite tends to align with the magnetic field. The energy required to change the direction of magnetization of a crystallite is called the crystalline anisotropy energy ($KV$) and depends both on the material properties and the crystallite size. As the crystallite size decreases, so does the

crystalline anisotropy energy, resulting in a decrease in the temperature at which the material becomes superparamagnetic [2,19]. The phenomenon of superparamagnetism is timescale-dependent due to the stochastic (random variable) nature of the thermal energy. The time scale for successful jump can be calculated by

$$\tau = \tau_o \, e^{-KV/kT} \tag{1.8}$$

Where attampt timescale ($\tau_o$) is about $10^{-9}$s and V is the volume of particle. This equation (1.8) describes the time scale over which the moment of particles ($\mu_p = M_s V$) attampts to jump the anisotropy energy ($KV$) barrier. Typical experiment with a magnetometer take 10 to 100 s; if $M_s$ reverse at times shorter than the experimental time scale, the system appears superparamagnetic. Using $\tau$ = 100 s and $\tau_o = 10^{-9}$ s , we can obtain the critical volume from equation (1.8)

$$V_{sp} = \frac{25kT}{K} \, . \tag{1.9}$$

A particle with volume smaller than this acts superparamagnetically on the 100 s experimental timescale . Equation (1.9) can be rearranged to yield

$$T_B = \frac{KV}{25k}. \tag{1.10}$$

$T_B$ is called the blocking temperature; below $T_B$ the free movement of moment of particles ($\mu_p = M_s V$) is blocked by the anisotropy; above $T_B$, $kT$ kicks the moment loose so that the system appears superparamagnetic.

# CHAPTER 2

# LITERATURE REVIEW

## 2.1 Magnetic Nanoparticles and Their Applications

Nanoparticles are typically defined as solid less than 100 nm in all three dimensions. The development of uniform nanometer-sized particles has been intensively pursued in the last two decades by the fact that small size and high surface to volume ratio of nanoparticles give unique mechanical, optical, electronic, magnetic and chemical properties [12, 26, 33]. Magnetic nanoparticles are of special interest owing to their unique magnetic properties due to their reduced size (< 100 nm). Magnetic nanoparticles have potential use in many technological applications [22].

## 2.2 Applications of Magnetic Nanoparticles

Depending on type of applications, magnetic nanoparticles are used in varieties of forms such as surface functionalized particles in biomedical applications, as particles arrays in magnetic storage media, as compacted powders in permanent magnets and in solutions as ferrofluids [21-34].

*2.2.1 Biomedical Applications*

Magnetic nanoparticles have been proposed for biomedical applications for several years [21, 73]. In recent years, nanotechnology has developed to a stage that makes it possible to produce, characterize and specifically tailor the functional properties of nanoparticles for applications. This shows considerable promise for applications in biomedical and diagnostic fields such as targeted drug delivery, hyperthermic treatment for malignant cell, and magnetic resonance imaging (MRI) [21-24, 26, 73]. There are three reasons why the magnetic nanoparticles are useful in biomedical applications. First, magnetic nanoparticles can have controllable size ranging from a few nanometers up to tens of nanometers, and are smaller than comparable in sizes to a cell ( 10-100μm ), a virus (20-450 nm), a protein (5 -50 nm) or a gene ( 2nm wide and 10 -100 nm long). They can get close to the cell or gene and they can be coated with biomoleclues to make them interact or bind with biological entity. Second, magnetic nanoparticles can be manipulated by an external magnetic field gradient. They can be used to deliver a package, such as an anticancer drug to a targeted region of the body such as a tumor. Third, magnetic nanoparticles can also be made to resonantly respond to a time-varying magnetic field, with an associated transfer of energy from the field to the nanoparticles. They can be made to heat up, which leads to their use as hyperthermia agents, delivering toxic amounts of thermal energy to targeted bodies such as tumors or as chemotherapy [21-24, 73]. As highlighted above for biomedical application, magnetic nanoparticles must (i) have a good thermal stability; (ii) have a larger magnetic moment; (iii) be biocompatible; (iv) be able to form stable dispersion so the particles

could be transported in living system; (v) response well to AC magnetic fields. Furthermore, better control of particle size and properties will be necessary to use these particles in biomedical application, in which uniformity of the properties will ensure accurate dosing and delivery [73]. The widely used magnetic nanoparticles for biomedical applications are magnetite ($Fe_3O_4$) and related oxides which are chemically stable, nontoxic, non-carcinogenic and have attractive magnetic properties [27].

### *2.2.2 Magnetic Recording Media*

Synthesis and assembly of magnetic nanoparticles have attracted great attention because of their potential application in ultrahigh-density magnetic recording [28]. Continue increase in the areal density of hard disk drive will be limited by thin film media in which each bit of information is stored over hundreds of grains. Self-assembled nanoparticle media and patterned media, in which data are stored in an array of single-domain magnetic particle have been suggested as means to overcome this limitation and to enable recording density up to 1 Tbit $inch^{-2}$ [29]. In such ultrahigh-density media, because of high recording density, a small material grain and narrow size distribution are required. To obtain both high signal-to-noise and thermal stability of the media, isolated, noninteracting or very weekly interacting nanoparticles with very high magnetic anisotropy energy $K_u$ are required [30]. Extensive researches are being done on $CoFe_2O_4$ and FePt nanoparticles for high density recording media [30, 32]. $CoFe_2O_4$ nanoparticles are well-known material with very high cubic magnetocrystalline anisotropy, good coercivity, and moderate saturation magnetization [32-34]. These

properties make $CoFe_2O_4$ nanoparticles a promising material for high-density magnetic recording devices. FePt $L1_0$ nanoparticles are one of the best candidates for ultrahigh density recording media with very high magnetocrystalline anisotropy ($K_u$ is $10^8$erg/cm$^3$), which is much higher than those of the currently used CoCr-based alloys [30]. This large crystalline anisotropy allows for thermally stable grain diameters down to 2.8 nm [57]. However, the as-synthesized FePt nanoparticles are superparamagnetic and have the face-centered cubic (fcc) structure. These particles have to be annealed at temperature as high as 580$^o$ C to transform into face-centered tetragonal (fct) structure and retain magnetic orientation to be useful for recording. The post-annealing leads to poor control over arrangement of nanoparticles through extensive particle aggregation which also makes magnetic easy axes alignment difficult, limiting their technological applications [28, 80]. Recently, Liu et al. [58] have made a break though by successfully preparing monodisperse FePt fct nanoparticles with high coercivity, which make it possible the direct application of fully converted fct FePt nanoparticles in high density magnetic media.

### *2.2.3 Exchange-Coupled Nanocomposite Magnets*

Exchange-coupled nanocomposite magnet consists of a uniform mixture of exchange coupled magnetically hard and soft phases [12, 16, 18]. This type of magnets are promising for advanced permanent magnetic applications as high energy products $(BH)_{max}$ and relatively high coercivities can be developed in these nanocomposite magnets. A small grain size (less than 20 nm) and a uniform mixture of the hard and

soft phases are required for effective exchange coupling between the hard and the soft phases. Zeng *et al.* in 2002 demonstrated that exchange-coupled nanocomposite magnet such as FePt-$Fe_3Pt$ can be made using monodisperse nanoparticles of FePt and $Fe_3O_4$ as precursors by self assembly technique [12]. In exchange-coupled isotropic FePt-$Fe_3Pt$ nanocomposite the energy product of 20.1 MGOe was achieved, which is 50% higher than that expected theoretically from a single phase, non-exchange-coupled isotropic FePt.

Recently, the same group prepared an exchange-coupled bimagnetic core/shell nanoparticles system with ferromagnetic FePt core and ferrimagnetic $MFe_2O_4$ (M=Fe, Co) shell [52]. The advantage of this system is that the magnetic properties such as magnetization and coercivity can be controlled by tuning the core/shell dimensions, and by tuning the material parameters of both core and shell. This system shows the great promise for achieving the potential high energy products in exchange-coupled nanocomposite magnets. An anisotropic nanocomposite magnet with both the hard and soft phases aligned is expected to show much higher energy product than the isotropic one [11]. However, controlling morphology including grain size and grain alignment in nanocomposite magnet remains a great challenge [24].

### *2.2.4 Ferrofluids*

A ferrofluid is a special solution of magnetic nanoparticles in a colloidal suspension whose flow can be controlled by magnets or magnetic fields [68]. Particles are coated with a surfactant that disperse the particles and prevents agglomeration by

overcoming the van der Waals forces that exists between the particles [26]. As a result when fluid is not in presence of external magnetic field it has zero net magnetization. When a strong magnet is brought close to the ferrofluid, several spikes will appear, as the fluid arranges itself along the magnetic field lines of the magnet. When the field is removed, the particles again disperse randomizing their orientation and establishing no net magnetization [26, 36]. These unique properties make ferrofluids have applications in numerous fields of technology. The most common application of ferrofluids is the cooling of loudspeakers. The ohmic heat produced in the voice coil can be transmitted to the outer structure by the fluid which increases the cooling approximately by a factor 3. In sealing technology, a drop of ferrofluid is put into the gap between a magnet and a high permeable rotating shaft. In the small gap a strong magnetic field fixes the ferrofluid, and pressure differences about 1 bar can be sealed without serious difficulties [36]. Some of the other technological applications of ferrofluid include bearing, dampers, stepping motors, and sensors [26, 35, 37, 88].

### *2.2.5 Synthesis Techniques*

The preparation of discrete nanoparticles can be accomplished through "bottom-up" or "top-down" methods. In a bottom-up approach small building blocks such as atoms and clusters are assembled into nanoparticles; examples of this approach include chemical synthesis, laser-induced assembly, and colloidal aggregation [38-48, 49, 50]. In the top-down approach, large objects are broken down to finer particles such as mechanical milling [51, 66].

Various synthesis strategies for preparation of magnetic nanoparticles have been investigated which include chemical co-precipitation [33, 41], sonochemical reactions [48, 60], sol-gel [64, 65], microwave heating [61, 69], mechanochemical [32, 70], micelle microemulsion [40, 44-47, 63], hydrothermal [62, 40], and ball milling [51, 66]. Compared to other methods, chemical routes have often been found the better methods for the production of high quality nanoparticles.

### *2.2.6 Chemical Synthesis- Concepts and Mechanism [26, 32]*

The synthesis of nanoparticles in a solution occurs by chemical reactions forming stable nuclei with subsequent particle growth. Upon the addition of precipitating, reducing, or oxidizing reagents to the solution containing the reactants, chemical reactions occur and solution becomes supersaturated with products. The thermodynamics equilibrium state of the system is restored by condensation of nuclei of the reaction product. Kinetic factors compete with the thermodynamics of the system in a growth process. The kinetic factors such as reaction rates, transport rates of reactants, accommodation, removal, and redistribution of matter compete with influence of thermodynamics in particles growth. The particle morphology is influenced by factors such as supersaturation, nucleation and growth rate, colloidal stability, recrystalization and aging process. When the nuclei are formed nearly at the same time in a supersaturated solution, subsequent growth of these nuclei results in the formation of particles with a very narrow size distribution. To maintain a narrow size distribution, it

is very important to prevent agglomeration, Ostwald ripening, and continued nuclei formation.

Nanoparticles possess large surface areas and often form agglomerates as a result of attractive van der Waals forces and the tendency of the system to minimize the total surface or interfacial energy. Agglomeration of particles can occur during any of the following stages: synthesis, drying, handling, and processing. In many applications and processing where dispersed particles or stabilized dispersions are required, undesirable agglomeration in each synthesis and processing step must be prevented. Surfactant is any substance that lowers the surface or interfacial tension of the medium in which it is dissolved. Surfactants are used during nanoparticles synthesis in order to reduce interparticle interaction through an increase in repulsive forces. They are used to control particle size and distribution in most chemical synthesis routes.

### *2.2.7 Ferrite ($Fe_3O_4$ & $CoFe_2O_4$) Nanoparticles*

There is an increasing interest in magnetic ferrite nanoparticles in recent years because of their broad applications in several technological fields including permanent magnets, magnetic fluids, magnetic drug delivery, and high density recording media as mentioned earlier [12, 21-35, 52]. The cubic $MFe_2O_4$ or $MO.Fe_2O_3$ (M = Fe, Co), is a common magnetic ferrite that has a cubic inverse spinel structure with oxygen forming a fcc closed packing and $M^{+2}$ and $Fe^{+3}$ occupy either tetrahedral or octahedral sites. Magnetic configuration of $MFe_2O_4$ material can be engineered by adjusting the chemical identity of $M^{+2}$ to provide a wide range of magnetic properties [38, 67]. For

many applications synthesis of uniform-size nanoparticles is of key importance, because the magnetic properties depend strongly on their dimensions.

Recently, great efforts have been made by various groups to achieve a fine-tuning of the size of ferrite nanoparticles employing different synthesis techniques and varying the experimental parameters such as heating rate, and quantity of surfactants. Kim et al. prepared cobalt ferrite nanoparticles ranging from 2 to 14 nm by controlling co-precipitation temperature of $Co^{+2}$ and $Fe^{+2}$ ions in alkaline solution although the size distribution was pretty wide [33]. Chinnasamy et al. [34] employed a modified oxidation process to synthesize cobalt ferrite particles with diameters ranging from a few micrometers to about 15 nm. Rajendrain et al. demonstrated 6 to20 nm sized cobalt ferrites prepared in aqueous solution at room temperature by the oxidative co-precipitation of $Fe^{2+}$ and $Co^{2+}$ [41]. Morais et al. showed the size-controlled synthesis of the nanoparticles of 10 to15nm in aqueous solution at 95$^{o}$C by controlling stirring speed [42]. Moumen et al. used oil-in-water micelle to prepare size-controlled Co-ferrite in the range of 2 to5 nm [44]. Liu et al. [47] also reported the nanoparticles of 2 to 35 nm in diameter which were prepared in normal micelle using similar with the method of Moumen et al. Pillai et al. [46]. Very recently Sun et al. [38, 39] synthesized ferrite nanoparticles with sizes variable from 3 to 20 nm in diameter by combining nonhydrolytic reaction with seed-mediated growth method.

Ferrite nanoparticles have been synthesized by a wide variety of methods as mentioned above. Although these methods are able to produce nano-sized ferrite particles, the quality of the nanoparticles is often poor. In many cases, a large size

distribution is reported and size control is arbitrary. It is desirable to have nanoparticles of specific size and property for particular application. For example, magnetic nanoparticles must be superparamagnetic at room temperatures in order to avoid agglomeration to use as ferrofluids and in biomedical application such as MRI contrast agents [26]. However, the superparamagnetic state must be avoided in high-density information storage since the superparamagnetic relaxation of the data bits will cause the magnetic moment of each bit to fluctuate and as consequence all the stored information will be lost. Compared with other methods used for preparing ferrites nanoparticles, the chemical solution method [38, 39] has its unique advantages in producing small particles size (down to 3 nm) with very narrow size distribution, as well as good crystallinity and stability.

### *2.2.8 FePt Nanoparticles*

As mentioned above, FePt nanoparticles have attracted great interest because as the only type of hard magnetic nanoparticles they have potential applications in ultrahigh-density magnetic recording media [71], high performance permanent magnets [12] and sensors and drug carriers in biomedical technology [73]. Since Sun et al. reported their breakthrough in chemical synthesis of FePt nanoparticles [71], synthesis of monodisperse FePt nanoparticles with size ranging from 2 to 15 nm have been achieved successfully [71, 88- 90]. However, as-synthesized FePt nanoparticles are of fcc structure which do not provide the magnetocrystalline anisotropy required for the applications mentioned above. The fct FePt composition has very high

magnetocrystalline anisotropy. In order to transform the fcc structured nanoparticles to the fct structure, heat treatment at temperatures above 500$^{o}$C is necessary. Undesirably, coalescence and sintering of the nanoparticles also take place at these temperatures, which make of direct application of monodisperse hard magnetic nanoparticles impossible.

Extensive efforts have been made since 2000 to obtain monodisperse fct FePt particles. One of the approaches in such efforts is to lower the onset temperature for the fcc to fct phase transformation. Doping by elements such as Ag, Au and Cu in the FePt phase was tested resulting in the onset of the fct phase at 400°C [74-79]. Direct synthesis of the fct structured particles by the polyol process using high boiling point solvents is another major approach [80-83]. In this approach, higher synthesis temperatures can be applied which allows partial formation of the fct phase. Recently, fcc FePt nanoparticle arrays with coating were annealed at temperatures higher than 700$^{o}$C without sintering. Immiscible silica matrix [84], or polyethyleneimine linker molecules [85] were used as the coating materials. The coating approach, however, was only suitable for monolayers of the separated nanoparticles on substrates. Other approaches to obtaining monodisperse fct nanoparticles include rapid thermal annealing [86] and pulse laser annealing [87]. To date, all the reported approaches have been only successful in obtaining partially transformed fct nanoparticles and high coercivities have not been developed from the partially transformed particles. It is, therefore, highly desirable to find processing techniques to produce completely transformed fct FePt nanoparticles.

# CHAPTER 3

# EXPERIMENTAL PROCEDURES AND EQUIPMENT

## 3.1 Raw Materials

All the raw materials of reagents used in the experiments were commercially available. Ethanol, hexane, sodium chloride and octane were used as received. Phenyl ether (99%), benzyl ether (99%), octyl ether (99%) 1,2-hexadecanediol (97%), oleic acid (90%), oleyl amine (>70%), cobalt(II) acetylacetonate, iron(III) acetylacetonate, platinum acetylacetonate (II), and iron pentacarbonyl were purchased from Aldrich Chemical Co.

## 3.2 Experimental Procedure for Chemical Synthesis of $Fe_3O_4$ Nanoparticles

The synthesis was carried out using standard airless process. The reagents were obtained from commercial sources and used without further purification. The process involves chemical reduction of iron (III) acetylacetonate $Fe(acac)_3$, by 1,2-hexadecanediol at high temperature in solution phase. Particles diameter were tuned from 4 to 20 nm by varying reaction conditions or by seed-mediated growth method.

*3.2.1 Synthesis of 4 nm $Fe_3O_4$ Nanoparticles*

In typical synthesis, a mixture of 2 mmol (607 mg) of Fe $(acac)_3$, and 10 mmol (2584.44 mg) of 1,2-hexadecanediol was added to a 125 ml European flask containing a PTFE coated magnetic stir bar. Phenyl ether (20 ml) was then transferred into the flask and the content was stirred while purging with Ar for 30 min at room temperature.

The flask was then heated to 100 °C and held at 100 °C for 20 min. During this period, 6 mmol (2.04 ml) of oleylamine and 6 mmol (1.9 ml) of oleic acid were injected into the flask while continuing the Ar purge. After the 20 min holding, the mixture was maintained under an Ar blanket and heated to 200 °C and held for 20 minutes and then heated to 265 °C at a rate of approximately 10 °C per minute. The flask was maintained at the refluxing temperature of 265 °C for 30 min before it was cooled down to room temperature under the Ar blanket. The heating profile used for this process is shown in Fig 3.2 (A). Afterward, all procedure was performed open to the atmosphere.

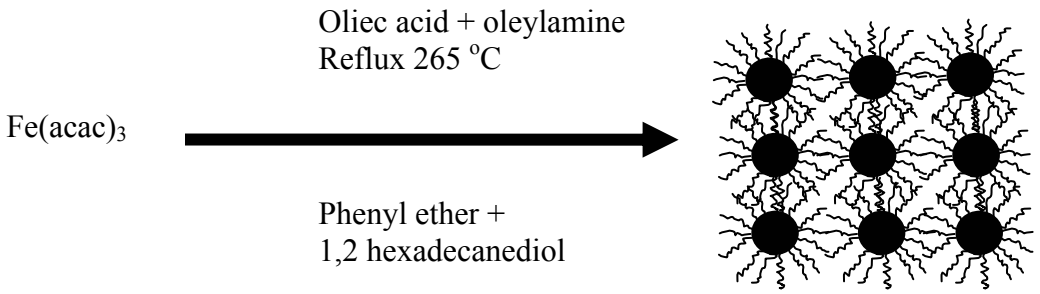


Figure 3.1 Scheme for synthesis of $CoFe_2O_4$ nanoparticles

Purification of the nanoparticles was accomplished as follows: 5 ml of the dispersion taken from the flask was added to 20 ml of ethyl alcohol (ethanol) and the mixture was centrifuged at 6000 rpm for 15 min. The supernatant was discarded and the precipitate redispersed in 10 ml of hexane and 5 ml of ethanol. Additional small amount of oleylamine and oleic acid is added to aid in redispersing the nanoparticles. This dispersion was centrifuged at 6000 rpm for 15 min. The supernatant was transferred to a new centrifuge tube, and any precipitate was discarded. An additional 15 ml of ethanol was added to this dispersion and centrifuged again. The supernatant was discarded and the remaining dark brown precipitate was re-dispersed in hexane to form 4 nm $Fe_3O_4$ nanoparticles. 6 nm particles were obtained following similar procedure described in the synthesis of 4 nm, only replacing the phenyl ether by benzyl ether and using different heating profile. In case of 6 nm, mixture was hold at 200 $^{\circ}$C for 2 hrs and then heated to reflux at 300 $^{\circ}$C for another 1 hr as shown in figure 3.2 (B).

*3.2.2 Synthesis of Larger (> 6 nm) $Fe_3O_4$ Nanoparticles*

To make larger $Fe_3O_4$ nanoparticles, a seed-mediated growth method was used. In this process, the smaller $Fe_3O_4$ nanoparticles (as seeds) were mixed with more precursor materials as mentioned above, and the mixture was heated as in the synthesis of 4 nm or 6 nm particles. By controlling the quantity of nanoparticles-seeds, $Fe_3O_4$ nanoparticles with various sizes can be synthesized. For example, mixing and heating 50 mg 4 nm $Fe_3O_4$ particles with 2 mmol of $Fe(acac)_3$, 10 nmol of 1, 2-hexadecanediol, 2 mmol oleic acid, 2 mmol of oleyl amine produced 8 nm $Fe_3O_4$ particles.

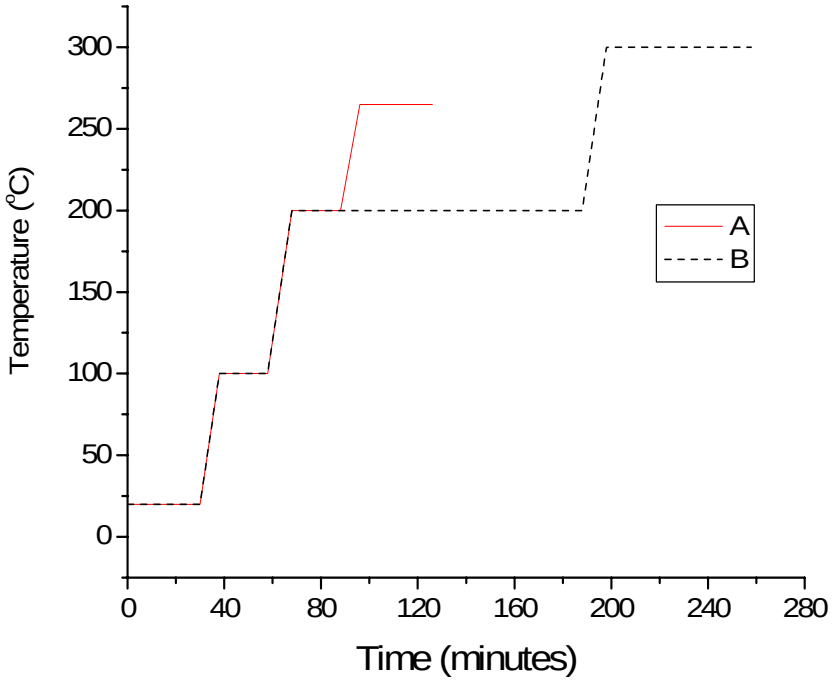


Figure 3.2 Heating profile for synthesis of (A) 4 nm and (B) 6 nm $Fe_3O_4$ nanoparticles

Similarly, mixture of 50 mg of 8 nm $Fe_3O_4$ seeds particle with 2 mmol of $Fe(acac)_3$, 10 mmol of 1,2-hexadecanediol, 2 mmol oleic acid, 2 mmol of oleylamine produced 12 nm $Fe_3O_4$ particles, while changing mass of seeds to 25 mg formed 20 nm $Fe_3O_4$ nanoparticles.

## 3.3 Experimental Procedure for Synthesis of $CoFe_2O_4$ Nanoparticles

Under similar conditions as described for synthesis of $Fe_3O_4$ nanoparticles above, Co-ferrite ($CoFe_2O_4$) nanoparticles were synthesized by simultaneous chemical reduction of iron (III) acetylacetonate $Fe(acac)_3$, and cobalt (II) acetylacetonate $Co(acac)_2$ , by 1,2-hexadecanediol at high temperature in solution phase. Particle

diameter was tuned from 3 nm to 20 nm by varying reaction conditions or by seed-mediated growth method.

*3.3.1 Synthesis of 4 nm $CoFe_2O_4$ Nanoparticles*

In the case of 4 nm particles the composition was controlled by varying the mole ratios of the precursors $Fe(acac)_3$ and $Co(acac)_2$ used during the chemical synthesis. Fe $(acac)_3$ (1 to 3 mmol), $Co(acac)_2$ (1 mmol), 1,2-hexadecanediol (10 mmol), oleic acid (5 mmol), oleyl amine (5 mmol), and phenyl ether (20 ml) were mixed and magnetically stirred under a flow of Ar for 30 minutes.

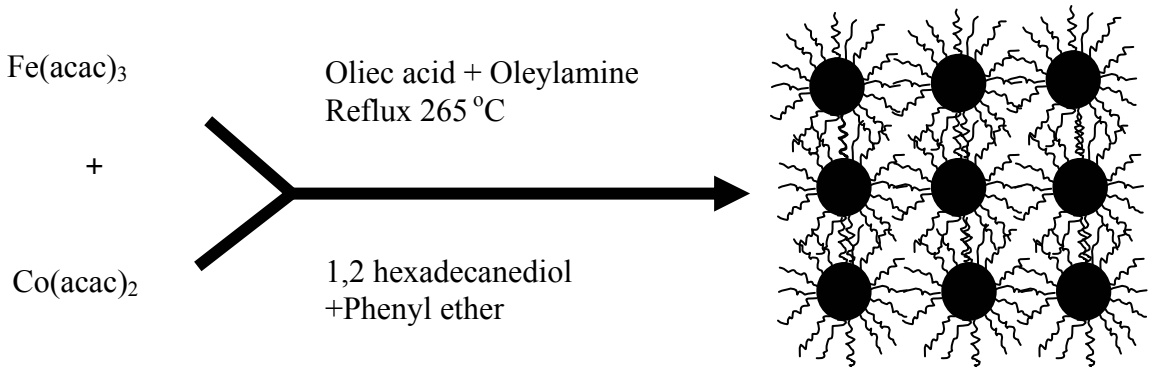


Figure 3.3 Scheme for synthesis of $CoFe_2O_4$ nanoparticles

The flask was then heated to 100 °C and held for 20 min. During this hold, 5 mmol (1.7 ml) of oleylamine and 5 mmol (1.6 ml) of oleic acid were injected into the flask while continuing the Ar purge. After the 20 min hold, the mixture was maintained under an Ar blanket and heated to 200 °C and held for 20 minutes and then heated to 265 °C at a rate of approximately 10 °C per minute. The flask was maintained at the refluxing temperature of 265 °C for 30 min before it was cooled down to room temperature under

the Ar blanket. The heating profile used for this process is same as used for $Fe_3O_4$ shown in Fig 3 (A). Following the similar purification process as mentioned above, 4 nm $CoFe_2O_4$ nanoparticles were obtained from the final product after a series of centrifugation. 6 nm particles were prepared by replacing phenyl ether with benzyl ether and following the similar heating profile (see Figure 3(B)) used for synthesis of 6 nm $Fe_3O_4$ nanoparticles.

*3.3.2 Synthesis of Larger (> 6 nm) $CoFe_2O_4$ Nanoparticles*

Mole ratios of 1.5:1 of $Fe(acac)_3$ and $Co(acac)_2$ was kept constant to prepare bigger particles in order to study the effect of size on the structural and magnetic properties. Particles of bigger size were prepared by seed-mediated growth method using the 4 nm and 6 nm as seeds. In this process, the smaller $CoFe_2O_4$ nanoparticles (as seeds) were mixed with more precursor materials and the mixture was heated as in the synthesis of 4 nm or 6 nm particles. By controlling the quantity of nanoparticle seed, $CoFe_2O_4$ nanoparticles with various sizes can be synthesized. For example, mixing and heating 60 mg 4 nm $CoFe_2O_4$ particles with 1.5 mmol of $Fe(acac)_3$, 1 mmol of $Co(acac)_2$, 8 mmol of 1, 2-hexadecanediol, 2 mmol of oleic acid, and 2 mmol of oleylamine formed 8 nm $CoFe_2O_4$ particles. Similarly, mixing and heating 50 mg of 8 nm $CoFe_2O_4$ seed particles with 2 mmol of $Fe(acac)_3$, $Co(acac)_2$ , 8 mmol of 1, 2-hexadecanediol, 2 mmol of oleic acid, and 2 mmol of oleylamine formed 12 nm $CoFe_2O_4$ particles , while changing to mass of seeds into 20 and 15 mg formed 15 and 20 nm $CoFe_2O_4$ nanoparticles respectively.

## 3.4 Experimental Procedure for Synthesis of Iron Platinum (FePt) Nanoparticles

FePt nanoparticles were synthesized by chemical reduction of platinum II acetylacetonate and $Pt(acac)_2$ and iron pentacarboyl $Fe(CO)_5$ , by 1,2-hexadecanediol at high temperature in solution phase. Particle diameter was tuned from 4 nm to 15 nm by varying reaction conditions [70, 88-90].

### *3.4.1 Synthesis of 4 nm FePt Nanoparticles*

In a typical synthesis route for 4 nm FePt nanoparticles, platinum acetylacetonate (197 mg, 0.5 mmol), 1,2-hexadecancediol (390 mg, 1.5 mmol), and dioctylether (20 ml) were mixed and heated to 100 $^{o}$C. Oleic acid (0.16 ml, 0.5 mmol), oleylamine (0.17 ml, 0.5 mmol) and $Fe(CO)_5$ (0.13 ml, 1 mmol) were added, and the mixture was heated to reflux (295 $^{o}$C). The refluxing was continued for 30 minutes. The heat source was then removed and the reaction mixture was allowed to cool to room temperature. The purification of nanoparticles was done by following the similar process as discussed above [Section 3.2.1].

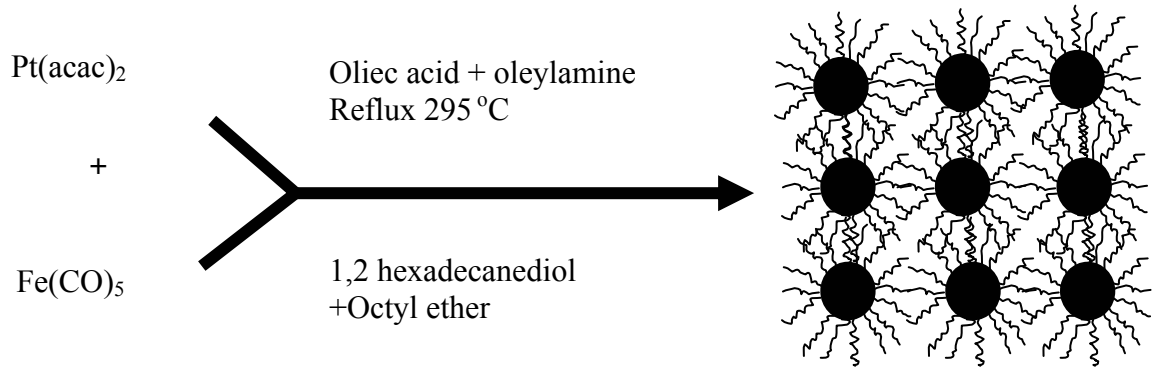


Figure 3.4 Scheme for synthesis of FePt nanoparticles

*3.4.2 Synthesis of Larger (> 4 nm) FePt Nanoparticles*

FePt nanoparticles larger than 4 nm, were synthesized by varying the reactions parameters in used to make 4 nm FePt nanoparticles. For instant, to make 8 nm FePt nanoparticles 10 ml of octyl ether was used with 8 times of surfactants [88]. To make 15 nm Pt/Fe3O4 core-shell particles, first 10 nm Pt cores were synthesized by addition of Pt precursor at 290°C in a mixture of octyl ether and surfactants and then the particles were coated with iron [90].

## 3.5 Preparation of Face-Centered Tetragonal FePt Nanoparticles

The face-centered cubic (fcc) 4, 8 and 15 nm FePt nanoparticles with different shape were used as precursors. The salt powder (NaCl) was ball milled for more than 24 hours to reach particle size smaller than 20 microns before they were mixed with the fcc FePt nanoparticles. The milling was carried out in a 500 ml Nalgene high density polyethylene plastic container inserted into a stainless steel container as shown in Figure 3.4 below. The milling load was as follows:

a) 25 grams of salt (NaCl) powder
b) 10 mm diameter 316 stainless steel balls, total weight = 500 grams
c) Ball to powder weight ratio = 20:1
d) Heptane 225 ml
e) Surfactant (oleyl amine) 2% of 225 ml.
f) RPM = 210

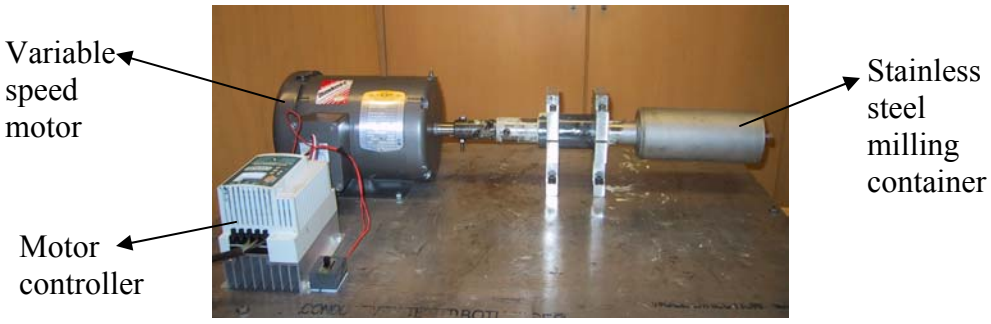


Figure 3.5 The ball milling set up used for milling of NaCl powders

A mixture of FePt fcc nanoparticles and ball-milled salt was dispersed in hexane and stirred by magnetic stir bar to mix them homogeneously and was continued stirring until mixture dried. Weight ratios of the salt to FePt fcc nanoparticles were varied. The mass ratios of ball-milled salt to FePt fcc particles including 1:1, 2:1, 4:1, 8:1, 20:1, 30:1, 40:1 and 100:1, 400:1 were tested. The mixture was then annealed at temperatures from 600-700$^{o}$C for 2-8 hours in forming gas (95% Ar + 5% $H_2$) in ceramic boats. After annealing, the salt was completely removed from the samples by washing the mixtures in water and ethanol followed by a series of centrifugation. The remaining particles were then rinsed with ethanol only and were centrifuged again to remove water. Dispersions of the fct FePt nanoparticles were eventually obtained in an organic solvent such as ethanol and cyclohexane. Surfactants were not necessary to stabilize the dispersion. Annealing experiments on selected samples were performed to determine the change in structural and magnetic properties due to phase transformation.

## 3.6 Annealing

Annealing experiments were carried out in a Lindberg Blue-M tube furnace. The maximum temperature that can be reached in this furnace was 1100 $^{\circ}$C. Annealing was done either in inert-Ar or reducing-forming gas (Ar + 7%$H_2$) atmosphere. The samples for annealing were prepared by depositing the nanoparticles dispersion liquids on silicon or glass substrate. Salt assisted annealing was done by using dry powder of the FePt fcc nanoparticles with NaCl in different ratio in ceramics boat as discussed above.

## 3.7 Characterization Techniques

Transmission electron microscopy (TEM), powder X-ray diffraction (XRD), Energy dispersive X-ray (EDX) were used for structural, morphological and compositional characterization of $Fe_3O_4$, $CoFe_2O_4$ and FePt nanoparticles. A laser particle size analyzer was also used for measuring the particle size. Inductively coupled plasma - optical emission spectroscopy (ICP-OES) was used for compositional characterization of FePt nanoparticles before and after annealing in salt matrix. Alternating gradient magnetometer (AGM) and superconducting quantum interference device (SQUID) magnetometer were used for magnetic property measurements.

### *3.7.1 Transmission Electron Microscope (TEM)*

JEOL's 1200EX TEM was used for observing the nanoparticles morphologies and crystal structure information. It uses an acceleration voltage of 120 kV and can be used for magnification up to 500k times. Bright field images as well as the selected area

diffraction patterns (SADP) were captured on to a negative, which were then developed and later scanned as a digital copy.

A 300 mesh copper grid with a carbon film deposited on a formvar backing, purchased from Ted Pella, were used for preparing the TEM samples. A drop of the nanoparticle dispersion liquid was put on the formvar side of the TEM grid and the solvent (octane/ hexane) was allowed to dry in air. Formvar is more hydrophobic than carbon and hence the solvent (which is also hydrophobic) can spread out more easily on the grid instead of staying agglomerated in the form of a small drop. Nanoparticles coated with surfactants assemble on the grid. For TEM imaging of the nanoparticles it is important that there is no excessive surfactant surrounding the nanoparticles. Excessive surfactant causes difficulty in the electron beam to be transmitted through the sample, reducing the contrast, and hence hinder clear observation of the nanoparticles.

*3.7.2 Compositional Characterization*

Grisham's EDX (Energy Dispersive X-ray) detector connected to the SEM was used for studying the elemental composition of samples. The samples were mounted on an Aluminum sample stub using a double sided carbon stick tabs. A thin layer of Au-Pd was also deposited on the samples to make them conductive. ICP (Inductively coupled plasma) analysis was done on some selected samples by Galbraith Research Labs.

*3.7.3 High Resolution TEM(HRTEM)*

HRTEM imaging and EDX analysis on some selected samples were done with Hitachi HF 2000 TEM at Georgia Institute of Technology. Sample preparation for HRTEM analysis is same as that for TEM.

*3.7.4 Laser Particles-size Analyzer*

Laser particle-size analyzer was used to analyze the particles size and size distribution of as-synthesis nanoparticles with Nanotrac, from Microtrac Inc. Sample for particles size analysis was prepared by dispersing as-synthesized nanoparticles in hexane. Surfactants, oleic acid and oleylamine) was added to make stable dispersion in case of larger particles (> 6 nm).

*3.7.5 X-ray Diffraction (XRD)*

Philips PW 1710 Diffractometer with Cu-Kα radiation (wavelength λ=1.54056 $A^o$) was used for studying the crystallinity of the samples. The samples were prepared by depositing them on glass substrate.

*3.7.6 Magnetic Measurements*

Magnetic measurements were made using Princeton Measurement Inc.'s MicroMag-2900 Alternating Gradient Magnetometer (AGM) and Quantum Design's MPMS-XL7 Superconducting Quantum Interference Device (SQUID).

#### 3.7.6.1 Sample Preparation for Magnetic Measurements

Samples for magnetic characterization were prepared by depositing a few drops of the final dispersion on a 3 × 3 mm silicon substrate and evaporating the solvent (hexane/ethanol) at room temperature, which led to the formation of the nanoparticles assemblies on the substrate. The samples were then dried in a vacuum to remove volatile organics from the assemblies. The samples were measured before and after annealing in forming gas (Ar + 7 % $H_2$) for different temperatures and annealing times. In case of fct FePt nanoparticles produced by salt assisted annealing, samples were prepared by dropping the nanoparticles dispersion in ethanol and were coated with epoxy when solvent was evaporated to prevent nanoparticles being flown. FePt fct nanoparticles samples were prepared by putting drops of mixture of nanoparticles with expoy/PVC–binder on Si substrates, and also by freezing nanoparticles dispersion in alcohol/water with and without magnetic field alignment.

#### 3.7.6.2 Alternating Gradient Magnetometer (AGM)

The sample is mounted on an extension rod attached to a piezoelectric element and then placed at the center of the poles that generates magnetic field. The sample is magnetized by a static DC field. An alternating gradient magnetic field produces an alternating force on the sample. This force ($F$) is proportional to the magnitude of the alternating magnetic field ($Mag$) and the magnetic moment ($M$) of the sample [68].

Thus,

$$F \infty (Mag) \,\&\, (M) \tag{3.1}$$

If (*Mag*) is kept constant;

$$F \infty M \tag{3.2}$$

This force is converted into a proportional voltage by a piezoelectric element and hence the moment of the sample is measured. The applied field is measured using a Hall probe sensor. The sensitivity of the AGM can reach up to 10 nemu. Due to availability only room-temperature measurements could be made using AGM. The maximum field that can be applied using AGM is limited to 14 kOe. Samples with dimension up to 5 mm x 5 mm can be measured using AGM.

3.7.6.3 Superconducting Quantum Interference Device (SQUID) magnetometer

SQUID uses a superconducting magnet, through which large amount of current can flow, generating large magnetic field. During magnetic moment measurement, the sample moves through a system of superconducting detection coils and the magnetic moment of the sample causes change in magnetic flux associated with the detection coils, resulting in electric current to be produced in the detection coils. The detection coils are connected to the SQUID sensor, which functions as a highly linear current to voltage converter, producing very accurate variations in the output voltage proportional to the moment of the sample. The maximum field that can be produced using SQUID is 70 kOe and can be operated in temperature range from 2 K to 400 K. The sensitivity of SQUID is 10 nemu up to applied field of 2.5 kOe and 0.6 μemu above that [69]. Liquid

helium is required to operate SQUID which makes it expensive to use. Sample dimension requirements are almost the same as in AGM, but in this case the sample can be longer in one of its dimension. Using AGM is much easier, faster, and less expensive to operate compared with SQUID. Hence room-temperature measurements of all samples that saturate below 14 kOe were measured using AGM.

# CHAPTER 4

# RESULTS AND DISCUSSIONS

## 4. 1 Iron Oxide ($Fe_3O_4$) Nanoparticles

Iron oxide ($Fe_3O_4$) nanoparticles were synthesized by chemical reduction of iron (III) acetylacetonate, $Fe(acac)_3$, by 1,2-hexadecanediol at high temperature in solution phase in presence of oleic acid and oleylamine as surfactants. The reaction of $Fe(acac)_3$ with surfactant at high temperature leads to formation of monodisperse $Fe_3O_4$ nanoparticles, which can be separated from the reaction by centrifugation of the resultant product as discussed in experimental section. Using phenyl ether as solvent, 4 nm $Fe_3O_4$ nanoparticles were obtained while the use of benzyl ether formed 6 nm particles. The boiling point of benzyl ether (~ 300 $^{\circ}$C) is higher than that of phenyl ether (~260 $^{\circ}$C), which indicates that higher refluxing temperature gives larger nanoparticles. It is important to heat the mixture at 200 $^{\circ}$C first and stay at that temperature for some time before it is heated to reflux 265 $^{\circ}$C to make monodisperse nanoparticles which is a key to fast nucleation and growth of the nuclei. Directly heating the mixture to reflux from room temperature leads to formation of wide size distribution because of slow nucleation and growth of nuclei, similar observation was made by *Sun et al*. [38].

Larger $Fe_3O_4$ nanoparticles were made by seed-mediated growth method, experimental details of which have been discussed in Chapter-3 (Section 3.2.2). $Fe_3O_4$ nanoparticles with sizes ranging from 4 to 20 nm were successfully produced by seeding techniques by varying the seed size, the quantity of the seed and the surfactants in the process of synthesis 4 nm particles. The nanoparticles obtained were characterized by EDX, TEM, laser particle-size analyzer, X-ray, and AGM/SQUID.

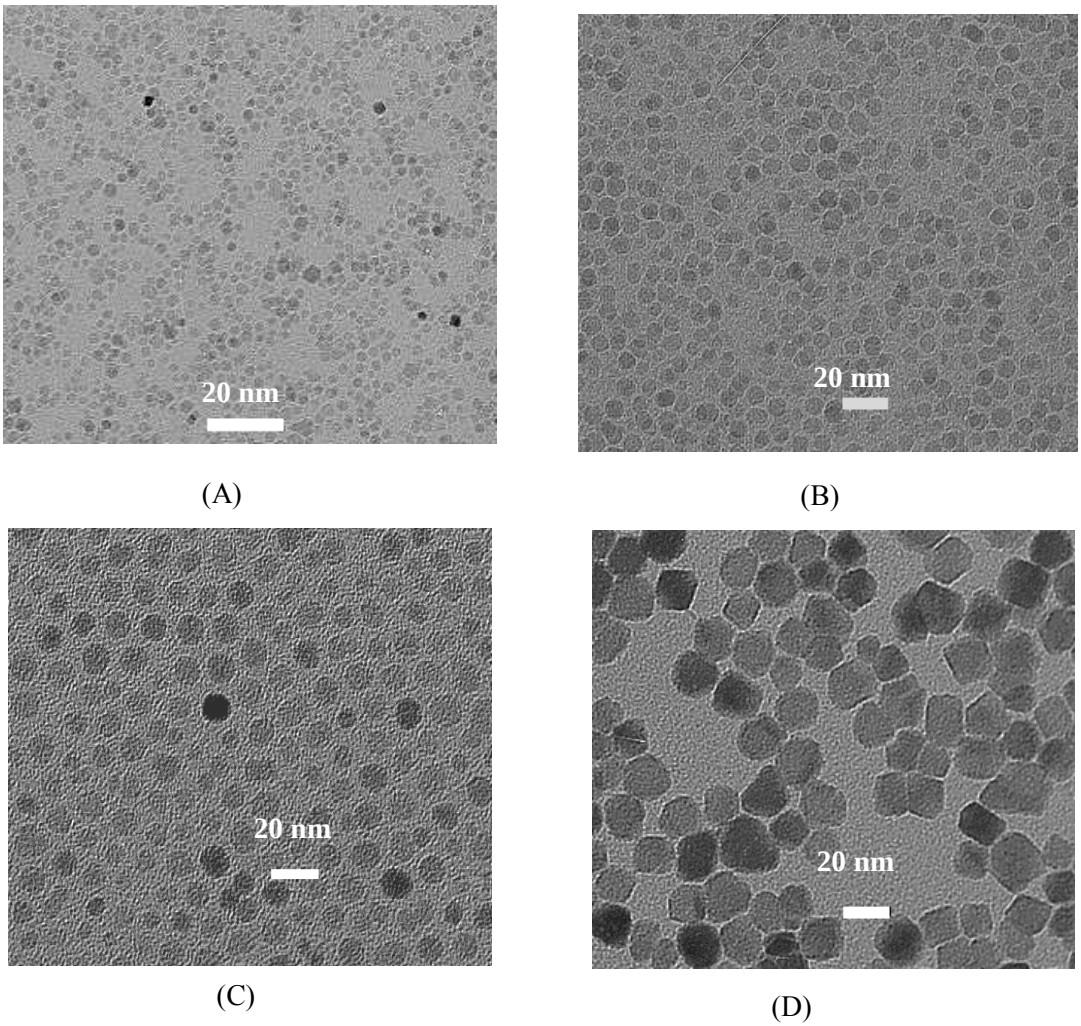


Figure 4.1 TEM bright field images of (A) 4 nm (B) 8 nm (C) 12 nm, and (D) 20 of $Fe_3O_4$ nanoparticles deposited from their hexane (or octane) dispersion on an amorphous carbon-coated copper grid and dried at room temperature

The composition of the as-synthesized $Fe_3O_4$ nanoparticles was measured using EDX detector in SEM. EDX shows presence of only Fe and O in the nanoparticles, which proves that there is no contamination in the as-synthesized nanoparticles.

TEM analysis shows that $Fe_3O_4$ nanoparticles as-synthesized in the first step and prepared by the seed-mediated method are monodisperse. Figure 4.1 shows typical TEM images of 4, 8, 12, and 20 nm $Fe_3O_4$ nanoparticles deposited on TEM carbon-coated copper grid from their hexane (or octane) dispersion and dried at room temperature. It can be seen from the TEM images that the particles have a very narrow size distribution and thus monodisperse.

Particle size and size distribution were also measured by laser particle-size analyzer from their hexane dispersion. Figure 4.2(A), 4.2(B), and 4.3(C) as representative histograms show a narrow size distribution of the nanoparticles. The average particle diameter calculated from laser particle-size analyzer is consistent with that observed in TEM images for small particles. However, when particles are larger than 8 nm, extra surfactant was needed to keep these particles dispersed in hexane. $Fe_3O_4$ nanoparticles which were bigger than 8 nm showed slightly larger size by laser particle-size analyzer as compared to what was observed from TEM. For example, laser particle-size analyzer showed an average particle size of 23 mm for 20 nm particles in TEM (see Figure 4.1(D) and 4.2(C)). In case of the bigger particles, the possible reason for difference in particle sizes measured by laser particle-size analyzer and TEM observation could be due to the formation of thick coating of surfactants on the surface of the nanoparticles.

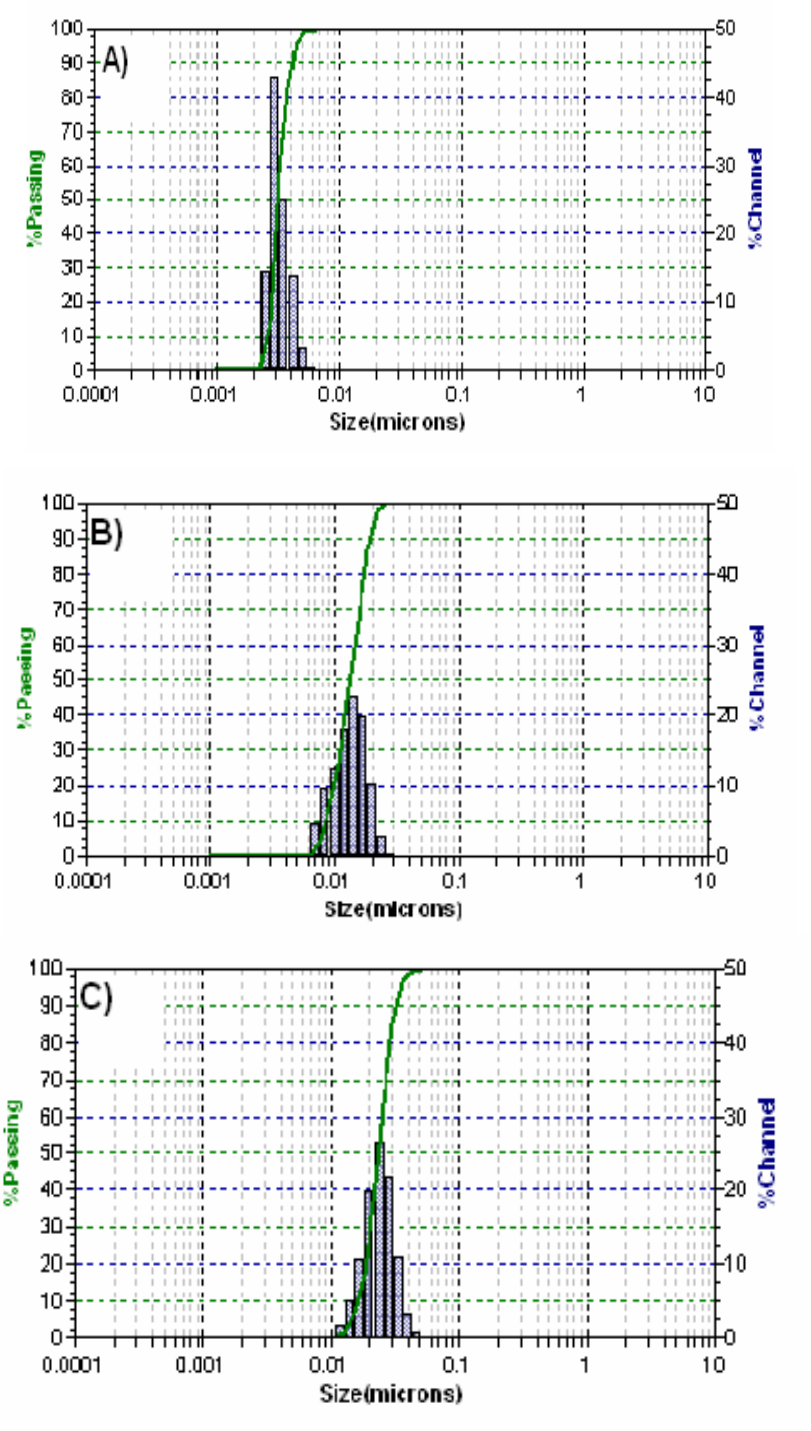


Figure 4.2 Histograms of $Fe_3O_4$ nanoparticles that show size distribution of A) 4 nm, B) 12 nm, and C) 20 nm measured by laser particle-size analyzer

XRD patterns in figure 4.3 show that the as-synthesized 4, 8, 12 and 20 nm $Fe_3O_4$ nanoparticles are highly crystalline in nature and the position and the relative intensity of peaks match well with that of standard $Fe_3O_4$ pattern. It can be seen that broadening of peaks decreases with increase in particle size due to the growth of the larger crystallites. Figure 4.3 also shows the XRD pattern of particles annealed in forming gas (Ar + 7% $H_2$) at 600 $^{\circ}$C for 30 minutes deposited on glass substrate. XRD analysis shows that the iron oxide particles were successfully reduced to Fe after annealing, indicated by the position and the relative intensity of peaks which match with standard bcc Fe pattern. Reduction leads to the increase in magnetization up to 210 emu/g.

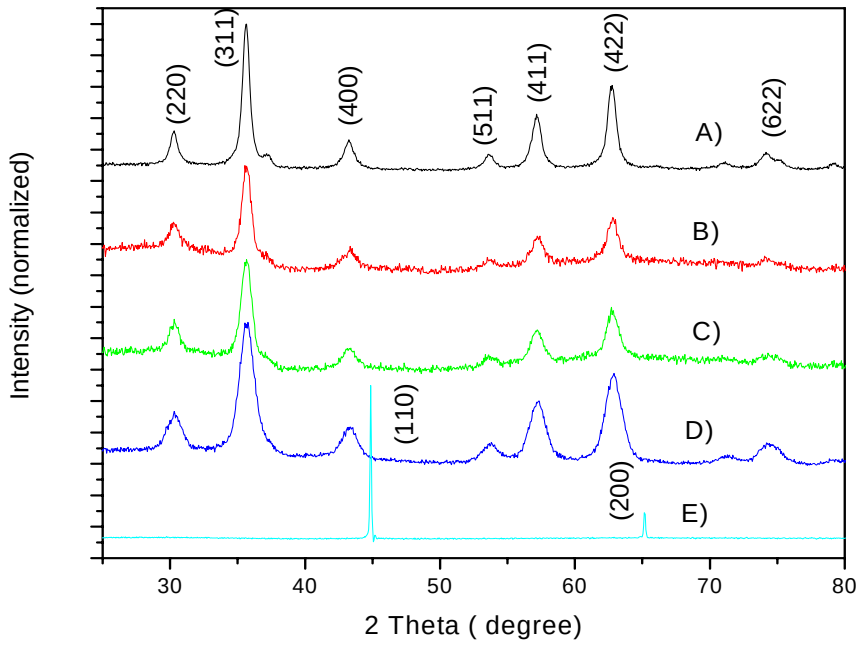


Figure 4.3 X-ray diffraction patterns of A) 20 nm, B) 12 nm, C) 8 nm, and D) 4 nm $Fe_3O_4$ nanoparticles assemblies, and E) annealed thin film of $Fe_3O_4$ nanoparticles assemblies at 600$^{o}$ C for 30 minutes in forming gas

### *4.1.1 Magnetic Properties of $Fe_3O_4$ Nanoparticles*

Magnetic properties of $Fe_3O_4$ nanoparticles at room temperature were measured by using AGM. All the as-synthesized $Fe_3O_4$ nanoparticles (4 to 20 nm) were superparamagnetic at room temperature, which indicates that the thermal energy can overcome the anisotropy energy barrier of the individual particles, and the net magnetization of the particle assemblies is zero in the absence of an external field. Figure 4.4 shows the in-plane hysteresis loops of as-synthesized 4, 8, 12, and 20 nm $Fe_3O_4$ nanoparticles at room temperature.

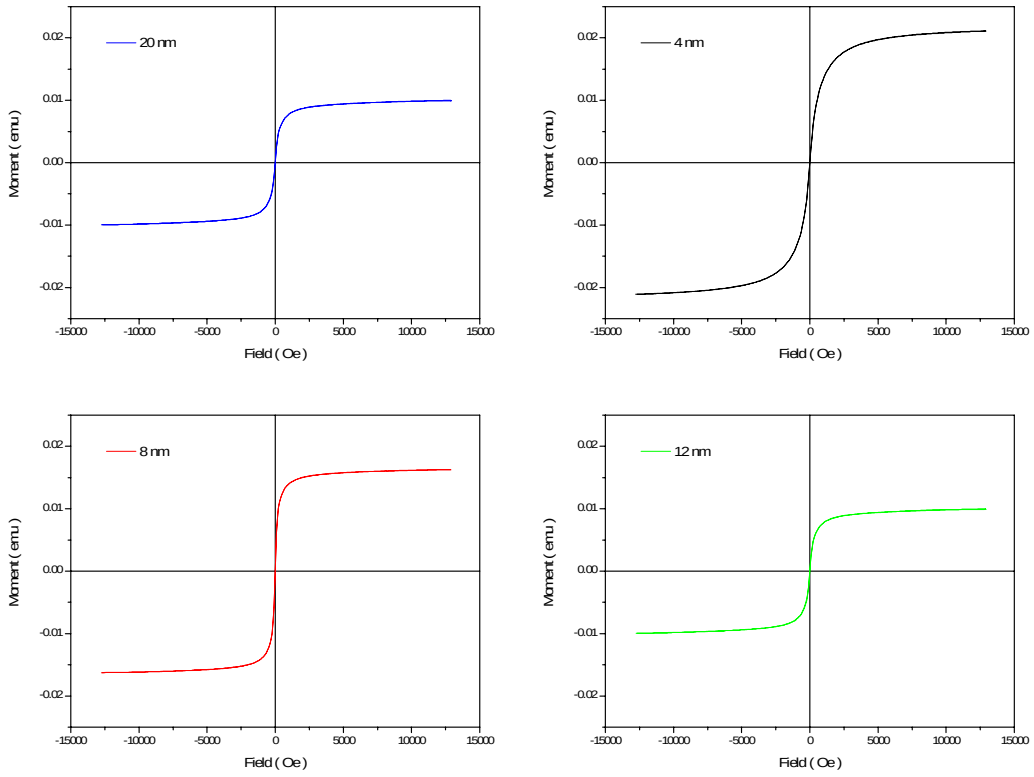


Figure 4.4 Hysteresis loops of the 4, 8, 12, and 20 nm $Fe_3O_4$ nanoparticles assemblies measured at room temperature in AGM

The temperature dependent magnetization was measured with zero-field cooling (ZFC) and field cooling (FC) procedures by SQUID. Figure 4.5 shows the plot of temperature versus normalized magnetization for 4, 6, 12 and 20 nm $Fe_3O_4$ nanoparticles with ZFC in an applied magnetic field of 100 Oe between 5 K and 330 K. The magnetization vs temperature (M-T) curves show peak characteristic of superparamagnetic particles.

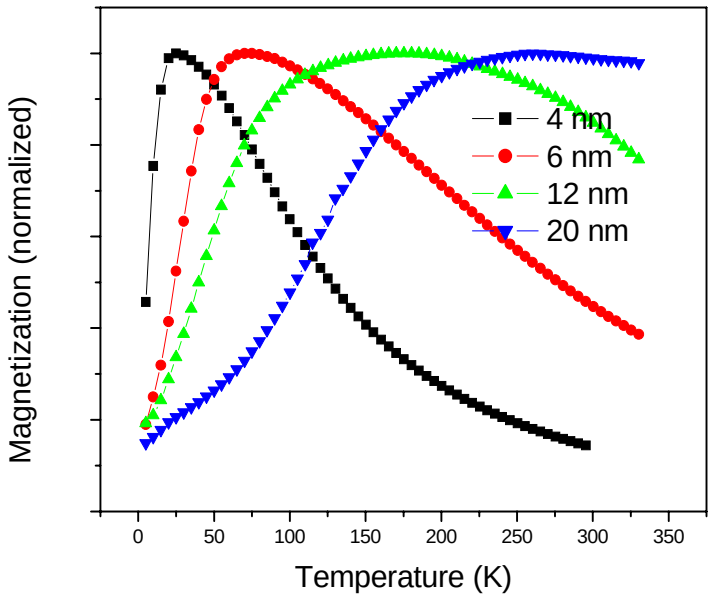


Figure 4.5 Magnetization vs temperature for 4, 6, 12 and 20 nm $Fe_3O_4$ nanoparticles with zero-field cooling at 100 Oe

All the iron oxide nanoparticles show superparamagnetic behavior at high temperature (300 K). However, on zero-field-cooling, the ZFC magnetization begins to drop and deviates from the field-cooled magnetization at blocking temperature, $T_B$, as shown in Figure 4.6 for 4 nm particles. The peak temperature in the M-T curve (blocking temperature) raises continuously with the increasing particle diameters. The

$T_B$ values are 25, 75, 175 and 260 K for 4, 6, 12 and 20 nm particles respectively (see Figure 4.5). It can be seen that the smaller particles have sharper transition peak (from superparamagnetic to ferromagnetic) and broadening of transition peaks increases with increase in particle diameters.

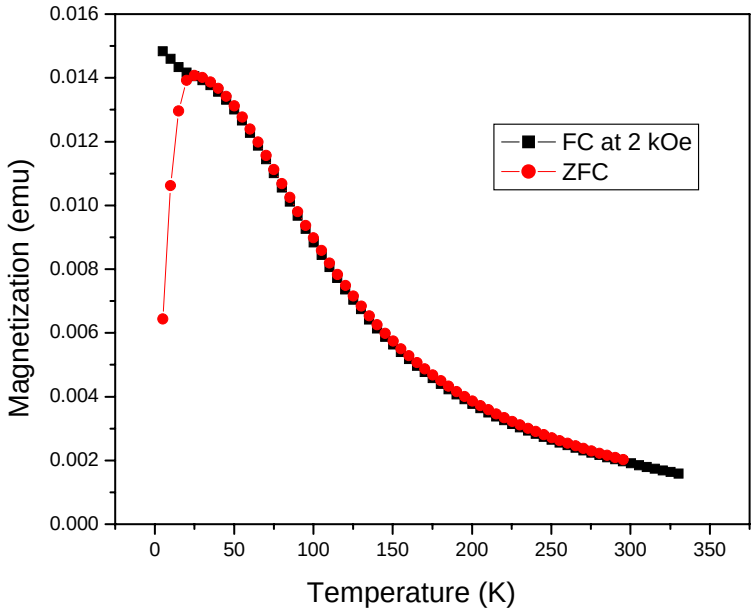


Figure 4.6 ZFC and FC curves of the 4 nm $Fe_3O_4$ particles from 5 K to 330 K measured at 100 Oe

*4.1.2 Conclusions*

Monodisperse $Fe_3O_4$ nanoparticles with tunable particle size from 4 nm to 20 nm have been synthesized by chemical solution methods. Particle size larger than 4 nm can be synthesized by varying the reaction conditions or by seed-mediated growth method. This process is simple and easy to achieve the desired size distribution and readily to be scaled up for large scale production. All the as-synthesized $Fe_3O_4$

nanoparticles up to 20 nm in diameter showed superparamagnetic behavior at room temperature, whereas all the particles were ferromagnetic at low temperature. The blocking of temperature $T_B$ of $Fe_3O_4$ nanoparticles increases with particles diameters. These iron oxide nanoparticles have great potential in magnetic nano-device and biomedical applications.

## 4.2 Cobalt Ferrite ($CoFe_2O_4$) Nanoparticles

Cobalt ferrite ($CoFe_2O_4$) nanoparticles were synthesized by simultaneous chemical reduction of iron (III) acetylacetonate, Fe $(acac)_3$, and cobalt (II) acetylacetoneate, $Co(acac)_2$, by 1,2-hexadecanediol at high temperature in solution phase in presence of surfactants oleic acid and olyle amine. Experimental details for the synthesis of $CoFe_2O_4$ nanoparticles have been discussed in chapter-3 (section 3.3). The reaction of $Fe(acac)_3$ and $Co(acac)_2$ with surfactants at high temperature leads to formation of monodisperse $CoFe_2O_4$ nanoparticles, which were separated from the reaction by a series of centrifugation of the end products .Using phenyl ether as solvent 4 nm $CoFe_2O_4$ nanoparticles were obtained. 6 nm particles could be obtained following the similar process as used in the synthesis of 6 nm $Fe_3O_4$ nanoparticles by replacing phenyl ether with benzyl ether and increasing the refluxing time by 30 minutes.

In the case of 4 nm particles, the final particle composition was controlled by varying the mole ratios of the precursors $Fe(acac)_3$ and $Co(acac)_2$. $Fe(acac)_3$ (1 to 3 mmol), $Co(acac)_2$ (1 mmol), 1,2-hexadecanediol (10 mmol), oleic acid (5 mmol), oleyl amine (5 mmol), and phenyl ether (20 ml) were tested. The magnetization of annealed

nanoparticles was found to increase rapidly with increasing mole ratio of precursors up to 1:1.5 and then decreased as the ratio is increased further to 1:3(Figure 4.7). It was observed that 1.5:1 mole ratio of $Fe(acac)_3$: $Co(acac)_2$ resulted in the highest magnetization value of 223 emu/g after their reduction process at 700 °C 30 minutes in forming gas (Ar + 7% $H_2$).

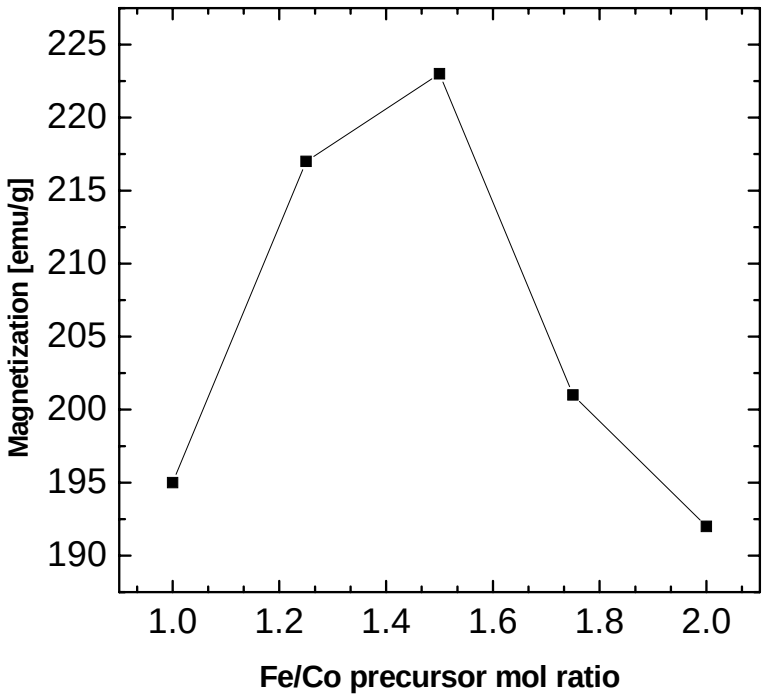


Figure 4.7 The mole ratio of 1.5:1 of $Fe(acac)_3$:$Co(acac)_2$ resulted in the highest magnetization value of 223 emu/g after annealing in forming gas at 700 °C for 30 minutes

At the optimized composition (1.5:1 precursor-mole ratio), larger $CoFe_2O_4$ particles were also made by seed-mediated growth method. $CoFe_2O_4$ nanoparticle sizes ranging from 3 to 20 nm were successfully produced by seeding techniques by varying size, and quantity of seeds and surfactants in the initial scheme of synthesis of 4 nm

particles as discussed in experimental section. The nanoparticles obtained were characterized by EDX, TEM, HRTEM, laser particles-size analyzer, X-ray, AGM and SQUID.

The composition of as-synthesized $CoFe_2O_4$ nanoparticles was determined by using EDX detector in HRTEM. The EDX spectra were acquired from 11 different areas in the sample. The EDX analysis software gives average composition of Fe = 68.78 ± 3.5 atomic percentage. Figure 4.8 shows typical EDX spectrum of $CoFe_2O_4$ nanoparticles deposited on Cu grid.

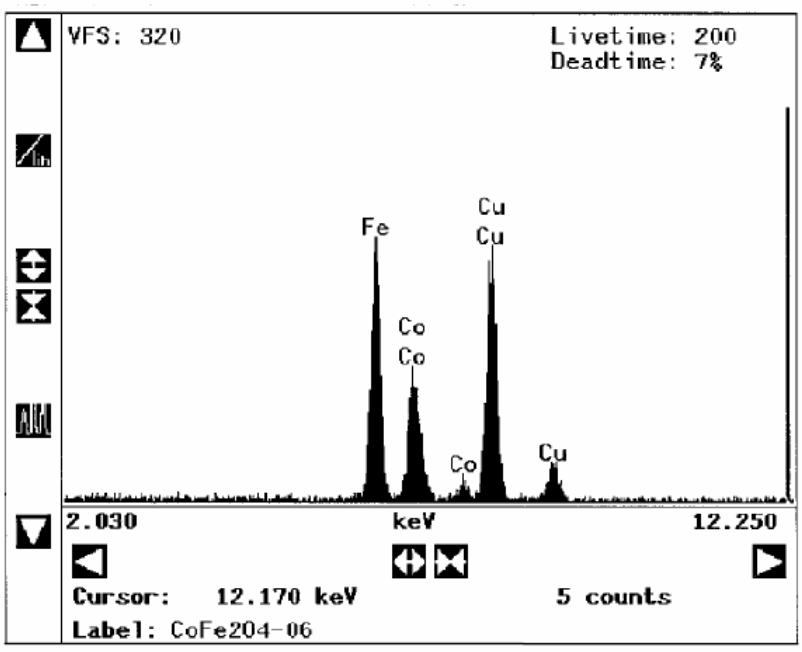


Figure 4.8 EDX spectrum of as-synthesized $CoFe_2O_4$ nanoparticles

TEM analysis shows that $CoFe_2O_4$ nanoparticles as-synthesized in first step and prepared by seed-mediated method are monodisperse. Figure 4.9(A), 4.9(B), 4.9(C),

4.9(D), and 4.9(E) show typical TEM images of 4, 6, 10, 16 and 20 nm $CoFe_2O_4$ nanoparticles deposited on TEM carbon-coated copper grid from their hexane (octane) dispersion and dried at room temperature. It can be seen from the TEM images that the particles have a narrow size distribution. Figure 4.9 (F) and 4.9(G) show the selected area electron diffraction (SAED) pattern obtained from a 20 nm $CoFe_2O_4$ nanoparticles assembly. The reflections of $CoFe_2O_4$ {220}, {311}, {400}, {400}, {422}, {511} are visible in the Figure 4.9(F). The electron diffraction rings indicate the nature of single phase crystallite with $CoFe_2O_4$ and match well with the XRD results (see Figure 4.11).

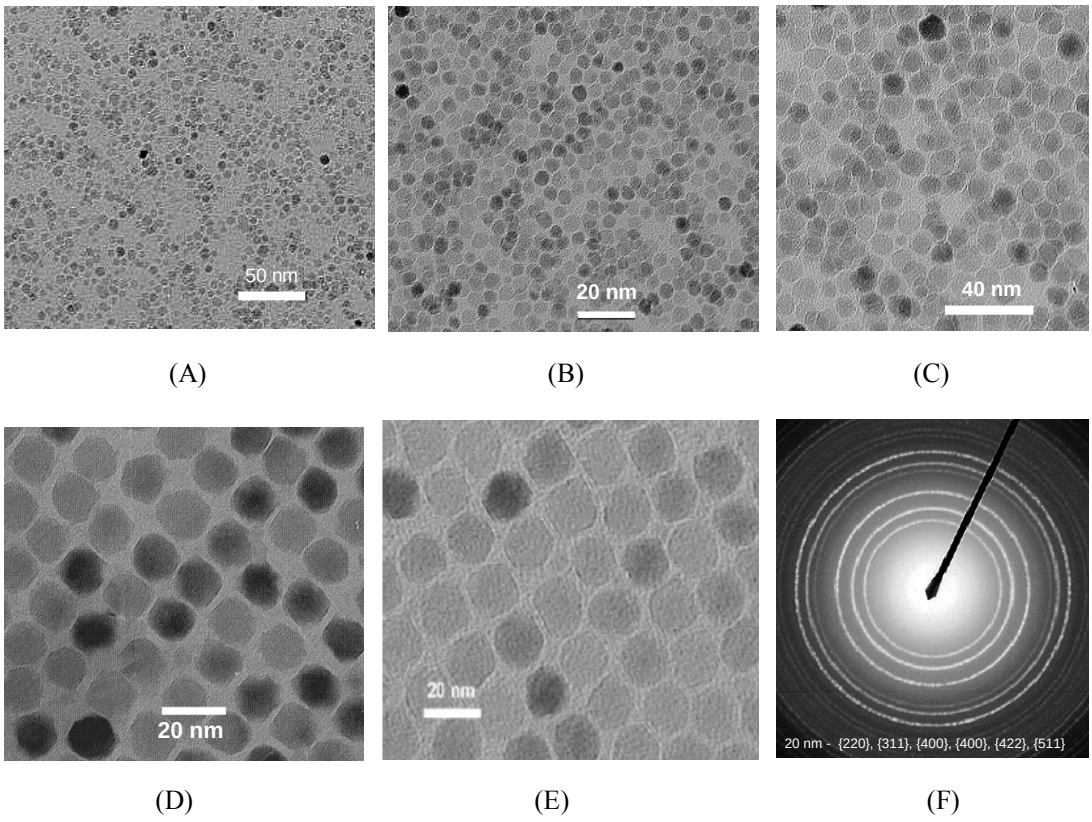


Figure 4.9 TEM bright field images of (A) 4 nm, (B) 6 nm, (C) 10 nm, (D) 16 nm, (E) 20 nm, and (F) selected area diffraction (SAED) of 20 nm $CoFe_2O_4$ nanoparticles deposited from their hexane (octane) dispersion on an amorphous carbon-coated copper grid and dried at room temperature

Particles size and size distribution were also analyzed by laser particle-size analyzer from their hexane dispersion. Figure 4.10(A), 4.10 (B), and 4.10(C) are some selected histogram of $CoFe_2O_4$ nanoparticles. It can be seen that particles have narrow size distribution. The average particle diameter calculated from laser particle-size analyzer is consistent with that observed by TEM micrograph for small particles. However, when particles are larger than 8 nm, extra surfactant is needed to make these particles disperse in hexane. As observed in $Fe_3O_4$ nanoparticles, bigger than 8 nm $CoFe_2O_4$ particles also showed slightly larger size by laser particle-size analyzer compared to what is observed from TEM. For example, laser particle-size analyzer showed average size of 24 mm for 20 nm particles in TEM (see Figure 4.9(E) and 4.10(C)). It is believed that the deviation in particle sizes measured by laser particle-size analyzer compared to TEM observation could be due to the formation of thick coating of surfactants on the surface of nanoparticles.

XRD patterns in Figure 4.11 show that the as-synthesized 3, 6, 10 and 20 nm $CoFe_2O_4$ nanoparticles are highly crystalline in nature and the position and the relative intensity of peaks match well with the standard $CoFe_2O_4$ pattern.

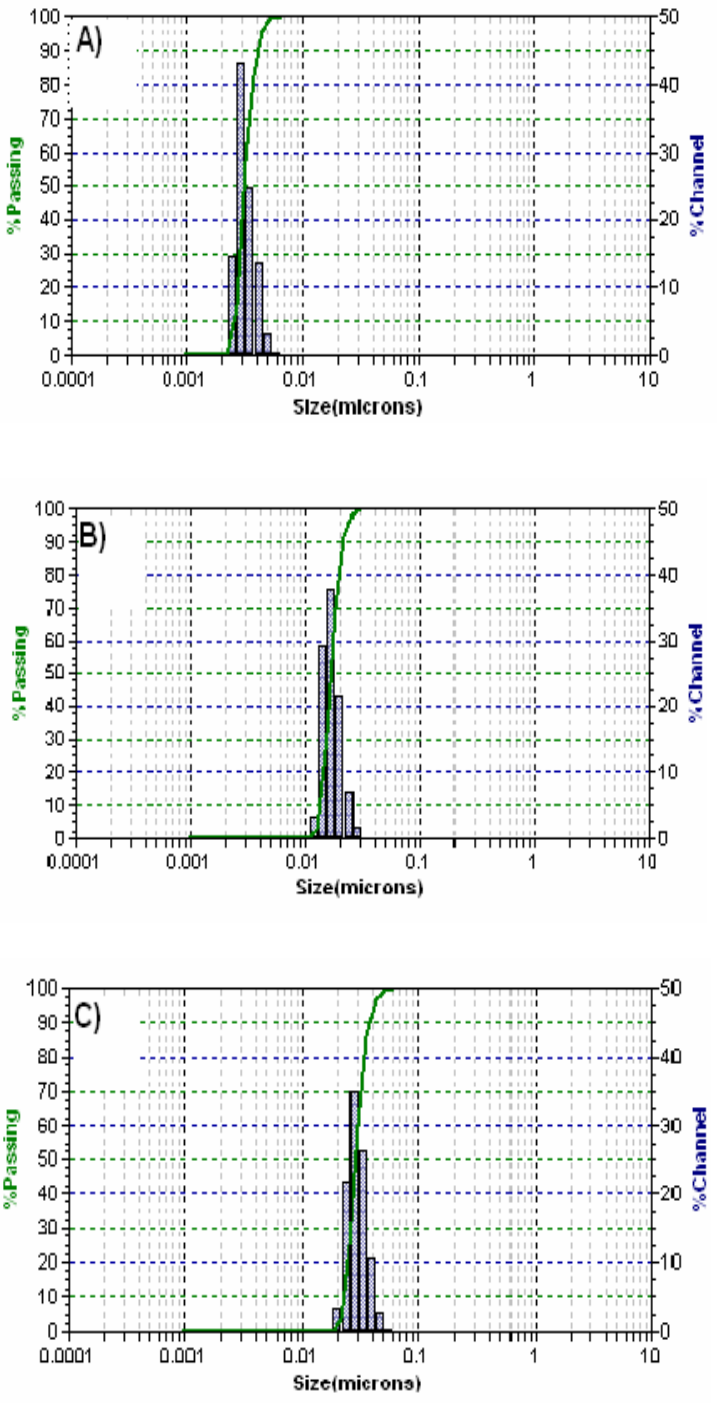


Figure 4.10 Histograms of $CoFe_2O_4$ nanoparticles that show size distribution of A) 3 nm, B) 16 nm, and C) 20 nm measured by laser particle-size analyzer

Broadening of peaks can be seen with decrease in particle sizes due to the formation of large crystal. Figure 4.11(E) also shows the XRD pattern of particles annealed in forming gas (Ar + 7% $H_2$) at 600$^o$ C for 30 minutes depositing on glass substrate. XRD analysis shows the ferrite particles can be successfully reduced to FeCo after annealing in forming gas. The position and the relative intensity of the peaks of annealed nanoparticles match well with standard FeCo pattern. Reduction leads to increase in magnetization up to 223 emu/g, which is close to the value for bulk.

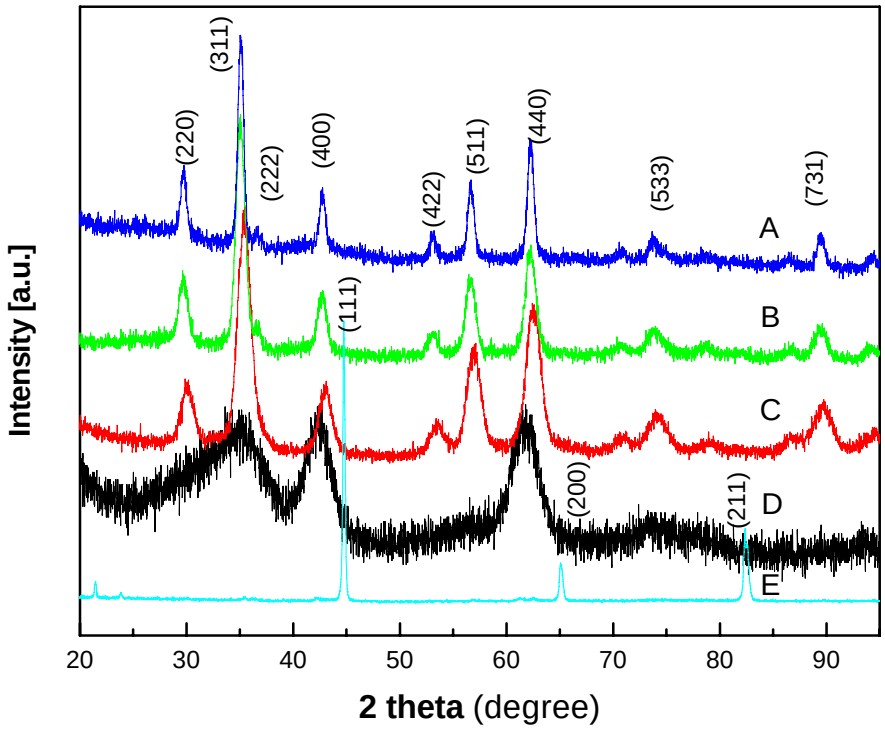


Figure 4.11 X-ray diffraction patterns of A) 20 nm, B) 10 nm, C) 6 nm, and D) 3 nm, $CoFe_2O_4$ nanoparticle assemblies, and E) annealed thin film of $CoFe_2O_4$ nanoparticles assemblies at 600$^o$ C for 30 minutes in forming gas

*4.2.1 Magnetic Properties of $CoFe_2O_4$ Nanoparticles*

Magnetic properties of nanoparticles at room temperature were measured by using AGM. Figure 4.12 shows the in-plane hysteresis loops of 3, 6, 10 and 20 nm $CoFe_2O_4$ nanoparticle synthesized using a precursor mole ratio of $Fe(acac)_3$:$Co(acac)_2$ of 1:1.5. It has been found that particle sizes less than 12 nm are superparamagnetic at room temperature.

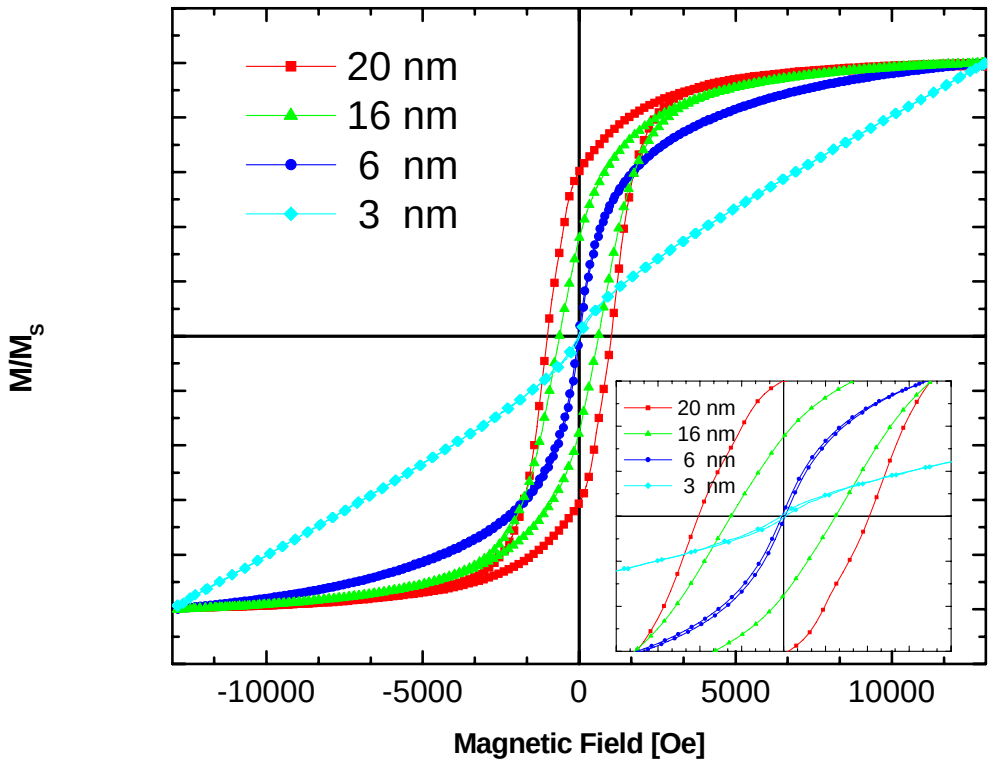


Figure 4.12 Hysteresis loops of the 3, 6, 16 and 20 nm $CoFe_2O_4$ nanoparticles ssemblies measured at room temperature

This indicates that the thermal energy can overcome the anisotropy energy barrier of individual particles, and the net magnetization of particles assemblies is zero in the absence of an external field. Particles with size greater than 12 nm are ferromagnetic at

room temperature. Figure 4.12 shows that coercivity of particle size greater than 12 nm increases with increase in particle diameters and 20 nm particles shows a coercivity of 1 kOe at room temperature.

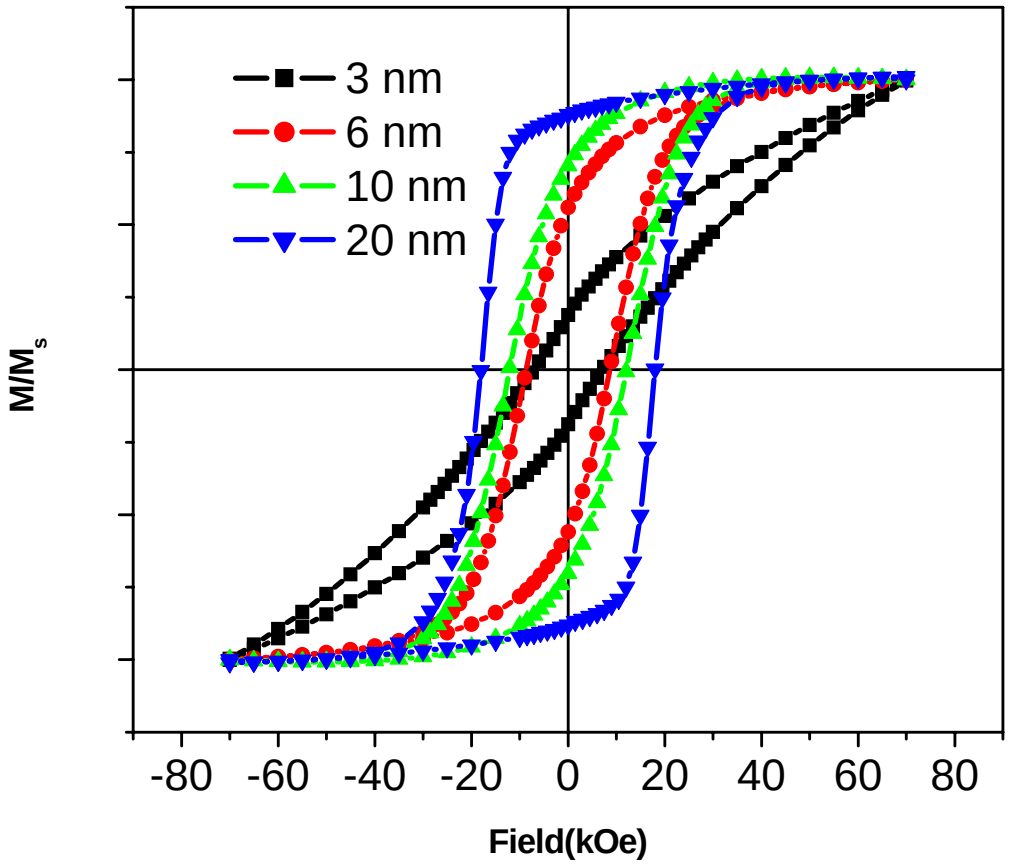


Figure 4.13 Hysteresis loops of the 3, 6, 10 and 20 nm $CoFe_2O_4$ nanoparticle assemblies measured at10 K

At low temperature magnetic properties of as-synthesized $CoFe_2O_4$ nanoparticles were measured by using SQUID. Figure 4.13 shows the hysteresis loops of 3, 6, 10 and 20 nm $CoFe_2O_4$ particles at 10 K. All the particles are ferromagnetic at this temperature. It is observed that coercivity of particles at low temperature is also size dependent and increases with particle diameters up to 20 nm. 20 nm particles

showed a coercivity of 18 kOe at 10 K. Figures 4.14 and 4.15 show the temperature dependent coercivities of 3 and 10 nm $CoFe_2O_4$ particles measured in different temperatures. The increase in coercivity with the decease of temperature is because of presence of Co cation in the Fe-O matrix which greatly increase the magnetic anisotropy of the material.

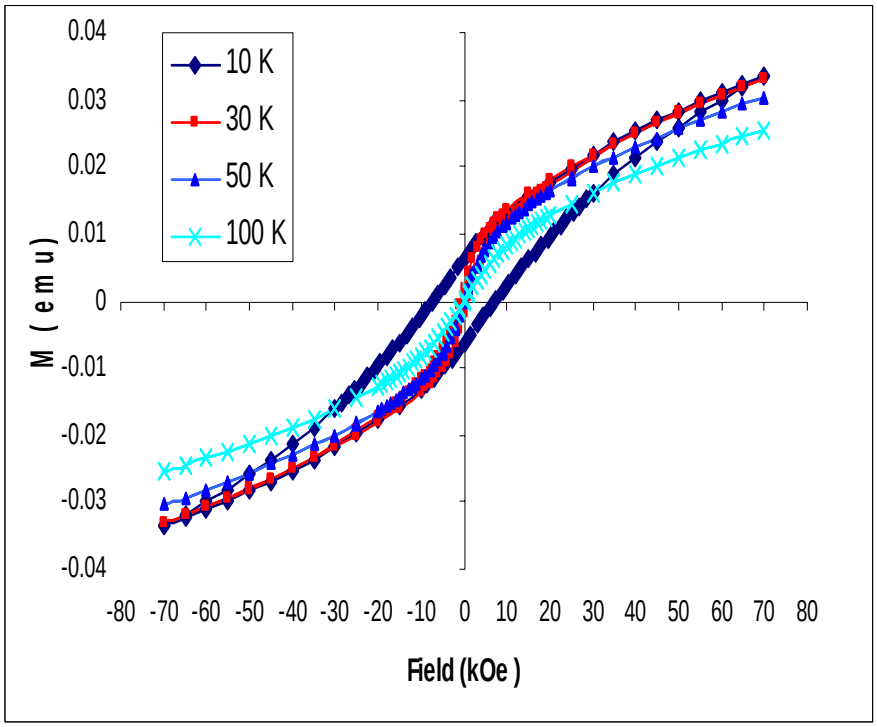


Figure 4.14 Hysteresis loops of 3 nm $CoFe_2O_4$ nanoparticle assembly measured at different temperatures.

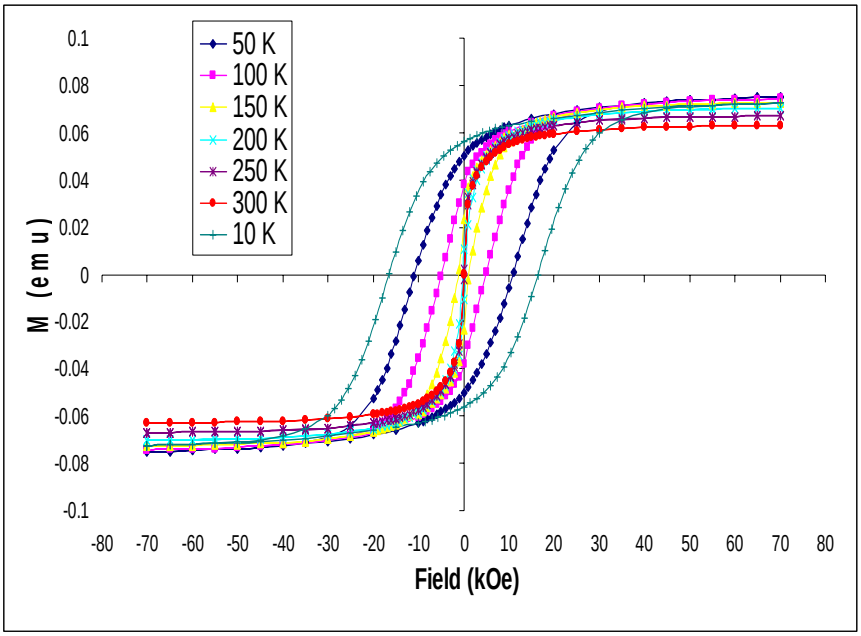


Figure 4.15 Hysteresis loops of 10 nm $CoFe_2O_4$ nanoparticle assembly measured at different temperatures

The temperature dependent magnetizations of different sized particles were measured with zero-field cooling (ZFC) and field cooling (FC) procedures. Figure 4.16 shows the plot of temperature versus normalized magnetization for 3, 6, and 10 nm $CoFe_2O_4$ nanoparticles with ZFC in an applied magnetic field of 100 Oe between 5K and 330K. The *M* vs *T* curves show peaks characteristic of superparamagnetic particles. The peak temperature in the *M* vs *T* curve (blocking temperature $T_B$), rises with the increasing particle size. The $T_B$ values are 30, 210 and 250 *K* for 3, 6 and 10 nm particles respectively.

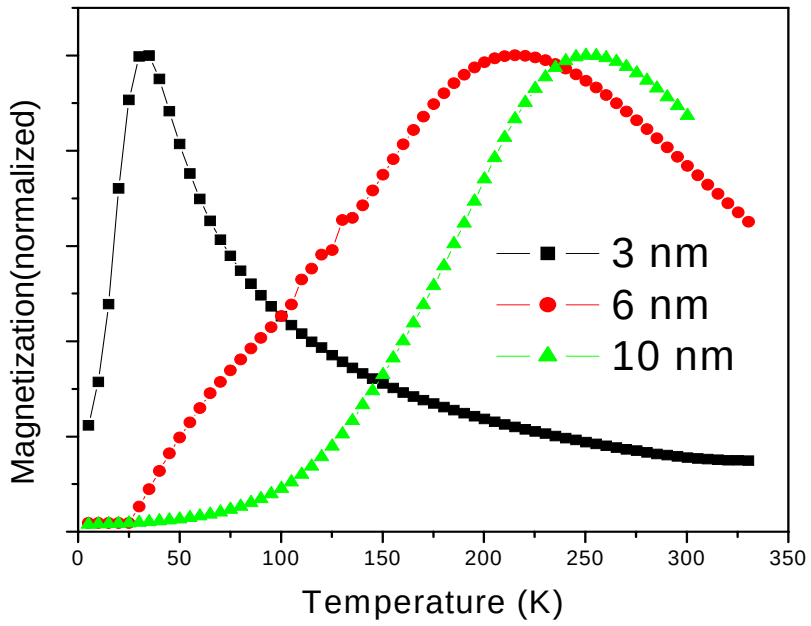


Figure 4.16 Magnetization verses temperature for 3, 6 and 10 nm $CoFe_2O_4$ nanoparticles with zero-field cooling at 100 Oe

Magnetization measurement with ZFC and FC processes between 5 and 330 K temperature interval were done on 4 nm particles for different applied fields. As seen in Figure 4.17, the difference between ZFC magnetization and FC magnetization starts to deviate at a temperature $T_F$, and shows irreversibility in the magnetization, indicating the onset of the freezing process. The strong irreversibility occurs below the blocking temperature $T_B$. Both temperatures decreased to a lower temperature as the field increased. $T_F$ changes from 247 K for lower field to 50 K for field above 20 kOe. $T_B$ changes between 40 K and 25 K.

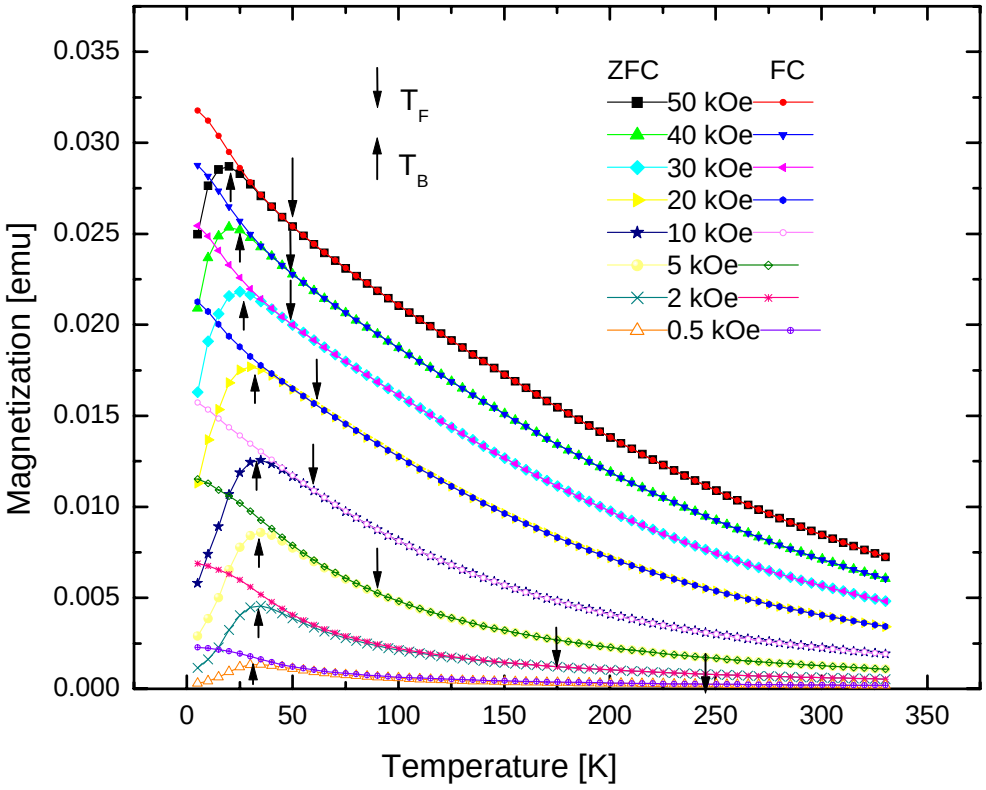


Figure 4.17 ZFC and FC curves of the 4 nm Co-ferrite particles from 5 K to 330 K

The origin of this transition is still under investigation. It could be spin glass state at the surface of particles or the increase in the anisotropy of the particles. Since the distribution of our particle size is narrow, the paramagnetic contribution to the blocking temperature is not expected.

While measuring FC properties, exchange bias were observed in smaller than 4 nm $CoFe_2O_4$ nanoparticles. Exchange bias field of 3 kOe have been observed for 3 nm $CoFe_2O_4$ nanoparticles as seen in Figure 4.18 The exchange bias in nanoparticles may

be associated with frustrated spins on the particles surface or presence of more than two phases. More work is needed to understand the exchange bias in the small particles.

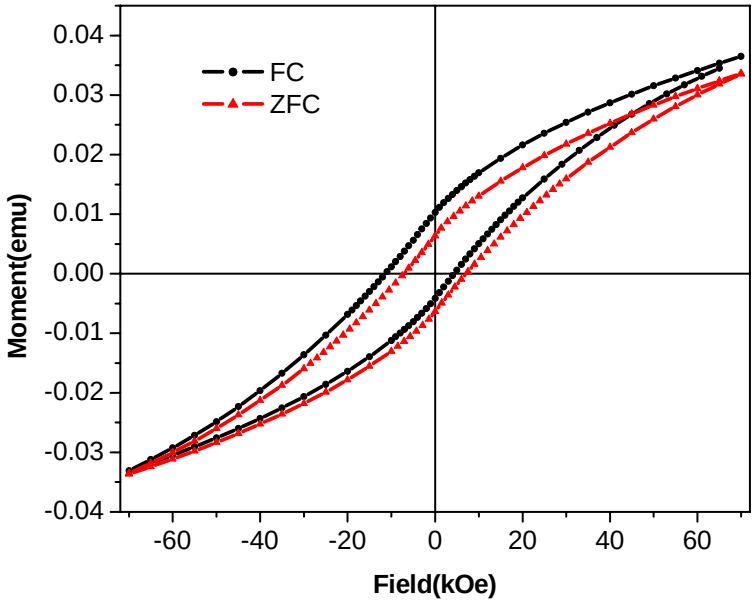


Figure 4.18 Hysteresis loops of the 3 nm $CoFe_2O_4$ nanoparticles assembly measured in ZFC and FC at 5 Tesla field of temperature at 10 K

*4.2.2 Conclusions*

Monodispersed Co-ferrite nanoparticles with particle size from 3 nm to 20 nm have been synthesized by chemical solution methods. Particles larger than 6 nm were synthesized by seed-mediated growth method. The composition was controlled by varying the mole ratios of the precursors iron(III) acetylacetonate and cobalt(II) acetylacetonate) in the solution. It was observed that the 1.5:1 mole ratio of $Fe(acac)_3$: $Co(acac)_2$ results in the highest magnetization value of 223 emu/g after annealing in forming gas at 600 ˚C. Low temperature (10 K) and room temperature (300 K)

magnetic measurements on these particles showed strong dependence of the magnetic properties on the particle size. Particle size greater than 12 nm showed ferromagnetic behavior at room temperature, whereas particles size less than 12 nm showed ferromagnetic behavior below room temperature. The blocking temperature $T_B$ values are 30, 210 and 250 K for 3, 6 and 10 nm particles respectively. A coercivity value of 1.8 T was obtained at 10 K for the 20 nm particles. The zero field cooling and field cooling measurements were done for 3 nm-sized particles show the irreversible magnetization in the particle are temperature and field dependent. Exchange bias field of 3 kOe have been observed for 3 nm $CoFe_2O_4$ nanoparticles. The cause for exchange bias in smaller nanoparticles is not yet understood. Further research work is needed to investigate the exchange bias in the small particles.

## 4.3 Iron Platinum (FePt) nanoparticles

Monodisperse face-centered tetragonal (fct) FePt nanoparticles were prepared by salt-assisted annealing technique. The as-synthesized face-centered cubic (fcc) FePt nanoparticles were mixed with ball-milled salt powders and annealed at 700° C for different annealing time and FePt to NaCl ratios. The salt was then removed from the particles by washing the samples in water and ethanol by a series of centrifugation processes. Experimental detail has been discussed in chapter-3 (Section 3.5). Figure 4.19, 4.20, and 4.21 show XRD patterns of the 4, 8, and 15 nm annealed FePt nanoparticles in a NaCl matrix under different conditions. It can be seen clearly that well defined (001) and (110) peaks for fct FePt appear in samples annealed at 700° C

for 2 h in forming gas. Diffraction peaks associated with NaCl or any other phases were not found in the XRD patterns, which indicate a minimal contamination by the salt during the annealing. ICP analysis confirmed a low level of Na contamination of 0.099% (wt/wt basis) and an average particle composition of $Fe_{52}Pt_{48.}$

The magnetization values of the salt-matrix annealed FePt nanoparticles were measured to check if any deterioration was caused by the contamination from the salt matrix during annealing or from water exposure during washing. For the recovered particles of 15 nm with salt to particle ratio of 40: 1, for instance, the magnetization values at 7 T at room temperature (which are considered to be close to the saturation magnetization) are as follows: annealed at 600° C for 2 h, 733.5 emu/$cm^3$; 700° C, 2 h, 744 emu/$cm^3$; 700° C, 4 h, 841.5 emu/$cm^3$. These magnetization values are comparable to FePt particles annealed under the same conditions without salt. It is seen that the magnetization values increase with the annealing time and temperature, indicating a phase-transition (from disordered fcc to ordered fct structure) that resulted in an increase in magnetization. The higher the degree of the chemical order, the higher is the magnetization. A completely ordered fct bulk phase possesses very high saturation magnetization (1140 emu/$cm^3$ at room temperature [91]).

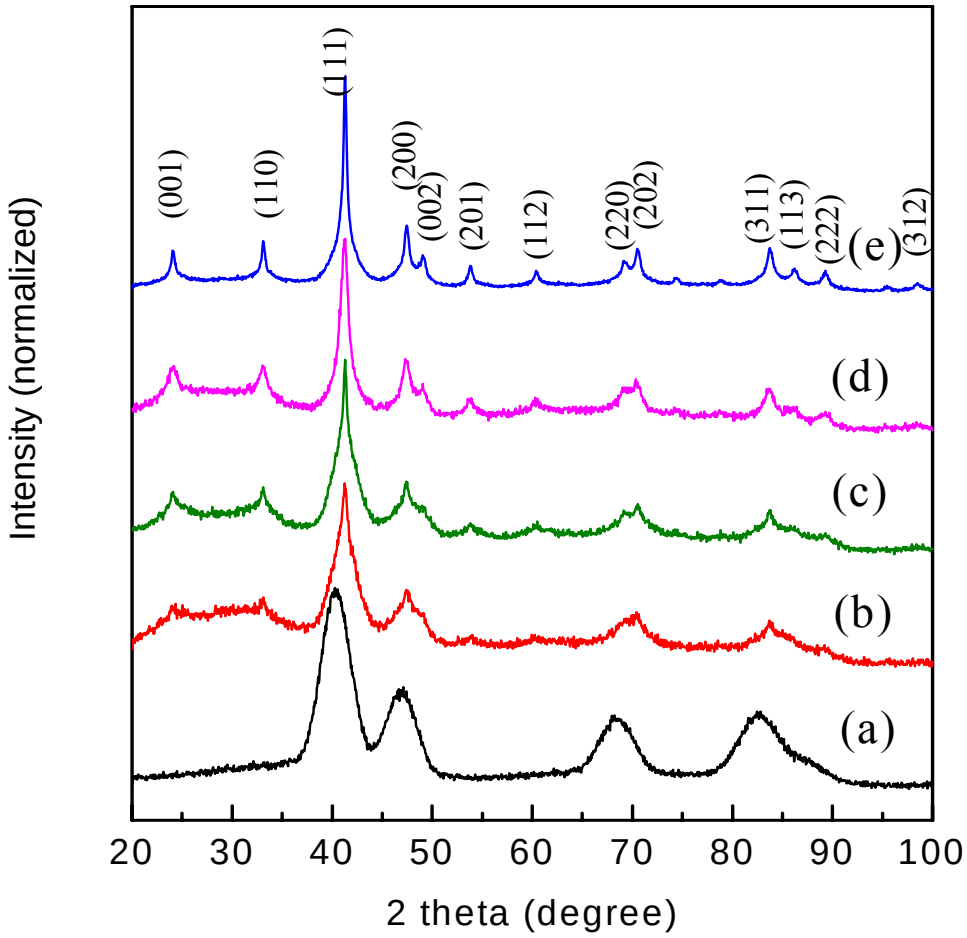


Figure 4.19 XRD patterns of the FePt nanoparticles (a) The as-synthesized 4 nm FePt particles, (b) particle annealed at 600°C for 2 h with NaCl : FePt ratio 40 : 1, (c) at 700°C for 2 h with the ratio 40 : 1, (d) 700°C for 4 h with the ratio 100 : 1 ,and (e) 700°C for 4 h with the ratio 40 : 1

The relatively low magnetization values at 7 T of the nanoparticles, even after sufficient annealing, may be attributed to the reduced magnetic moment of the surface atoms of the nanoparticles and the fact that the 7 T field is not enough to reach the saturation.

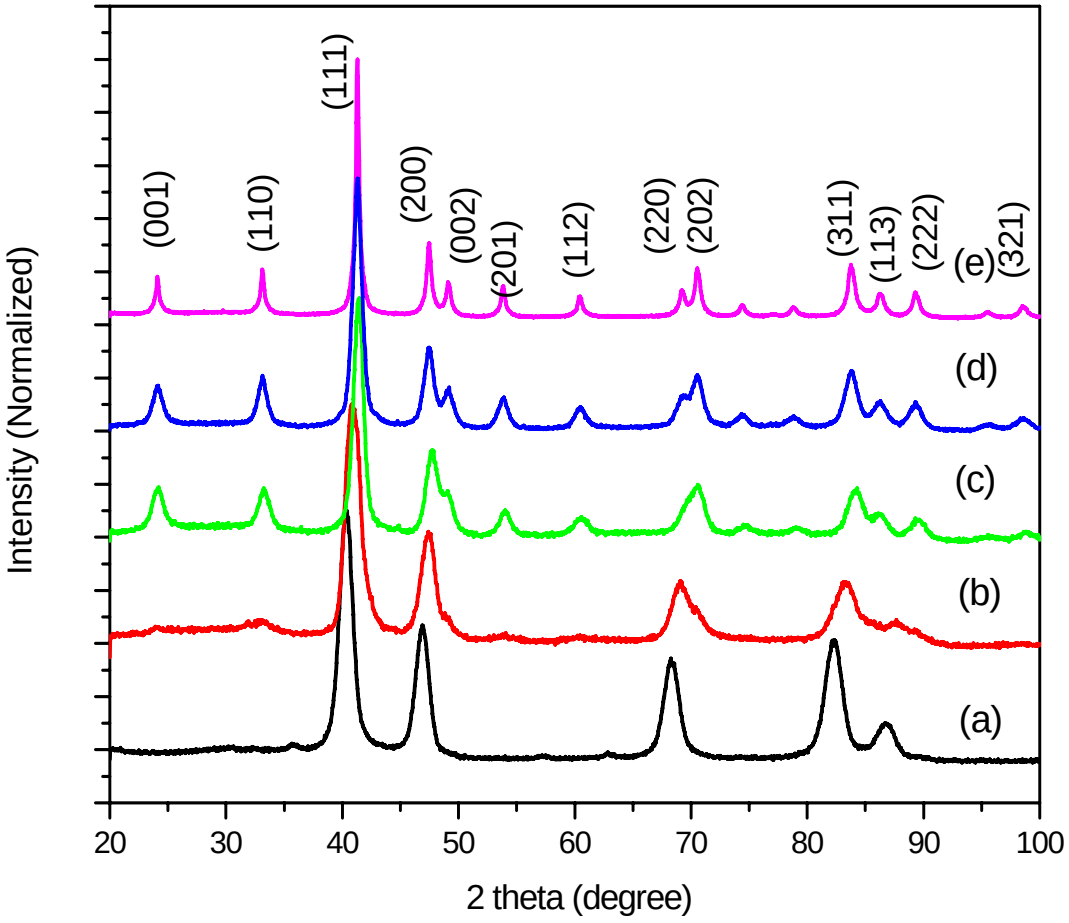


Figure 4.20 XRD patterns of 8 nm FePt nanoparticles (a) The as-synthesized FePt particles, (b) particle annealed at 600°C for 2 h with NaCl : FePt ratio 40 : 1, (c) at 700°C for 2 h with the ratio 40 : 1, (d) 700°C for 4 h with the ratio 100 : 1 , and (e) 700°C for 4 h with the ratio 40 :1

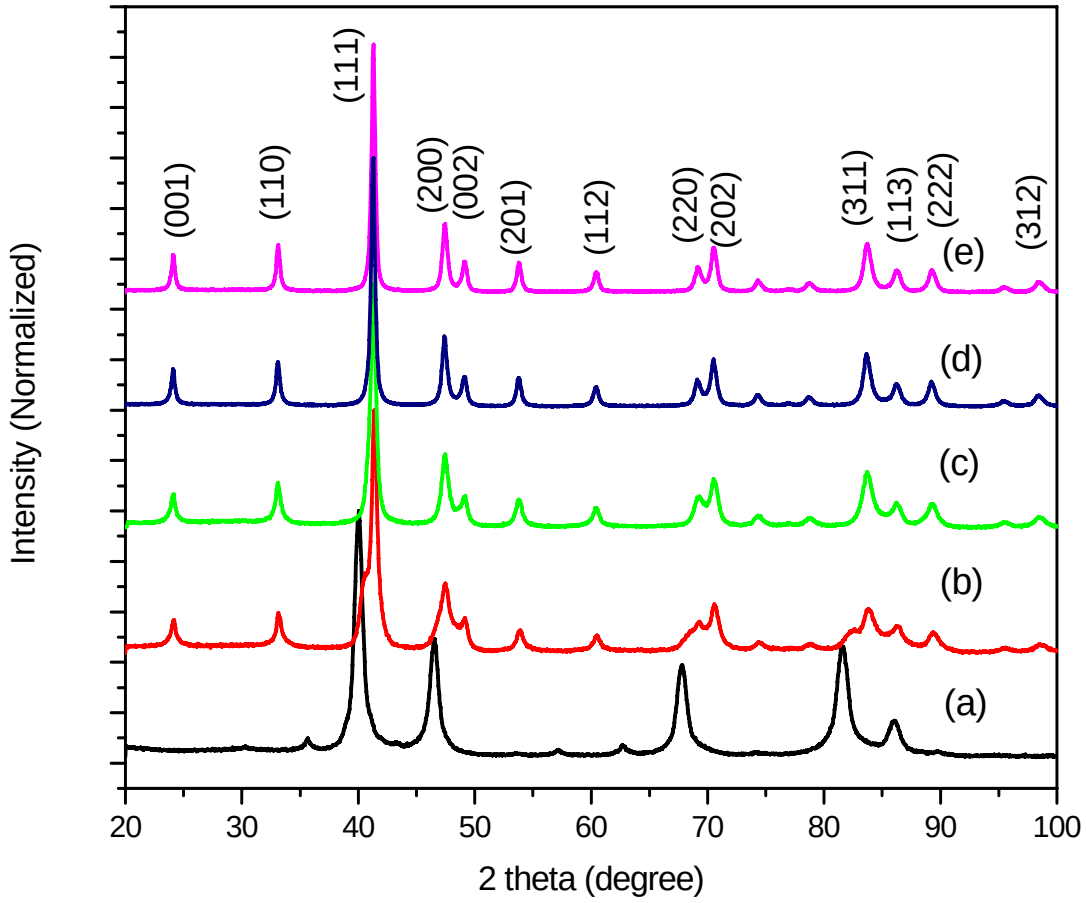


Figure 4.21 XRD patterns of the 15 nm FePt nanoparticles (a) The as-synthesized FePt particles, (b) particle annealed at 600°C for 2 h with NaCl : FePt ratio 40 : 1, (c) at 700°C for 2 h with the ratio 40 : 1, (d) 700°C for 4 h with the ratio 100 : 1 ,and (e) 700°C for 4 h with the ratio 40 :1

The morphology of the salt-matrix annealed nanoparticles was closely monitored by TEM observations and a laser particle-size analyzer. It was found that the annealed particles are easier to aggregate than the fcc particles because of the magnetic attraction force between the fct particles. This kind of aggregation can be re-dispersed by ultra-sonic vibration. Monodispersed nanoparticles can still be observed if the particles are properly deposited on TEM observation grids. Figure 4.22 shows images of

the particles annealed at 700° C for 2 h. It can be seen clearly that this methodology has successfully prevented the particles with sizes ranging from 4 to 15 nm from sintering and growing at 700° C, which is high enough for a complete phase transformation from the fcc to the fct structure. It has been found that the higher the salt to particle ratio, the lesser is the sintering. When the ratio is lower than 20: 1, monodisperse fct nanoparticles cannot be obtained from heat treatments at 700°C for 2 h. Lower salt ratios give significant particle sintering and agglomeration.

Annealing at higher temperatures and extended time should be accompanied by higher salt to FePt ratio in order to avoid sintering. From experimental observations, the salt particle size has no significant effect on the annealing and the presence of salts does not alter the fcc to fct transition temperature. From figures 4.22(*b*) and 4.22(*d*) it can be seen that most of the 8 nm particles have cubic or rectangular shapes, like their precursors before the annealing, indicating that nanoparticles shapes can be retained with this heat treatment technique. Figure 4.23 and 4.24 (a) show the TEM images of 4 and 8 nm particles annealed longer than 2 h with FePt to NaCl ratio up to 1:400. Figure 4.24 (b) shows the representative selected area electron diffraction (SAED) pattern of 8 nm FePt nanoparticles. The observed SAED patterns can be assigned to the fct FePt alloy.

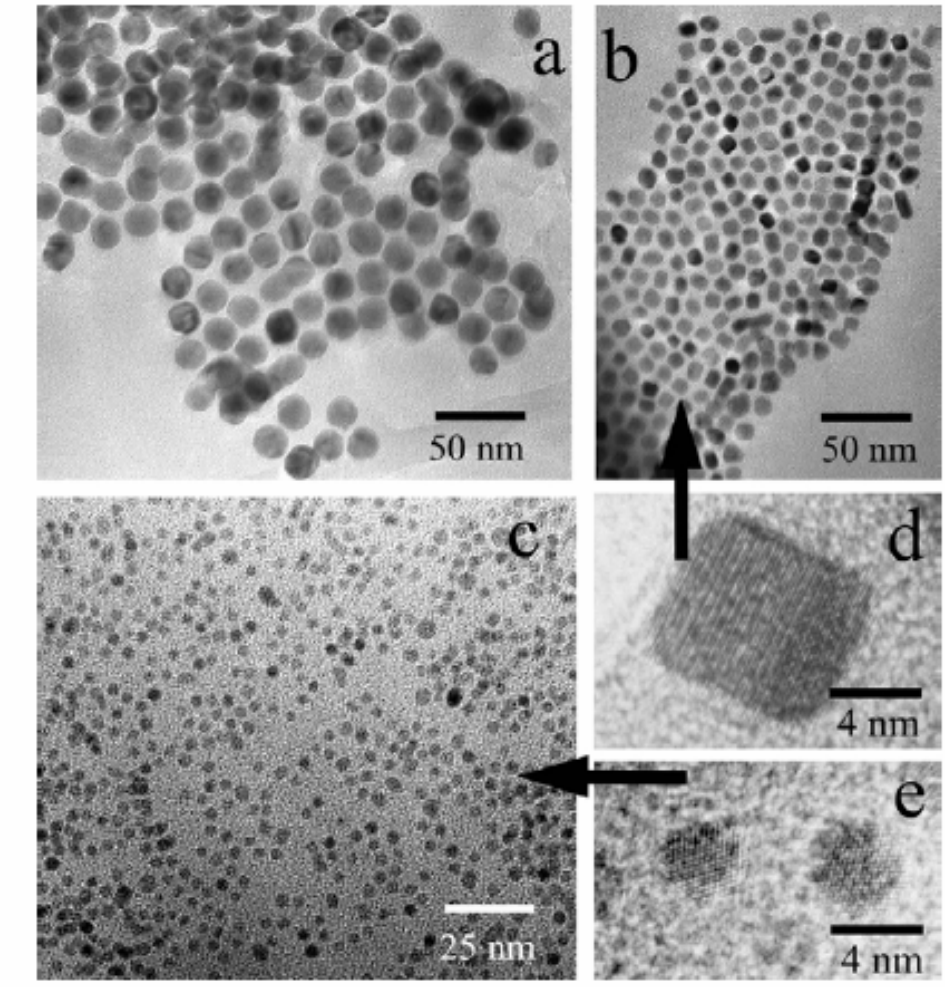


Figure 4.22 TEM images of salt-matrix annealed fct FePt particles annealed at 700°C for 2 h. (*a*) 15 nm with NaCl : FePt ratio of 100 : 1; (*b*) 8 nm with the ratio of 40 : 1; (*c*) 4 nm with the ratio of 40 : 1; (*d* ) and (*e*) are the high resolution TEM images for (*b*) and (*c*), respectively

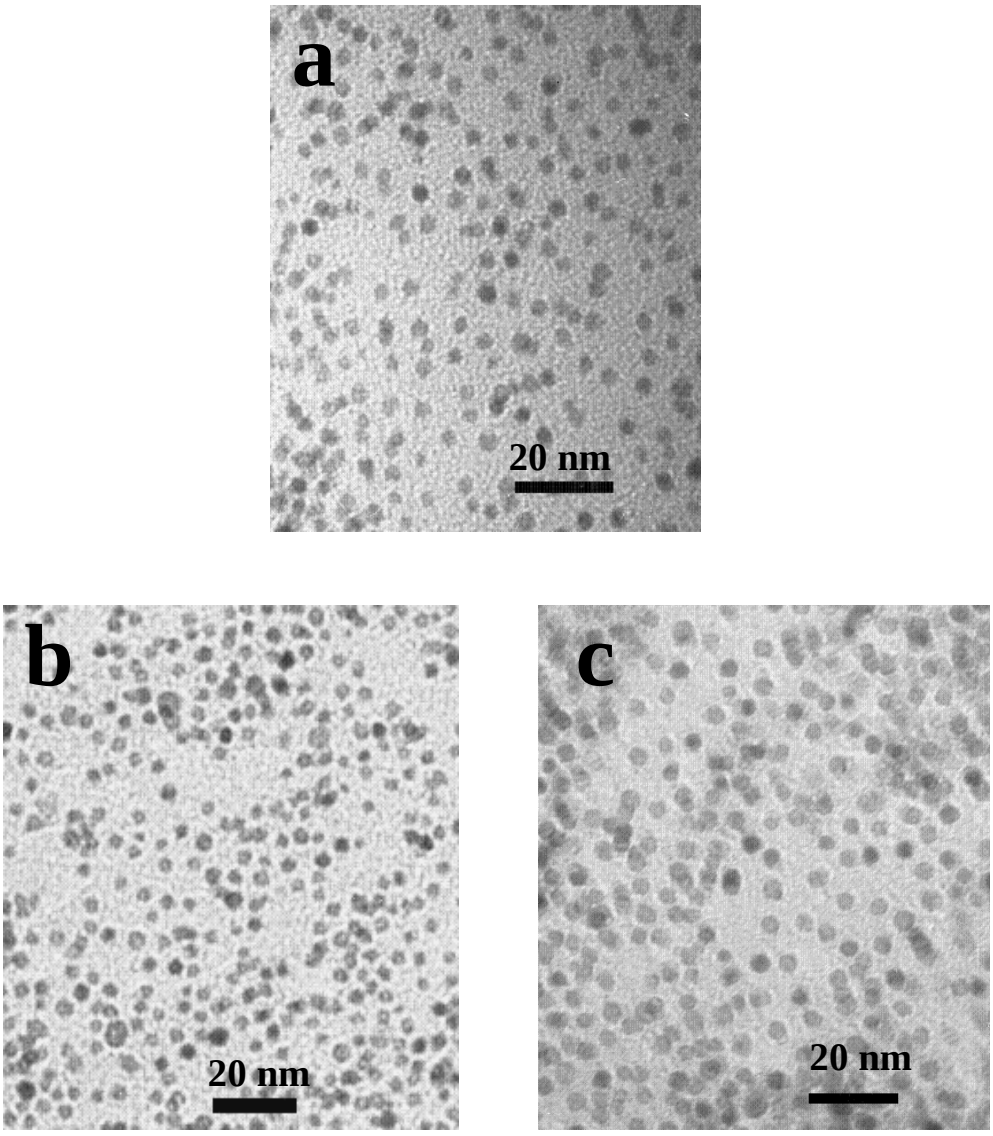


Figure 4.23 TEM images of salt-matrix annealed fct FePt particles annealed at 700°C for different time (*a*) 4 nm for 4 h with NaCl :FePt ratio of 100 : 1; (*b*) 4 nm for 6 h with the ratio of 400 : 1; and (*c* ) 4 nm for 8 h NaCl : FePt ratio of 400 :1

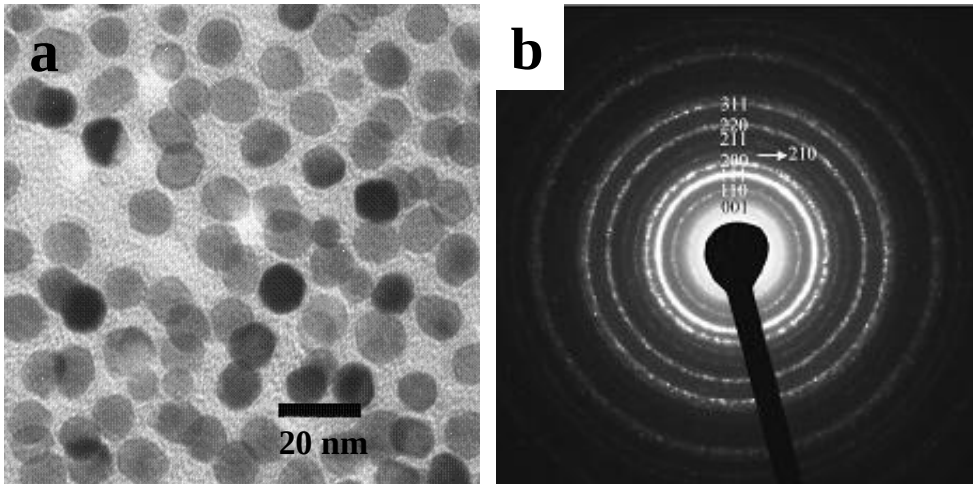


Figure 4.24 TEM images of salt-matrix annealed fct FePt particles annealed at 700°C for 2 h. (*a*) 8 nm with NaCl : FePt ratio of 100 : 1; (*b*) SAED of FePt nanoparticles

From the results discussed above, it appears that the salt-assisted annealing is effective in preventing the agglomeration and growth of nanoparticles. This technique can therefore, be readily applied to heat treatments of nanorods, nanowires and other isolated micro- and nanostructures as long as they can be mixed with salt powders and salt contamination can be avoided. The major reason for the great interest in FePt nanoparticles is that fct FePt phase has very high magnetic anisotropy and therefore, fct FePt nanoparticles should have high coercivity as long as their size is above the superparamagnetic critical dimension (2.8 nm). The annealed particles were mixed with epoxy to measure the magnetic properties. After the epoxy dried, the magnetization loops were measured with a SQUID in 7 Tesla field. Figures 4.25, 4.26, and 4.27 show demagnetization curves of annealed fct FePt nanoparticles with 4, 8, and 15 nm particles size in different annealing time and ratio of salts. The particles exhibited giant

coercivity, up to 30 kOe at room temperature (Figure 4.27). In all the cases of the annealed particles, when the XRD patterns showed the fct structure, coercivity values of the isolated particles in epoxy were normally above 15 kOe at room temperature. It is interesting to note that the 8 nm particles have higher coercivity than the rest. It may be attributed with the different shapes (cubic and rectangular) of the 8 nm particles. From figure 4.25, 4.26, and 4.27, it can also be seen that the demagnetization curves of the 4 and 8 nm particles show kinks with relatively low saturation magnetizations, indicating a two-phase magnetization behavior, which may be related to particle-size dependence of the phase-transition and is worth further investigation.

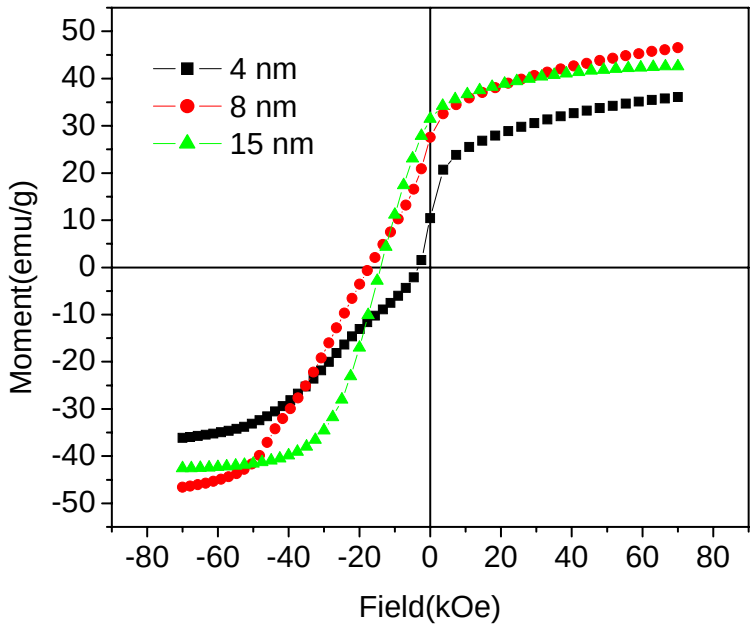


Figure 4.25 Demagnetization curves of the annealed fct FePt nanoparticles with 4, 8 and 15 nm particles size in NaCl matrix was performed at 700$^{o}$ C for 2 hrs in forming gas at ratio of FePt: NaCl = 1: 40

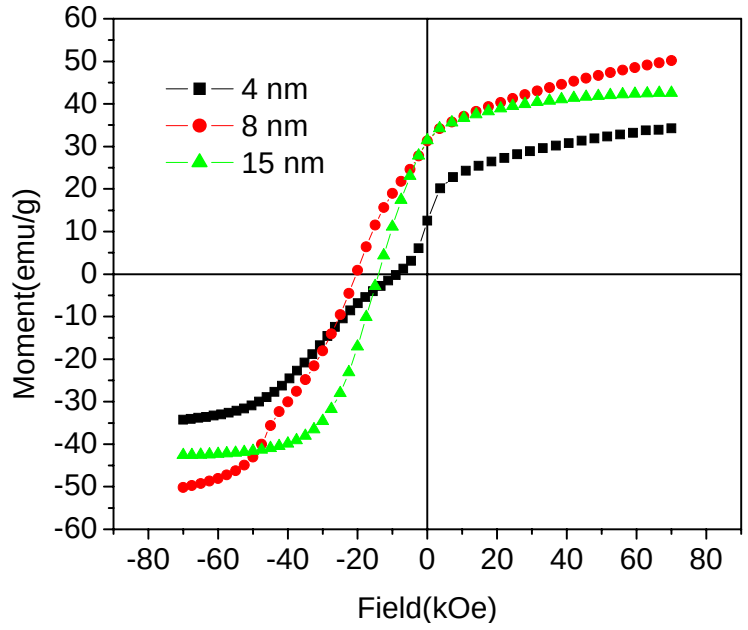


Figure 4.26 Demagnetization curves of the annealed fct FePt nanoparticles with 4, 8 and 15 nm particles size in NaCl matrix was performed at 700°C C for 4 hrs in forming gas at ratio of FePt: NaCl = 1: 40

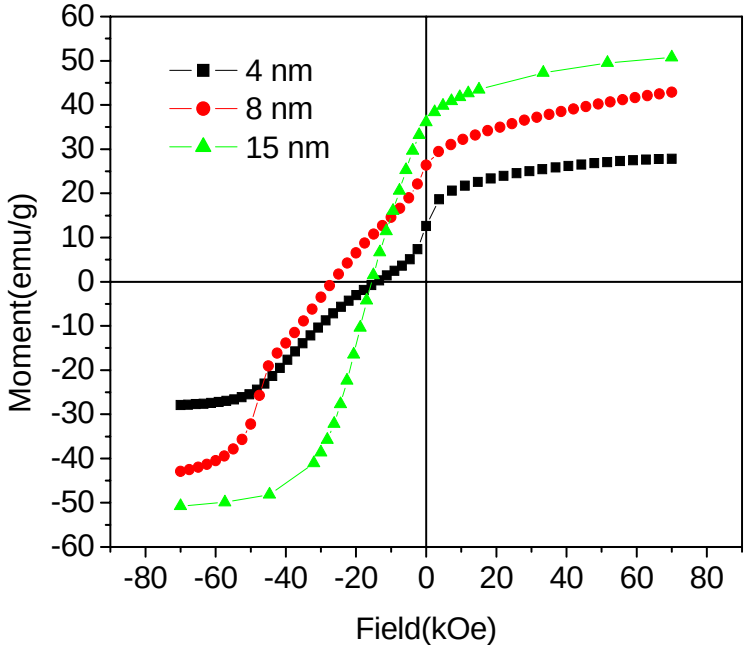


Figure 4.27 Demagnetization curves of the annealed fct FePt nanoparticles with 4, 8 and 15 nm particles size in NaCl matrix at 700° C for 2 hrs in forming gas at ratio of FePt: NaCl = 1: 100

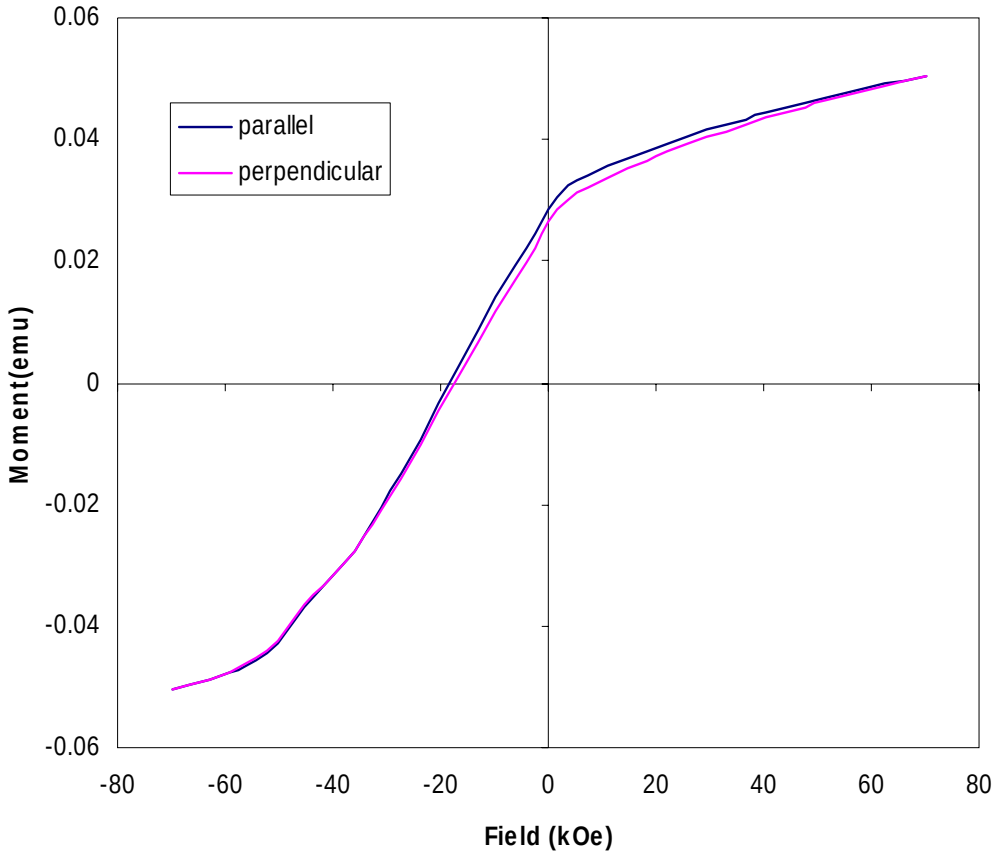


Figure 4.28 Demagnetization curves in parallel and perpendicular to field measured at room temperature from 8 nm FePt fct particles solidified in 2 Tesla field

It was supposed that the fct particles with magnetocrystalline anisotropy should be aligned in a magnetic field and therefore, the hardened epoxy/PVC specimens could give different magnetization curves in different directions. However, no obvious difference was found in the magnetization curves measured in the parallel and perpendicular directions (Figure 4.28).

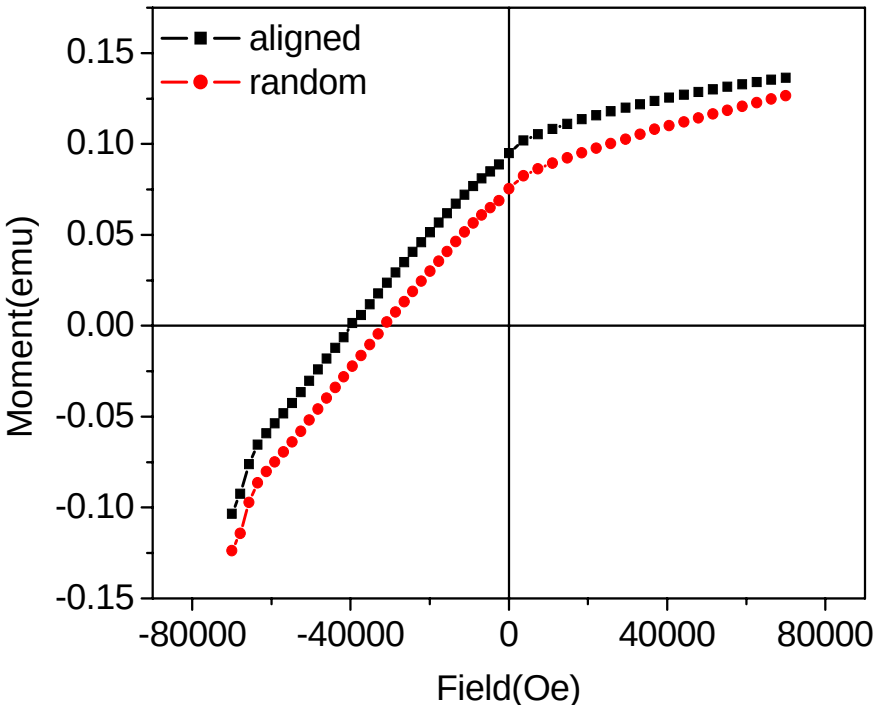


Figure 4.29 Demagnetization curves of the aligned and non-aligned fct particles measured at 10 K from the aligned 8 nm particles and the randomly aligned particles in frozen alcohol

One possible reason for this phenomenon is that the fct particles (each of them is a small permanent magnet) attract each other to form large aggregations, which makes the rotation of individual particles difficult. Another reason may be that it is difficult to rotate the very fine nanoparticles with 7 T field in epoxy because of the friction. The high viscosity of epoxy and the huge surface area of the nanoparticles can make an extremely high friction. Alignment with higher magnetic field may be needed. To reduce the friction, the particles were aligned in alcohol and water in a magnetic field of 7 T. The specimens were cooled down in the magnetic field, from room temperature at which alcohol and water are liquids, to temperatures below the ice points for alcohol

and water, and then the demagnetization curves were measured. These curves were then compared with the curves measured for the samples cooled without the magnetic field (randomly aligned particles). Figure 4.29 shows the demagnetizing curves measured from the aligned particles and the random particles in frozen alcohol at 10 K. A significant difference has been found, where high remanence and coercivity can be seen for aligned particles although we were not able to saturate the magnetization with 7 T magnetic field at 10 K. No kinks were observed in these minor-loop curves.

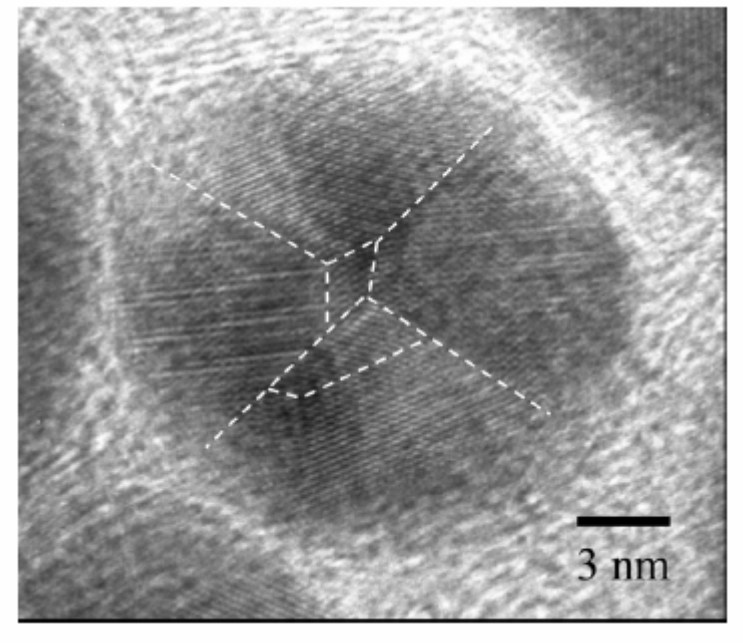


Figure 4.30 HRTEM image of an annealed fct FePt nanoparticles showing the polycrystalline morphology

Another reason for the difficulty in aligning the nanoparticles is associated with an observation of the polycrystalline feature of the annealed fct particles. Figure 4.30 shows an example of an annealed nanoparticle with a high resolution TEM image. In

the case of large sized particles (15 nm), the samples comprises of more than 50% of the plycrystalline particles, by a rough estimation. In the case of polycrystalline nanoparticles, the domain grain relationship can be complicated and the magnetization reversal cannot be described in a simple model. An extended understanding of this issue is on our wish list.

### *4.3.1 Conclusions*

Although further works are needed to produce aligned nanostructured magnetic assemblies or bulks, salt matrix annealing methodology reported here has marked the availability of building blocks of highly anisotropic fct FePt nanoparticles. The direct applications of fully converted fct FePt nanoparticles in magnetic-recording media and biomedical experiments are possible now. Based on a simple and economic processing feasible for industrial scale-up production, this technique can also be applied to the production of other isolated nanostructured materials where heat treatment, but not sintering, is required.

# CHAPTER 5

## SUMMARY

Monodisperse hard (FePt) and soft ($Fe_3O_4$, $CoFe_2O_4$) nanoparticles were successfully synthesized by chemical solution methods. Particle diameter was tuned from 3 to 20 nm by varying reaction conditions or by seed-mediated growth method. Both the hard and soft as-synthesized nanoparticles were highly crystalline. Monodisperse face-centered tetragonal (fct) FePt nanoparticles were prepared by annealing at 700 $^{o}$C the disordered face-centered cubic (fcc) FePt nanoparticles in NaCl matrix. It has been found that the magnetic properties of the as-synthesized $Fe_3O_4$ and $CoFe_2O_4$ of nanoparticles are dependent on particle size and measurement temperature. All of the as-synthesized $Fe_3O_4$ nanoparticles up to 20 nm in diameter were found to be superparamagnetic at room temperature, while $CoFe_2O_4$ nanoparticle with size greater than 12 nm were ferromagnetic. The blocking temperature $T_B$ of $Fe_3O_4$ and $CoFe_2O_4$ nanoparticles increases with particle diameters. High coercivity values of 1 kOe and 18 kOe were obtained for 20 nm $CoFe_2O_4$ nanoparticles at room temperature and 10 K respectively. Exchange bias was observed on field-cooling measurements of the $CoFe_2O_4$ nanoparticles smaller than 4 nm. Exchange bias field of 3 kOe was obtained for 3 nm $CoFe_2O_4$ particles. $Fe_3O_4$ and $CoFe_2O_4$ nanoparticles were successfully reduced to Fe and FeCo after annealing in forming gas (Ar +7% $H_2$). Reduction of $Fe_3O_4$ and $CoFe_2O_4$ nanoparticles resulted in magnetizations up to 210 emu/g and 223

emu/g respectively. The as-synthesized fcc FePt nanoparticles were superparamagnetic in nature while a very high coercivity of the isolated fct FePt nanoparticles up to 30 kOe at room temperature was obtained for 8 nm particles annealed in NaCl matrix.

In this study, the reported soft and hard magnetic nanoparticles have potential for many technological applications such as ultrahigh density recording media, biotechnology ferrofluids, and fabrication of exchange-coupled nanocomposite permanent magnets. The synthesis processes explored in this study are simple and easy to achieve the desired particle size distribution and can be scaled up for mass production.

Following issues are recommended for future work.

- The cause for exchange bias in smaller than 4 nm $CoFe_2O_4$ nanoparticles is not yet understood. More work is needed to investigate the exchange bias in the small particles.
- Salt-matrix annealing technique has been successfully adopted to prepare highly anisotropic fct FePt nanoparticles. The next step forward is to produce aligned nanostructured magnetic assemblies or bulks.

# APPENDIX A

# UNITS FOR MAGNETIC PROPERTIES

Table A.1 Units for magnetic properties [ 28]

| Quantity | Symbol | Gaussian & cgs emu [a] | Conversion factor, C [b] | SI & rationalized mks [c] |
|---|---|---|---|---|
| Magnetic flux density, magnetic induction | $B$ | gauss (G) [d] | $10^{-4}$ | tesla (T), $Wb/m^2$ |
| Magnetic flux | $\Phi$ | maxwell (Mx), $G \cdot cm^2$ | $10^{-8}$ | weber (Wb), volt second (V·s) |
| Magnetic potential difference, magnetomotive force | $U$, $F$ | gilbert (Gb) | $10/4\pi$ | ampere (A) |
| Magnetic field strength, magnetizing force | $H$ | oersted (Oe),[e] Gb/cm | $10^3/4\pi$ | A/m [f] |
| (Volume) magnetization [g] | $M$ | $emu/cm^3$ [h] | $10^3$ | A/m |
| (Volume) magnetization | $4\pi M$ | G | $10^3/4\pi$ | A/m |
| Magnetic polarization, intensity of magnetization | $J$, $I$ | $emu/cm^3$ | $4\pi \times 10^{-4}$ | T, $Wb/m^2$ [i] |
| (Mass) magnetization | $\sigma$, $M$ | emu/g | 1<br>$4\pi \times 10^{-7}$ | $A \cdot m^2/kg$<br>$Wb \cdot m/kg$ |
| Magnetic moment | $m$ | emu, erg/G | $10^{-3}$ | $A \cdot m^2$, joule per tesla (J/T) |
| Magnetic dipole moment | $j$ | emu, erg/G | $4\pi \times 10^{-10}$ | $Wb \cdot m$ [i] |
| (Volume) susceptibility | $\chi$, $\kappa$ | dimensionless, $emu/cm^3$ | $4\pi$<br>$(4\pi)^2 \times 10^{-7}$ | dimensionless<br>henry per meter (H/m), Wb/(A·m) |
| (Mass) susceptibility | $\chi_\rho$, $\kappa_\rho$ | $cm^3/g$, emu/g | $4\pi \times 10^{-3}$<br>$(4\pi)^2 \times 10^{-10}$ | $m^3/kg$<br>$H \cdot m^2/kg$ |
| (Molar) susceptibility | $\chi_{mol}$, $\kappa_{mol}$ | $cm^3/mol$, emu/mol | $4\pi \times 10^{-6}$<br>$(4\pi)^2 \times 10^{-13}$ | $m^3/mol$<br>$H \cdot m^2/mol$ |
| Permeability | $\mu$ | dimensionless | $4\pi \times 10^{-7}$ | H/m, Wb/(A·m) |
| Relative permeability [j] | $\mu_r$ | not defined | | dimensionless |
| (Volume) energy density, energy product [k] | $W$ | $erg/cm^3$ | $10^{-1}$ | $J/m^3$ |
| Demagnetization factor | $D$, $N$ | dimensionless | $1/4\pi$ | dimensionless |

*a.* Gaussian units and cgs emu are the same for magnetic properties. The defining relation is $B = H + 4\pi M$.
*b.* Multiply a number in Gaussian units by C to convert it to SI (e.g., $1\ G \times 10^{-4}\ T/G = 10^{-4}\ T$).
*c.* SI (*Système International d'Unités*) has been adopted by the National Bureau of Standards. Where two conversion factors are given, the upper one is recognized under, or consistent with, SI and is based on the definition $B = \mu_0(H + M)$, where $\mu_0 = 4\pi \times 10^{-7}$ H/m. The lower one is not recognized under SI and is based on the definition $B = \mu_0 H + J$, where the symbol $I$ is often used in place of $J$.
*d.* 1 gauss $= 10^5$ gamma ($\gamma$).
*e.* Both oersted and gauss are expressed as $cm^{-1/2} \cdot g^{1/2} \cdot s^{-1}$ in terms of base units.
*f.* A/m was often expressed as "ampere-turn per meter" when used for magnetic field strength.
*g.* Magnetic moment per unit volume.
*h.* The designation "emu" is not a unit.
*i.* Recognized under SI, even though based on the definition $B = \mu_0 H + J$. See footnote *c*.
*j.* $\mu_r = \mu/\mu_0 = 1 + \chi$, all in SI. $\mu_r$ is equal to Gaussian $\mu$.
*k.* $B \cdot H$ and $\mu_0 M \cdot H$ have SI units $J/m^3$; $M \cdot H$ and $B \cdot H/4\pi$ have Gaussian units $erg/cm^3$.

# APPENDIX B

# CRYSTRAL STRUCTURE OF FERRITE

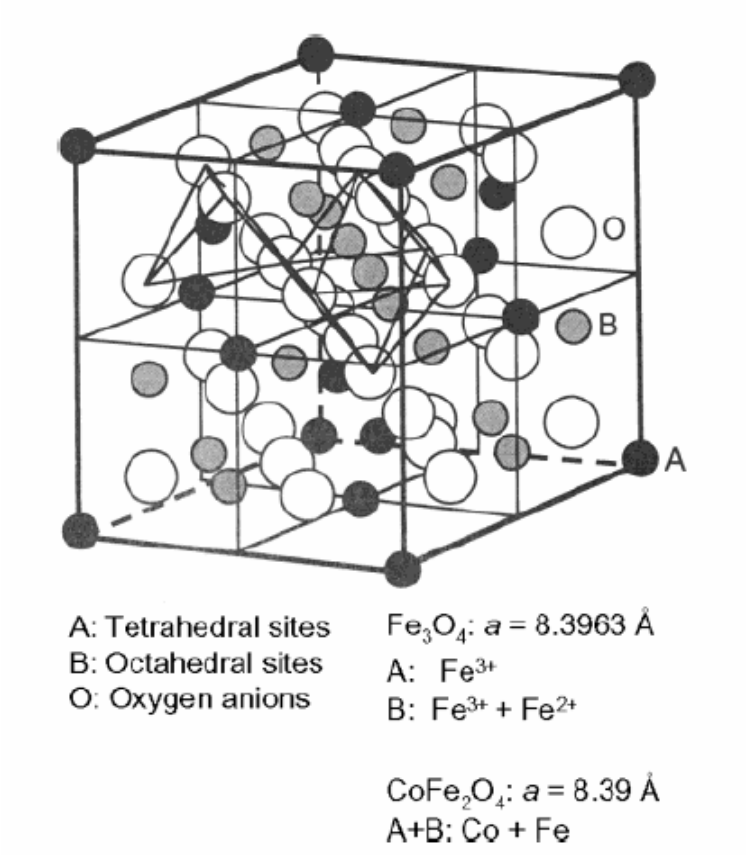


Figure B.1 Schematic model of the Spinel unite cell structure [67]

The Spinel structure has two cation sites: the tetrahedrally coordinated A sites and the octahedrally coordinated B sites. For $Fe_3O_4$, the A and B positions are occupied by $Fe^{3+}$and $Fe^{2+}$ cations, respectively. For $CoFe_2O_4$, the A and B positions are equally occupied by Co and Fe cations. $Fe_3O_4$ and $CoFe_2O_4$ have almost the same lattice parameters: $a$ = 8.3963 Å for $Fe_3O_4$, $a$ = 8.39 Å for $CoFe_2O_4$. The mass densities for $Fe_3O_4$ and $CoFe_2O_4$ are almost identical.

# APPENDIX C

## FePt PHASE DIAGRAM

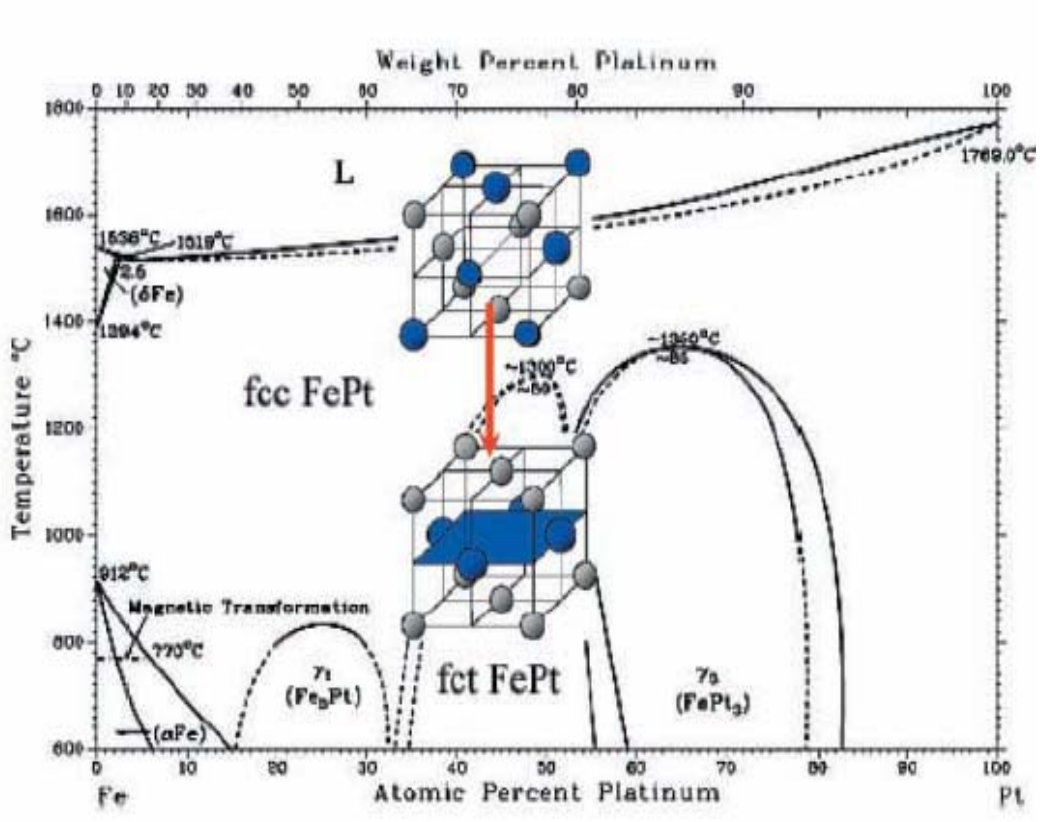


Figure C.1 FePt phase diagram and schematic representation of structure transformation between fcc and fct FePt. Gray circles represent Fe atoms and blue circles represent Pt atoms in unit cells [72]

# APPENDIX D

# RESEARCH ACOMPLISHMENTS

Awards:

- Awarded "Scharff Award Scholarship" on March 22, 2005 by University of Texas at Arlington, Department of Physics for research achievements.

List of Publications:

- Field-Ball Milling Induced Anisotropy in Magnetic Particles
  Narayan Poudyal, Baki Altuncevahir, Vamsi Chakka, Kanghua Chen, Truman D. Black, J. P. Liu, Yong Ding and Zhong Lin Wang, *Journal of Physics D: Applied Physics,* **37,** L45 (2004).

- Monodisperse face-centered tetragonal FePt nanoparticles with giant coercivity
  Kevin Elkins, Daren Li, Narayan Poudyal, Vikas Nandwana, Zhiqiang Jin, Kanghua Chen and J. Ping Liu, *Journal of Physics D: Applied Physics,* **38,** 2306 (2005).

Presentations:

- Effect of Ball Milling on Magnetic Hysteresis of SmCo Particles
  Narayan Poudyal, Baki Altuncevahir, Truman D. Black, and J. Ping Liu
  Poster presentation in the International Conference on Photonic, Excitonic, Spintronic Processes in Nanostructures in the University of Texas at Dallas, USA, January, 2004.

- Tailoring the Magnetic Properties of $Co_xFe_{3-x}O_4$ Nanoparticles
  Narayan Poudyal, Tejaswi Vedantam, Baki Altuncevahir,Vamsi Chakka, J. P. Liu
  Poster presentation at the DARPA Meta-Materials PI Review, Washington DC, August, 2004.

- Tailoring Magnetic Properties of Co-ferrite Nanoparticles
  Narayan Poudyal, Tejaswi Vedantam, Baki Altuncevahir, Vamsi Chakka, J. P. Liu
  Poster presentation at the SPRING 04 Conference on research in nanotechnology in the University of Texas at Dallas, USA in November, 2004.

- Tailoring Magnetic Properties of Co-ferrite Nanoparticles
  Narayan Poudyal, Tejaswi Vedantam, J. P. Liu.
  Paper presentation in American Physical Society (APS) March meeting in Los Angles, California, 2005.

News Articles:

- Just Add Salt titled news articles published in Physics Web in August 4, 2005.
  Link to the articles: http://physicsweb.org/articles/news/9/8/3/1

- For nanoparticles, just add salt titled news articles published in Nanotechweb.org Link to the articles: http://www.nanotechweb.org/articles/news/4/8/6/1

- Physicists Discover Table Salt is Solution to Creating the Smallest Magnets titled news articles published in UTA Today in August 15, 2005

REFERENCES


1. Soshin Chikasumi, “Physics of Magnetism” John Wiley and Sons, (1964).

2. B. D. Cullity, “Introduction to Magnetic Materials”, Addison-Wesley Publishing, (1972).

3. Nicola A. Spaldn, “ Magnetic Materials: Fundamentals and Device Applications”, Cambridge University Press, (2003)

4. William D. Callister, Jr., “Material Science and Engineering: An Introduction”, John Wiley & Sons, 2000.

5. Robert C. O’ Handley, “Modern Magnetic Materials: Principles and Applications”, Wiley & Sons, 2000.

6. J.C. Anderson, “Magnetism and Magnetic Materials”, Chapman and Hall Ltd. (1968).

7. J. M. D. Coey, “Magnetic Materials”, *Journal of Alloys and Compounds,* **326**, 2 (2000).

8. S. R. Trout, “Understanding Permanent Magnet Materials: An Attempt at Universal Magnetic Literacy”, *Magnequench International, Inc.*

9. J. M. D. Coey, “Permanent Magnetism”, *Solid State Communications*, **102**, 101 (1997).

10. E.F. Kneller, andvR. Hawing “The exchange-spring magnet: new material for permagnet magnets”, IEEE Transactions on Magnetics, 27, 3588 (1991).

11. R. Skomski, J.M.D. Coey, “Giant energy product in nanostructured two-phase magnets”. Physical. Review B, 48, 15812(1993).
12. Hao Zeng, Jing Li, J.P. Liu, Zhoung L. Wang, and Shouheng Sun, “Exchange-coupled nanocomposite magnets by nanoparticles self-assembly” Nature, 420,395 (2002).

13. J.P. Liu, “Novel approaches to the synthesis and processing of nanocomposite magnets”, 18th International workshop on high performance magnets and their applications, Annecy (France) (2004).

14. J. Sort, S. Surmach, J. S. Munoz, and M. D. Baro, "Improving the energy product of hard magnetic materials", Physical Review B, 65, 174420(2002).

15. D.C. Jiles, "Recent advances and future directions in magnetic materials", *Acta Meterialia*, **15**, 5907 (2003).

16. Eric E. Fullerton, J. S. Jiang, S. D. Bader, "Hard/Soft magnetic heterostructures: model exchange-spring magnets", *Journal of Magnetism and Magnetic Materials*, **200**, 392 (1999).

17. R. Skomski and J.M.D Coey, "Exchange Coupling and Energy Product in Random Two phase Aligned Magnets", *IEEE Transactions on Magnetics*, **30**, 607(1994).

18. J. P. Liu, "Nanosturctured Soft and Hard Magnetic Materials", Chapter-6 of Handbook of nanophase and nanostructured materials, ed. by Z.L. Wang, Y. Liu and Z. Zhang, Kluwer Academic/Plenum Publishers and Tsinghua University Presss, **3**, 244-268 (2003).

19. Kenneth J. Klabunde, "Nanoscale Materials in Chemistry", John & Sons, Inc. (2001).

20. D. Goll and H. Kronmuller, "High-performance Permanent Magnets", Naturwissenschaften, 87,423(2000).

21. Catherine C. Berry and Adam S. G. Curtis, "Fictionalization of magnetic nanoparticles for application in biomedicine", *Journal of Physics. D: Applied Physics*, **36**, R198 (2003).

22. Taeghwan Hyeon, "Chemical synthesis of magnetic nanoparticles", *Chemical communication, 927(2003).*

23. Adam Curtis, "Biomedical aspects of magnetic nanoparticles", *Euro physics News*, **34**, 6 (2003)

24. M. Chastellain1, A. Petri1, M. Hofmann and H. Hofmann, "Synthesis and patterning of magnetic nanostructures", *European Cells and Materials*, **3**, 1, 11 (2002).

25. D.K. Kim W. Voit, W. Zapka, B. Bjelke, M. Muhammed, and K.V. Rao, "*Material Research Society Symp. Proc*." **676**, (2001).

26. M. A. Willard, L.K. Kulrihara, E.E. Carpenter, S. Calvin and V.G. Harris, "Chemically prepared magnetic nanoparticles", *International Material Reviews*, **49**, 3(2004).

27. L. Fu, V.P. Dravid, K. Klug, X. Liu and C.A. Mirkin, " Synthesis and patterning of magnetic nanostructures", *European Cell and Materials, 3 Suppl.* 2, 156(2002).

28. R.B. Goldfarb and F.R., U.S. Department of Commerce, National Bureau of Standards, Boulder, Colorado 80303, March 1985. NBS Special Publication 696. For sale by the Superintendent of Documents, U.S. Government Printing Office, Washington, DC 200402.

29. CA Ross, "Patterned Magnetic Recording Media", *Annual Review of Material Research*, **31**, 203(2001).

30. S. Okamoto, O. Kitkami, N. Kickuchi, T. Miyazaki, and Y. Shimada, "Size dependences of magnetic properties and switching behavior in FePt $L1_0$ nanoparticles", *Physical Review B*, **67**, 094422 (2003).

31. D. Weller, M. F. Doerner, "Extremely high-density longitudinal magnetic recording media" Annual review of materials science, **30**, 611(2000).

32. Y. Shi, J. Ding and H. Yin, "$CoFe_2O_4$ nanoparticles by the mechanochemical method", *Journal of Alloys and Compounds*,**303**, 290(2002).

33. Yeong II Kim, Don Kim, and Choong Sub Lee, "Synthesis and characterization of $CoFe_2O_4$ magnetic nanoparticles prepared by temperature-controlled co-precipitation method", *Physica B*, **337**, 42 (2003).

34. C.N. Chinnasamy, M. Senoue, B. Jeyadevan, Oscar Perales-Perez, K. Shinoda, and K. Tohji, " Synthesis of size-controlled cobalt ferrite particles with high coercivity and squareness ratio", *Journal of colloid and interface science* , **263**, 80(2003).

35. http://www.carolina.com/physics/aboutferro.asp

36. http://www.zarm.uni-bremen.de/2forschung/ferro/basic_info/applic/index.htm

37. S. H. Gee, Y.K. Hong, D.W. Erickson, M.H. Park, and J.C. Sur "Synthesis and aging effect of spherical magnetite ($Fe_3O_4$) nanoparticles for biosensor applications", *Journal of Applied Physics*, **93**, 10 (2003).

38. Shouheng Sun, Hao Zeng, David B. Robinson, Simone Raoux, Philip M. Rice, Shan X. Wang, and Guanxiong Li, "Monodisperse $MFe_2O_4$ (M = Fe, Co, Mn) Nanoparticles", *Journal of Applied Chemical Society*, **126**, 273 (2004).

39. Shouheng Sun, and Hao Zeng, "Size-Controlled Synthesis of Magnetite Nanoparticles", *Journal of Applied Chemical Society*, **124**, 8204(2002).

40. Christy R, Vestal and Z. John Zhang, "Magnetic spinel ferrite nanoparticles from microemulsions" *International Journal of Nanotechnology*", **1** 1/2(2004).

41. M. Rajendran, R. C. Pullar, A. K. Bhattacharya, D. Das, S. N. Chintalapudi and C. K. Majumdar, "Magnetic properties of nanocrystalline $CoFe_2O_4$ powders prepared at room temperature: variation with crystallite size", *Journal of Magnetism and Magnetic Materials,* **232** ,71(2001).

42. P.C. Morais, V.K. Garg , A.C. Oliveira, L.P. Silva, R.B. Azevedo, A.M.L. Silva, E.C.D. Lima, " Synthesis and characterization of size-controlled cobalt-ferrite-based ionic ferrofluids", *Journal of Magnetism and Magnetic Materials,* **225** , 37 (2001).

43. T. Pannaparayil and S. Komarneni, "Synthesis and characterization of ultra fine cobalt ferrites", *IEEE Transactions on magnetics*, **25**, 5(1989).

44. N. Moumen , P. Veillet M.P. Pileni, "Controlled preparation of nanosize cobalt ferrite magnetic particles", *Journal of Magnetism and Magnetic Materials*, **149**, 67(1995).

45. Yangkyu Ahn , Eun Jung Choi , Sehun Kim , Hang Nam Ok , "Magnetization and Mössbauer study of cobalt ferrite particles from nanophase cobalt iron carbonate", *Materials Letters,* **50** , 47(2001).

46. V. Pillai, and D.O. Shah, " Synthesis of high-coercivity cobalt ferrite particles using water-in-oil microemulsions", Journal *of Magnetism and Magnetic Materials*, **163**, 243(1996).

47. Chao Liu, Bingsuo Zou, Adam J. Rondinone, and Z. John Zhang "Chemical Control of Superparamagnetic Properties of Magnesium and Cobalt Spinel Ferrite Nanoparticles through Atomic Level Magnetic Couplings", *Journal of American Chemical Society*, **122**, 6263(2000).

48. R. Vijayakumar, Yu Koltypin, I. Felner, A. Gedanken, "Sonochemical synthesis and characterization of pure nanometer-sized $Fe_3O_4$ particles", *Material Science and Engineering A*, **286**, 101(2000).

49. V. V. Yakovlev, V. Lazarov, J. Reynolds, and M. Gajdardziska-Josifovska, "Laser-induced phase transformations in semiconductor quantum dots", *Applied Physics Letters*, **76**, 2050(2000).

50. W. D. Ristenpart, I. A. Aksay, and D. A. Saville, "Assembly of colloidal aggregates by electro-hydrodynamic flow: Kinetic experiments", *Physical Review E,* **69**, 021405 (2004).

51. Gerardo F. Goya, "Handling the particles size and distribution of $Fe_3O_4$ nanoparticles through ball milling", *Solid state communications*, **130**,783(2004).

52. Hao Zeng, Shouheng Sun, J. Li and Z. L. Wang, and J. P. Liu, "Tailoring magnetic properties of core/shell nanoparticles", *Applied Physics Letters*, **85**, 792 (2004).

53. Carl C. Koch, "Nanostructured Materials: Processing, Properties, and Applications", *Noyes Publications*, (2002).

54. Vincent Rotello, "Nanoparticles: Building Blocks for Nanotechnology", *Kluwer Academics/Plenum Publishers*, New York (2004).

55. http://www.azom.com/details.asp?ArticleID=637

56. R. Coehoorn, D. B. de Mooij and C. de Waard "Meltspun permanent magnet materials containing $Fe_3B$ as the main phase", *Journal of Magnetism and Magnetic Material, Volume 80, 10(1989).*

57. S. Sun, Eric E. Fullerton, D. Weller and C. B. Murray, " Compositionally controlled FePt nanoparticle Materials", *IEEE Transactions on magnetics*, **37**,1239(2001).

58. Kevin Elkins, Daren Li, Narayan Poudyal, Vikas Nandwana, Zhiqiang Jin, Kanghua Chen and J. Ping Liu, " Monodisperse face-centered tetragonal FePt nanoparticles with giant coercivity", *Journal of Physics D: Applied Physics,* **38**, 2306(2005).

59. Kurikka V.P.M. Shafi, Aharon Gedanken, Ruslan Prozorov, Judit Balohgh, "Sonochemical Preparation and Size-Dependent Properties of Nanostructured $CoFe_2O_4$ Particles", *Chemical Material*, **10**, 3445(1998).

60. Kurikka V.P.M. Shafi, Aharon Gedanken, Ruslan Prozorov, Judit Balohgh, "Sonochemical Preparation and Size-Dependent Properties of Nanostructured $CoFe_2O_4$ Particles", *Chemical Material*, **10**, 3445(1998).

61. F. Bensebaa, F. Zavaliche, P. L. Ecuyer, R.W. Cochrane, T. Veres, " Microwave synthesis and characterization of Co-ferrite nanoparticles" *Journal of Colliod and Interface Science*, **277**, 104(2004).

62. G. B. Ji, S.L. Tang, S.K. Ren, F.M. Zhang, B.X. Gu, Y.W. Du, "Simplified synthesis of single-crystalline magnetic $CoFe_2O_4$ nanorods by a surfactant-assisted hydrothermal process", *Journal of Crystal Growth*, **270**,156(2004).

63. Xinyong Li, Charles Kutal, "Synthesis and characterization of superparamagnetic $Co_xFe_{3-x}O_4$ nanoparticles" *Journal of Alloys and Compounds*, **349**,264(2003).

64. Jae-gwang Lee, Jae Yun Park, Chul Sung Kin, "Growth of ultra-fine cobalt ferrite particles by a sol-gel method and their magnetic properties" *Journal of Material Science*, **33**, 3965(1998).

65. Tadao Sugimota, Yasuhiko Shimotsuma, Hiroyuki Itoh, " Synthesis of uniform cobalt ferrite particles from a highly condensed suspension of β-FeOOH and β-$Co(OH)_2$ particles" *Power Technology,* **96**, 85(1998)

66. S. Bid, A. Banerjee, S. Kumar, S. K. Pradhan, Udaya De, D. Banerjee, " Nanophase iron oxides by ball-mill grinding and their Mössbauer characterization", Journal of Alloys and Compounds, **326**, 292(2001).

67. Jing Li, Hao Zeng, Shouheng Sun, J. Ping Liu, and Zhong Lin Wang **, "**Analyzing the Structure of CoFe-$Fe_3O_4$ Core-Shell Nanoparticles by Electron Imaging and Diffraction", *Journal of Physical Chemistry B,* **108***,* 14005(2004).

68. http://www.carolina.com/physics/aboutferro.asp

69. Riki Hrpensess and Ahron Gedanken, "The microwave-assited polyol synthesis of nanosized hard magnetic material, FePt", *Journal of Material Chemistry,* **15**, 698, (2005).

70. W. Liu, P.G. McCormick, "Synthesis of $Sm_2Co_{17}$ alloy nanoparticles by mechanical processing" *Journal of magnetism and magnetic materials*, **195**, L297(1999).

71. S. Sun S, C. B. Murray, D. Weller, L. Folks and A. Moser, "Monodisperse FePt Nanoparticles and Ferromagnetic FePt Nanocrystal Superlattices", *Science,* **287** 1989(2000).

72. Ding Jun and Zhao Zeliang, "High Coercivity FePt Thin Films for High-density Perpendicular Recording Media , *Faculty of science, research newsletter*, **7**, 3, (2003).

73. Q. A. Pankhurst, J. Connolly J, S. K. Jones and J. Dobson J, "Applications of magnetic nanoparticles in biomedicine", *Journal of Physics D: Applied Physics*, **36,** R167 (2003).

74. O. Kitakami, Y. Shimada, K. Oikawa, H. Daimon and K. Fukamichi, "Low-temperature ordering of $L1_0$-CoPt thin films promoted by Sn, Pb, Sb, and Bi additives", *Applied Physics Letter*, **78** ,1104(2001).

75. T. Maeda, T. Kai, A. Kikitsu, T. Nagase and J. Akiyama, "Reduction of ordering temperature of an FePt-ordered alloy by addition of Cu", Applied Physics. Letter, 80, 2147(2002).

76. S. Kang, J. W. Harrell and D. E. Nikles , "Reduction of the fcc to L10 Ordering Temperature for Self-Assembled FePt Nanoparticles Containing Ag", Nano Letter, 2, 1033 (2002).

77. S. S. Kang, D. E. Nickles and W. J. Harrell, "Synthesis, chemical ordering, and magnetic properties of self-assembled FePt–Ag nanoparticle", *Journal of Applied Physics***, 93,** 7178 (2003).

78. X. Sun, S. Kang, J. W. Harrell, D. E. Nikles , Z. R. Dai, J. Li, and Z. L. Wang ,"Synthesis, chemical ordering, and magnetic properties of FePtCu nanoparticle films" , Journal of Applied Physics, **93**, 7337(2003).

79. C. L. Platt, K. W. Wierman, E. B. Svedberg, R. van de Veerdonk, J. K. Howard , A. G. Roy and D. E. Laughlin, "L–$1_0$ ordering and microstructure of FePt thin films with Cu, Ag, and Au addi" , Journal of Applied Physics, **92**, 6104 (2002).

80. B. Jeyadevan, A. Hobo, K. Urakawa, C. N. Chinnasamy, K. Shinoda, and K. Tohji, "Towards direct synthesis of fct-FePt nanoparticles by chemical route", Journal of *Applied Physics*, **93** 7574(2003).

81. B. Jeyadevan, K. Urakawa, A. Hobo, N. Chinnasamy, K. Shinoda, K. Tohji, David D. Julianto Djayaprawira, M.Tsunoda and M.Takahashi, "Direct Synthesis of fct-FePt Nanoparticles by Chemical Route", Japanese Journal of Applied Physics, **42**, 350(2003)

82. K. Sato, B. Jeyadevan and K. Tojhi, *Journal of Magnetism and Magnetic Materials,* **266** 227(2003)

83. S. Kang, Z. Jia , S. Shi , D. E. Nikles and J.W. Harrell , "Easy axis alignment of chemically partially ordered FePt nanoparticles", *Applied Physics Letter*, **86** 62503(2005).

84. Y. Ding, S.A. Majetich, J. Kim, K. Barmak, H. Rollins and P. Sides, "Sintering prevention and phase transformation of FePt nanoparticles", *Journal of. Magnetism and Magnetic Materials,* **284**, 336(2004).

85. M. Mizuno, Y. Sasaki, A. C. C. Yu and M. Inoue "Prevention of Nanoparticle Coalescence under High-Temperature Annealing" *Langmuir,* **20**, 11305(2004).

86. H. Zeng, S. Sun , R. L. Sandstrom and C.B. Murray, "Chemical ordering of FePt nanoparticle self-assemblies by rapid thermal annealing**",** *Journal of. Magnetism and Magnetic Materials,* **266,** 227(2003).

87. S. Saita and S. Maenosono, "Chemical ordering of FePt nanoparticles by pulsed laser annealing", *Journal of Physics: Condensed Matter,* **16,** 6385(2004).

88. Kevin E. Elkins , Tejaswi S. Vedantam, J. P. Liu, Hao Zeng, Shouheng Sun, Y Ding, and Z. L. Wang, *Nano Letter,* **3,** 1647(2003).
89. M. Chen, J.P. Liu, and S. Sun, "One-Step Synthesis of FePt Nanoparticles with Tunable Size**",** Journal *of American Chimerical Society,* **126**, 8394(2004).

90. X. Teng and H. Yang "Synthesis of Face-Centered Tetragonal FePt Nanoparticles and Granular Films from Pt@$Fe_2O_3$ Core-Shell Nanoparticles", *Journal of American Chemical Society,* **125,** 14559(2003).

91. T. Klemmer, D. Hoydick, H. Okumura, B. Zhang and W. A. Soffa "Magnetic hardening and coercivity mechanisms in $L1_0$ ordered FePd ferromagnets"**,** *Scr. Metall. Mater,.* **33,** 1793 (1995).

## BIOGRAPHICAL INFORMATION

Narayan Poudyal was born in Nepal. After his high school education his native country, Mr. Poudyal pursued his higher secondary education in Pune, India. He then completed his Bachelor's Degree in Science (B. Sc.), and Master's Degree in Physics from the Tribhuvan University, Kathmandu, Nepal. After completing a Master's Degree in Physics, he worked as a lecturer in Tribhuvan University, Kathmandu, Nepal, for two years. He also served as an executive member and Head of the Department of Science and Mathematics in Occidental Public School, Kathmandu, Nepal, for four years. In due course of teaching experience, the author felt the need of a better understating and broader knowledge of physics that motivated him to continue higher education in physics. Subsequently, he joined the Department of Physics at the University of Texas at Arlington (UTA), Texas, USA, in 2002 and was awarded Master's Degree in Physics in August 2005. Currently, he is in the Ph D program in Physics at UTA. The opportunity of working on the synthesis of magnetic nanoparticles by chemical method has enriched his knowledge and experience in the area of nano-scale magnetism and nanotechnology, which has drawn the great attention around the world. The work he was involved in the development of advanced nanomaterials (magnetic nanoparticles), was reported in the Physics Web for its significant contributions to the relevant research fields. Mr. Poudyal is exploring more in the area while pursuing his Doctoral Degree in Physics under his advisor, Professor J. Ping Liu.